

# **Regulation of the Tumor Necrosis Factor Receptor-1 signaling by palmitoylation**

Dissertation

zur Erlangung des Doktorgrades

der Mathematisch-Naturwissenschaftlichen Fakultät

der Christian-Albrechts-Universität zu Kiel

vorgelegt von

**Philipp Zingler**

Kiel

2019

Erster Gutachter:	Prof. Dr. Axel Scheidig
Zweiter Gutachter:	Prof. Dr. Stefan Schütze
Tag der mündlichen Prüfung:	11. Februar 2019

## **I. Table of contents**

<b>I. Table of contents</b> .....	<b>3</b>
<b>II. Abbreviations</b> .....	<b>7</b>
<b>III. List of Figures</b> .....	<b>9</b>
<b>IV. List of Tables</b> .....	<b>11</b>
<b>1.1 Summary</b> .....	<b>12</b>
<b>1.2 Zusammenfassung</b> .....	<b>12</b>
<b>2. Introduction</b> .....	<b>15</b>
2.1 Programmed cell death .....	15
2.2 Caspase dependent programmed cell death - apoptosis.....	15
2.3 The biology of TNF .....	20
2.4 Tumor necrosis factor receptor 1 signaling.....	21
2.5 Post translational modification of TNF-R1 - palmitoylation .....	23
2.6 Aims of the dissertation.....	27
<b>3. Materials and Methods</b> .....	<b>28</b>
3.1 Materials .....	28
3.2 Methods.....	38
3.2.1 Cell culture .....	38
3.2.2 Preparation of whole cell lysates .....	38
3.2.3 Protein quantification .....	39
3.2.4 SDS-PAGE/Western blot.....	39
3.2.5 Acyl-resin-assisted capture .....	40
3.2.6 Electroporation .....	41
3.2.7 Purification of Fc60TNF .....	41

## I. Table of contents

---

3.2.8 Immunoprecipitation via Fc60TNF .....	41
3.2.9 Nucleofection .....	42
3.2.10 Generation of U937 knockout cells by CRISPR/Cas9 plasmids .....	42
3.2.11 Generation of TNF-R1 constructs.....	43
3.2.12 Recloning.....	44
3.2.13 Agarose gel electrophoresis.....	45
3.2.14 Isolation of DNA fragments from agarose gel.....	45
3.2.15 Competent cells.....	45
3.2.16 Transfection of Mach1 T1 <sup>R</sup> competent cells .....	46
3.2.17 Sequencing .....	46
3.2.18 Mini-/ Maxi-preparation .....	46
3.2.19 Retroviral gene transduction .....	47
3.2.20 Apoptosis assay .....	48
3.2.21 Detection of cleaved Caspase-3, PARP1 and phosphorylated MLKL .....	48
3.2.22 IκB degradation .....	48
3.2.23 Surface expression staining of TNF-R1.....	49
3.2.24 Surface expression staining of TNF-R2.....	49
3.2.25 Internalization assay .....	49
3.2.26 Immunofluorescence .....	50
3.2.27 Sucrose density gradient ultracentrifugation .....	50
3.2.28 PTE activity assay.....	51
3.2.29 Generation of APT2 knockdown cells .....	51
3.2.30 Generation and purification of recombinant APT2 .....	51
3.2.31 rAPT2 activity assay.....	52
3.2.32 <i>In vitro</i> depalmitoylation of TNF-R1 by rAPT2 .....	53
3.2.33 Caspase-3 activity assay .....	53
3.2.34 Ceramide detection assay .....	53
<b>4. Results .....</b>	<b>54</b>
4.1 Palmitoylation of TNF-R1 .....	54
4.1.1 Inhibition of (de)-palmitoylation interferes with TNF-R1 internalization.....	54
4.1.2 Long term Fab <sub>TNF</sub> stimulation revealed a constitutively palmitoylation of TNF-R1 .....	55

## I. Table of contents

---

4.1.3	Generation of TNF-R1 knockout U937 cells .....	56
4.1.4	Determination of putative cysteines responsible for TNF-R1 palmitoylation ....	57
4.1.5	Expression of mutant TNF-R1 in TNF-R1 knockout U937 cells .....	58
4.1.6	AcylRAC of mutant receptor expressing cells revealed double or triple palmitoylation of TNF-R1 .....	60
4.1.7	Mutant receptor C248S reveals apoptosis rescue .....	61
4.1.8	Mutagenesis of putative cysteines affects NF- $\kappa$ B activation in U937 cells.....	62
4.1.9	Mutagenesis of cysteines alters surface expression but not the ability for internalization .....	63
4.1.10	Verification of TNF-R1 knockout HeLa80 cells .....	66
4.1.11	TNF-R1 palmitoylation also occurs in HeLa80.....	67
4.1.12	Expression of mutant TNF-R1 in TNF-R1 knockout HeLa80 cells.....	68
4.1.13	AcylRAC reveals triple palmitoylation of TNF-R1 .....	70
4.1.14	Mutagenesis of putative cysteines affects NF- $\kappa$ B activation in HeLa80 cells ...	71
4.2	Depalmitoylation of TNF-R1.....	73
4.2.1	Long term TNF stimulation reveals TNF-R1 depalmitoylation.....	73
4.2.2	Analysis of TNF-R1 palmitoylation in HeLa80 cells upon TNF stimulation .....	74
4.2.3	Detection of several putative Acyl-protein thioesterases .....	74
4.2.4	Acyl-protein thioesterase activity assay disclose APT2 activation upon TNF stimulation .....	76
4.2.5	Inhibition of APT2 blocks TNF-R1 depalmitoylation .....	77
4.2.6	Purification of active recombinant APT2 .....	78
4.2.7	Recombinant APT2 deplamitoylates TNF-R1 <i>in vitro</i> .....	79
4.2.8	Inhibition of APT2 alters TNF-R1 internalization and apoptosis induction.....	80
4.2.9	Inhibition of APT2 increases apoptosis induction.....	81
4.2.10	Blocking of TNF-R1 depalmitoylation triggers ceramide formation by nSMase .....	82
4.2.11	Lipid raft isolation revealed altered receptor localization and translocation ..	84
4.3	zDHC5 interferes with TNF-R1 signaling.....	86
4.3.1	Interaction of the protein acyltransferase 5 (zDHC5) with the TNF-receptor complex .....	86
4.3.2	Generation of zDHC5 knockout U937 cells.....	87
4.3.3	Characterization of zDHC5 knockout U937 cells regarding apoptosis and internalization of TNF-R1 .....	88

## I. Table of contents

---

4.3.4 Kinetic of zDHHC5 palmitoylation upon TNF stimulation .....	89
4.4 (De)-palmitoylation of TNF-R2 .....	90
4.4.1 Kinetic of TNF-R2 palmitoylation upon TNF stimulation .....	90
4.4.2 Generation of TNF-R2 knockout U937 cells .....	91
<b>5. Discussion .....</b>	<b>93</b>
5.1 Identification of TNF-R1 palmitoylation and its effect on subcellular localization and signaling .....	93
5.2 APT2 alters TNF-R1 distribution in the plasma membrane by receptor depalmitoylation.....	99
5.3 zDHHC5 promotes TNF-receptosome maturation in TNF-R1 signaling.....	102
5.4 TNF-R2 palmitoylation may contribute to TNF-receptor crosstalk .....	102
5.5 Model of TNF-R1 palmitoylation.....	104
<b>6. References.....</b>	<b>106</b>
<b>7. List of publication .....</b>	<b>121</b>
<b>8. Eidesstattliche Erklärung.....</b>	<b>122</b>
<b>9. Danksagung.....</b>	<b>123</b>
<b>10. Wissenschaftlicher Werdegang .....</b>	<b>124</b>

## II. Abbreviations

APT2	acyl protein thioesterase 2
aSMase	acid sphingomyelinase
Bcl2	B cell lymphoma protein 2
C/Cys	cysteine
Cas9	CRISPR-associated 9
Caspase	cysteine-aspartic protease
CD	cluster of differentiation
CHX	cycloheximide
ciAP	cellular inhibitor of apoptosis
CRISPR	clustered regulatory interspaced short palindromic repeats
Ctrl	control
DD	death domain
DHHC	aspartate-histidine-histidine-cysteine
DISC	death-inducing signaling complex
DNA	deoxyribonucleic acid
DR	death receptor
ER	endoplasmic reticulum
FADD	FAS-associated death domain
FCS	fetal calf serum
FLICE	FADD-like interleukin 1 $\beta$ -converting enzyme
FLIP	FLICE-like protease inhibitory protein
HRP	horseradish peroxidase
I $\kappa$ B	inhibitor of kabba B
MOMP	mitochondrial outer membrane permeabilization
NF- $\kappa$ B	nuclear factor kappa-light-chain-enhancer of activated B cells

## II. Abbreviations

---

nSMAse	neutral sphingomyelinase
PAGE	polyacrylamide gel electrophoresis
PARP1	poly (ADP-ribose)-polymerase 1
PAT	protein acyltransferase
PBS	phosphate buffered saline
PCD	programmed cell death
PPT	palmitoyl protein thioesterase
PTE	protein thioesterase
RIP1	receptor-interacting protein 1
RNA	ribonucleic acid
RT	room temperature
SD	standard deviation
SDS	sodium dodecyl sulfate
siRNA	small interfering RNA
TMD	transmembrane domain
TNF	tumor necrosis factor
TNF-R	tumor necrosis factor receptor
TRADD	TNFR-associated death-domain
TRAF2	TNFR-associated factor-2
WB	Western blot
WT	wild type
XIAP	X-linked inhibitor of apoptosis
zVAD	benzyloxycarbonyl-Val-Ala-Asp-fluoromethylketone

Commonly used abbreviations are not listed.



### III. List of Figures

- Figure 1: Schematic representation of the TNF superfamily belonging death receptors and their respective ligands
- Figure 2: Apoptosis signaling pathway of death receptor CD95 and TRAILR1
- Figure 3: Signaling pathway of TNF-R1
- Figure 4: Substrate palmitoylation by a protein acyltransferase PAT
- Figure 5: Substrate depalmitoylation by a protein acylthioesterase PTE
- Figure 6: Internalization of TNF-R1 in U937 cells pre-incubated with (de)-palmitoylation inhibitors
- Figure 7: AcylRAC of untreated U937 and Fab<sub>TNF</sub> treated U937 cells
- Figure 8: Generation of TNF-R1 knockout U937 cells
- Figure 9: Topology model of Tumor Necrosis Factor Receptor-1
- Figure 10: Western blot for TNF-R1 mutants in TNF-R1 knockout U937 cells
- Figure 11: Western blot of for TNF-R1 mutants in TNF-R1 knockout U937 cells
- Figure 12: AcylRAC of WT U937,  $\Delta$ TNF-R1 and mutant TNF-R1 expressing cells
- Figure 13: Apoptosis assay of mutant TNF-R1 expressing cells
- Figure 14: I $\kappa$ B $\alpha$  degradation of WT U937,  $\Delta$ TNF-R1 and mutated TNF-R1 expressing cells
- Figure 15: Surface expression of WT and mutant TNF-R1 in U937 cells
- Figure 16: Internalization of WT and mutant TNF-R1 in U937
- Figure 17: Verification of TNF-R1 deficiency in HeLa80 cells by Western blot and immunofluorescence
- Figure 18: AcylRAC of HeLa80 cells
- Figure 19: Western blot of mutant receptors in TNF-R1 knockout HeLa80 cells
- Figure 20: AcylRAC of WT HeLa80,  $\Delta$ TNF-R1 HeLa80 and mutant TNF-R1 expressing cells
- Figure 21: I $\kappa$ B $\alpha$  degradation of WT HeLa80,  $\Delta$ TNF-R1 HeLa80 and mutated TNF-R1 expressing cells
- Figure 22: AcylRAC of a TNF treated kinetic for different points of stimulation in U937 cells
- Figure 23: AcylRAC of HeLa80 cells pre-treated with cycloheximide (CHX)

### III. List of Figures

---

- Figure 24: Mass spectrometry data and immunoprecipitation via Fc60TNF of thioesterases APT1, APT2 and PPT1
- Figure 25: Thioesterase activity assay of U937 pre-incubated with fluorescent depalmitoylation probes
- Figure 26: AcylRAC of APT2 inhibited U937 cells
- Figure 27: Purification and activity of recombinant APT2
- Figure 28: AcylRAC of U937 cells pre-incubated with APT-2
- Figure 29: Internalization and apoptosis in U937 cells pre-treated with depalmitoylation inhibitors
- Figure 30: Analysis of apoptosis and necroptosis in ML349 treated U937 cells
- Figure 31: Ceramide formation and caspase-3 activation in response to TNF co incubated with ML349
- Figure 32: Plasma membrane fragmentation by sucrose density gradient ultracentrifugation in WT U937, C248S and shAPT2 U937 cells
- Figure 33: Mass spectrometry data and immunoprecipitation via Fc60TNF of protein acyltransferases zDHHC5 and zDHHC20
- Figure 34: Verification of the knockout of zDHHC5 in U937 cells by Western blot analysis and acylRAC
- Figure 35: Apoptosis and internalization of zDHHC5 knockout U937 cells
- Figure 36: Analysis of zDHHC5 palmitoylation in response to TNF stimulation
- Figure 37: AcylRAC of a TNF treated kinetic for different points of stimulation in U937 cells probing for TNF-R2
- Figure 38: Verification of the knockout of TNF-R2 in U937 cells by Western blot analysis acylRAC and surface expression
- Figure 39: Alignment of TNF-R1 amino acid sequence from different mammals
- Figure 40: Model of TNF-R1 palmitoylation

## **IV. List of Tables**

Table 1:	Cell culture solutions
Table 2:	Growth media for bacteria
Table 3:	Laboratory equipment
Table 4:	Chemicals
Table 5:	Reagents and utensils
Table 6:	Software used for documentation and analysis
Table 7:	Bacterial strain
Table 8:	Primary antibodies
Table 9:	Secondary antibodies
Table 10:	Kits
Table 11:	Oligonucleotides
Table 12:	CRISPR/Cas9 plasmids
Table 13:	TNF-R1 constructs

### 1.1 Summary

The cytokine Tumor Necrosis Factor (TNF) is a pleiotropic mediator responsible for multiple biological outcomes in the organism ranging from cell expansion, differentiation and regeneration to inflammation and cell destruction. The main receptor transducing the external signal into the cell is the Tumor Necrosis Factor Receptor-1 (TNF-R1). Ligand binding either causes cell survival or cell death. The decision between these diametrically opposed effects is regulated by multiple posttranslational modifications of TNF-R1. In this thesis, a yet unknown posttranslational modification of TNF-R1 was identified that regulates the outcome of receptor engagement by affecting its subcellular localization within biological membranes. Dynamic S-acylation controls the selective signaling of TNF, leading either to receptor retention in discrete plasma membrane microdomains promoting cell survival or to receptor internalization associated with increased cell death.

In the first part of the thesis, the constitutive palmitoylation of TNF-R1 was identified and respective palmitoylation sites were defined using TNF-R1-deficient U937 and HeLa80 cells generated by the CRISPR/Cas9 method. Mutational analyses of putative palmitoylation sites in reconstituted U937 and HeLa80 cells revealed that TNF-R1 is triple-palmitoylated at cysteines C223, C248 and C304. However, the mutation of palmitoylation site C248 already changed the signaling outcome of TNF-R1 regarding cell death induction or NF- $\kappa$ B activation. A C248S exchange resulted in an altered subcellular localization and reduced receptor expression on the cell surface.

In the second part, the protein thioesterase (PTE) APT2 was identified as the depalmitoylase for TNF-R1 after TNF stimulation. Pharmacological inhibition of APT2 altered the internalization and subcellular translocation of TNF-R1 and thus increased cell death induction and reduced NF- $\kappa$ B activation. Mechanistically, APT2 inhibition trapped TNF-R1 at the plasma membrane which resulted in an increase of apoptosis due to the production of ceramide mediated by the neutral sphingomyelinase (nSMase).

Third, palmitoylated proteins in TNF signaling were investigated. It turned out that the protein acyltransferase (PAT) zDHHC5 is involved in the intracellular maturation, transport and apoptosis-induction of TNF-receptosomes after receptor internalization. Interestingly, also TNF-R2, the second cellular receptor for TNF displays a palmitoylation upon TNF stimulation.

### 1.2 Zusammenfassung

Tumor-Nekrose-Faktor (TNF) ist ein pleiotropes, proinflammatorisches Zytokin, welches von Zellteilung und -regeneration bis hin zu Entzündungen und Zelltod zahlreiche biologische Prozesse im Organismus reguliert. Der Rezeptor, der Signalweiterleitung ins Zellinnere vermittelt, ist der Tumor-Nekrose-Faktor-Rezeptor-1 (TNF-R1), der je nach Komposition der Signalkomplexe entweder das Überleben der Zellen fördert oder deren Tod durch Apoptose einleitet. Die Entscheidung zwischen diesen beiden entgegengesetzten Effekten wird letztendlich bereits durch mehrere posttranslationale Modifikationen am Rezeptor reguliert.

In dieser Arbeit konnte erstmals eine posttranslationale Modifikation charakterisiert werden, die die TNF-R1-Signaltransduktion über die subzelluläre Lokalisation in der Plasmamembran reguliert. Eine dynamische S-Acylierung steuert dabei die von TNF ausgelösten Ereignisse in der Zelle. Über eine Retention des Rezeptors in speziellen Plasmamembran-Mikrodomänen wird das Überlebenssignal weitergeleitet. Wird der Rezeptor dagegen internalisiert, wird der Zelltod eingeleitet.

Im ersten Teil der Arbeit konnte die konstitutive Palmitoylierung von TNF-R1 mit den entsprechenden Palmitoylierungsstellen in mittels CRISPR/Cas9 Technologie erzeugten TNF-R1-defizienten U937- und HeLa80 Zellen nachgewiesen werden. Mutationsanalysen der mutmaßlichen Palmitoylierungsstellen in rekonstituierten U937- und HeLa80-Zellen ergaben, dass TNF-R1 an den Cysteinen C223, C248 und C304 dreifach palmitoyliert vorliegt. Eine C248S Mutation änderte die TNF-R1 induzierte Signaltransduktion hinsichtlich der Zelltodinduktion oder der NF- $\kappa$ B-Aktivierung. Mechanistisch änderte sich die subzelluläre Lokalisation des TNF-R1 einhergehend mit einer Verringerung der Rezeptordichte an der Zelloberfläche.

Im zweiten Teil konnte gezeigt werden, dass die Protein-Thioesterase (PTE) APT2 nach TNF-Stimulation die Depalmitoylierung von TNF-R1 katalysiert. Die Hemmung von APT2 veränderte die Rezeptor-Internalisierung und die subzelluläre Translokation und ebenfalls die TNF-R1-Signaltransduktion hinsichtlich Zelltodinduktion oder NF- $\kappa$ B-Aktivierung. Aktivierter TNF-R1 verbleibt bei Hemmung von APT2 an der Plasmamembran, was in diesem experimentellen Setting zu einer Zunahme der Apoptose führt. Mechanistisch katalysiert die TNF-induzierbare neutrale Sphingomyelinase (nSMase) die Produktion des pro-apoptotischen Neutrallipids Ceramid an der Zellmembran.

## 1.2 Zusammenfassung

---

Außerdem wurden weitere palmitoylierte Proteine in der TNF-Signalkaskade identifiziert. So ist die Protein-Acyltransferase (PAT) zDHH5 nach Rezeptor-Internalisierung an der intrazellulären Reifung, dem Transport von TNF-Rezeptosomen und der Apoptose-Induktion nach Rezeptor-Internalisierung beteiligt. Darüber hinaus konnte auch für TNF-R2, dem zweiten Rezeptor für TNF, eine Palmitoylierung nach TNF-Stimulation nachgewiesen werden.

## **2. Introduction**

### **2.1 Programmed cell death**

In 1990 researchers began to understand that cell death does not only happen after an overwhelming damage and is not just an accidental part of life. Cell death is rather a highly controlled, energy-dependent, active process, afterwards termed as programmed cell death (PCD) [Lockshin and Zakeri, 2001]. PCD is one key driver in cellular development and homeostasis of multicellular organisms as well as in the elimination of potential harmful cells and in immune defense reactions [Green and Llambi, 2015].

Nowadays, programmed cell death is subdivided into two classes: the caspase-dependent and the caspase-independent PCD. Caspase-independent PCD comprises autophagy and regulated necrosis which have been discovered and characterized as PCD only in the last decade [Degterev et al., 2005; Gump and Thorburn, 2011].

### **2.2 Caspase dependent programmed cell death - apoptosis**

The best known and characterized form of PCD is the caspase-dependent cell death termed apoptosis, which was first described morphologically by Lockshin and Williams in 1964, working on intersegmental muscles of silkworms [Lockshin and Williams, 1964]. However, the term apoptosis, deriving from the ancient Greek word for “falling off”, was then coined by Kerr and colleagues in 1972 [Kerr et al., 1972]. Apoptosis is hallmarked by various morphological as well as biochemical changes such as cell shrinkage, chromatin condensation (pyknosis), nuclear fragmentation (karyorrhexis), dynamic plasma membrane blebbing, loss of adhesion to neighbor cells and/or to extracellular matrix, exposure of phosphatidylserine to the outer membrane leaflet and debris clearance by phagocytes and neighboring cells [Elmore 2007; Doherty and Baehrecke, 2018]. Apoptosis can be assigned into two main pathways triggered by different stimuli: the mitochondrial or intrinsic pathway and the death receptor or extrinsic pathway, both of which are linked and influence each other [Igney and Krammer, 2002].

The intrinsic or mitochondrial pathway is initiated when cells are damaged beyond their ability to self-repair caused by a plethora of stimuli such as the withdrawal of growth factors, hormones or cytokines, ER stress, DNA damage and free radicals as well as environmental influences as radiation, toxins, hypoxia, hyperthermia and viral infections [Elmore, 2007; Green and Llambi, 2015].

## 2. Introduction

---

Such stimuli lead to the activation of the protein family Bcl2 (B cell lymphoma protein 2) which serve as a main signaling node in the decision of life and death, governing the mitochondrial membrane permeability [Yang et al., 1995]. To date, 25 Bcl2 proteins have been identified, sharing one or more Bcl2 homology (BH) regions, defined by sequence, structure and function [Derfuss et al., 1998]. Three main classes compete for the control, regulation and opening of the mitochondrial permeability transition pore. Pro-apoptotic Bcl2 proteins such as Bax (Bcl2 associated X protein) and Bak (Bcl2 antagonist or killer) are necessary for the pore formation, which can be blocked by anti-apoptotic Bcl2 proteins such as Bcl2, Bclx or BclXL (B cell lymphoma extra-large), whereby BH3-only proteins such as Bid (BH3-interacting domain death agonist), Bim and Noxa either activate the pro-apoptotic and/or neutralize the anti-apoptotic Bcl2 proteins [Kvansakul and Hinds, 2013].

As soon as pro-apoptotic Bcl2s predominates, transition pores are formed, forcing the mitochondrial outer membrane permeabilization (MOMP), resulting in the release of sequestered pro-apoptotic proteins such as cytochrome c, Smac (Second mitochondria-derived activator of caspases)/Diablo (Direct IAP-binding protein with low PI) and HtrA2 (High temperature requirement protein A2)/Omi from the intermembrane space into the cytoplasm [Saelens et al., 2004; Garrido et al., 2006]. Once in the cytosol, cytochrome c interacts with APAF1 (apoptotic protease-activating factor 1) assembling and activating the apoptosome which enables another main player of apoptosis to interact with the apoptosome and thus auto-activate, pro-caspase-9, triggering the execution phase of apoptosis [Hill et al., 2004; Yuan and Kroemer, 2010].

Caspases are **cysteine-aspartic proteases**, orchestrating the morphological changes that characterize apoptosis and are widely expressed as inactive proenzymes. Once activated, a proteolytic caspase cascade is initiated activating other caspases which amplifies apoptotic signaling, resulting in a rapid death. 17 different caspases are known in mammals which cleave proteins at their aspartic acid residues with diverse specificities due to neighboring amino acids at the recognition site [Cohen, 1997; Green and Llambi, 2015]. Based on their function, human caspases are subdivided into three subgroups: initiator caspases (caspase-2, caspase-8, caspase-9, caspase-10), effector caspases (caspase-3, caspase-6, caspase-7) and inflammatory caspases (caspase-1, caspase-4, caspase-5) [Rai et al., 2005].



## 2. Introduction

---

Upon release into the cytoplasm, Smac/Diablo and HtrA2/Omi serve as antagonists of XIAP (X-linked inhibitor of apoptosis) by hindering the inhibition of caspase-9, caspase-3 and caspase-7 through XIAP interaction and thus potentiating the apoptosome activity [Eckelman et al., 2006].

The extrinsic or death receptor pathway is characterized by activation of death receptors. These death receptors belong to the tumor necrosis factor (TNF) receptor family which is a subgroup of the TNF superfamily of cytokines comprising 19 ligands and 29 receptors [Aggarwal, 2003; Schütze et al., 2008]. Death receptors such as TNF-R1 (TNF receptor 1), CD95 (FasR (first apoptosis signal receptor) or Apo-1 (apoptosis antigen 1)), TRAILR1 (TNF-related apoptosis inducing ligand receptor 1), also termed DR4, TRAILR2 (TNF-related apoptosis inducing ligand receptor 2), also termed DR5, as well as DR3 and DR6 share a cysteine-rich extracellular domain and a conserved 80 amino acid sequence at their cytoplasmic tail, the death domain (DD) (Figure 1). This DD enables the relay of the extracellular stimulus by ligand-triggered receptor activation to the intracellular signaling pathway [Ashkenazi and Dixit, 1998]. In most death receptors such as CD95 and TRAILRs, ligand binding with concomitant receptor clustering allows the recruitment of the adaptor protein FADD (FAS-associated death domain protein) to the receptor via DD-DD interaction. This leads to the assembly of the caspase activation platform DISC (death-inducing signaling complex) by association of FADD and pro-caspase-8 via their DEDs (death effector domain). After DISC formation, caspase-8 undergoes autocatalytic cleavage resulting in the initiation of the execution phase of apoptosis [Wajant, 2002; Rubio-Moscardo et al., 2005].

## 2. Introduction

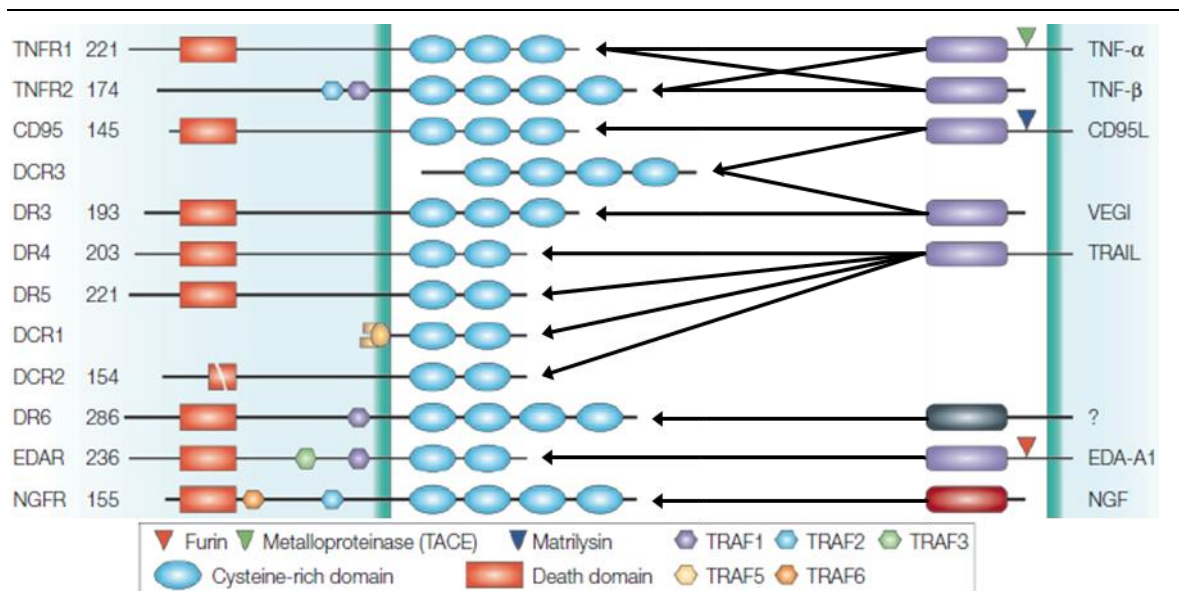


**Figure 1: Schematic representation of the TNF superfamily belonging death receptors and their respective ligands.** Death receptors are type I transmembrane proteins. Today, eight different death receptors have been identified, death receptor 1 (DR1, TNF-R1), DR2 (CD95), DR3, DR4 (TRAILR1), DR5 (TRAILR2), DR6, EDAR (ectodysplasin A receptor) and NGFR (nerve growth factor receptor). DCR1 (Decoy receptor 1) is anchored by a covalently linked C-terminal glycolipid. DCR3 (Decoy receptor 3) lacks transmembrane domain and is secreted as soluble protein. All ligands are type II transmembrane proteins with a carboxy-terminal extracellular domain, an amino-terminal intracellular domain and a single transmembrane domain, except for lymphotoxin- $\alpha$  (TNF- $\beta$ ) and vascular endothelial cell growth inhibitor (VEGI) which are secreted. The C-terminal extracellular domain, known as the tumor-necrosis factor (TNF) homology domain (purple domain), has 20 – 30 % amino acid identity between the superfamily members and is responsible for binding to the receptor. Most members of the TNF superfamily are released from the cell surface by proteolysis by distinct proteases. TNF is released by the metalloprotease TACE (tumor necrosis factor alpha convertase), CD95L by matrilysin and EDA-A1 (ectodysplasin A1) by a member of the furin family. The numbers on the left represent the number of amino acids in the cytoplasmic domain of the receptors. TRAF, TNFR-associated factor; TNF- $\alpha$ , tumor necrosis factor  $\alpha$ ; CD95L, CD95 ligand; TRAIL, tumor necrosis factor receptor related apoptosis inducing ligand; NGF, nerve growth factor (**adopted and modified from Aggarwal, 2003**).

Both pathways culminate in the execution phase, the final pathway of apoptosis. This phase is initiated by the proteolytic cleavage of effector caspases mainly caspase-3 and caspase-7 mediated by the activated initiator caspases caspase-9 and caspase-8 defining the outcome of the initial stimuli [Figure 2; Green and Llambi, 2015]. The activation of the execution caspases leads to the processing and cleavage of at least 1000 proteins resulting in either a gain or a loss of function of the proteins. In addition to the activation of endonucleases and proteases which degrade nuclear material and cytoskeletal and nuclear proteins, cytokeratins, PARP1 (Poly(ADP-ribose)-polymerase 1), p75 subunit of complex I of the respiratory chain, CAD (caspase-activated deoxyribonuclease), gelsolin and ROCK I (Rho-associated coiled-coil protein kinase 1) to name just a few are also directly processed by the execution caspases, leading ultimately to the dismantling of the cell [Elmore, 2007; Crawford and Wells, 2011; Green and Llambi, 2015; Ricci et al., 2004; Enari et al., 1998; Kothakota et al., 1997; Coleman et al., 2001].

## 2. Introduction

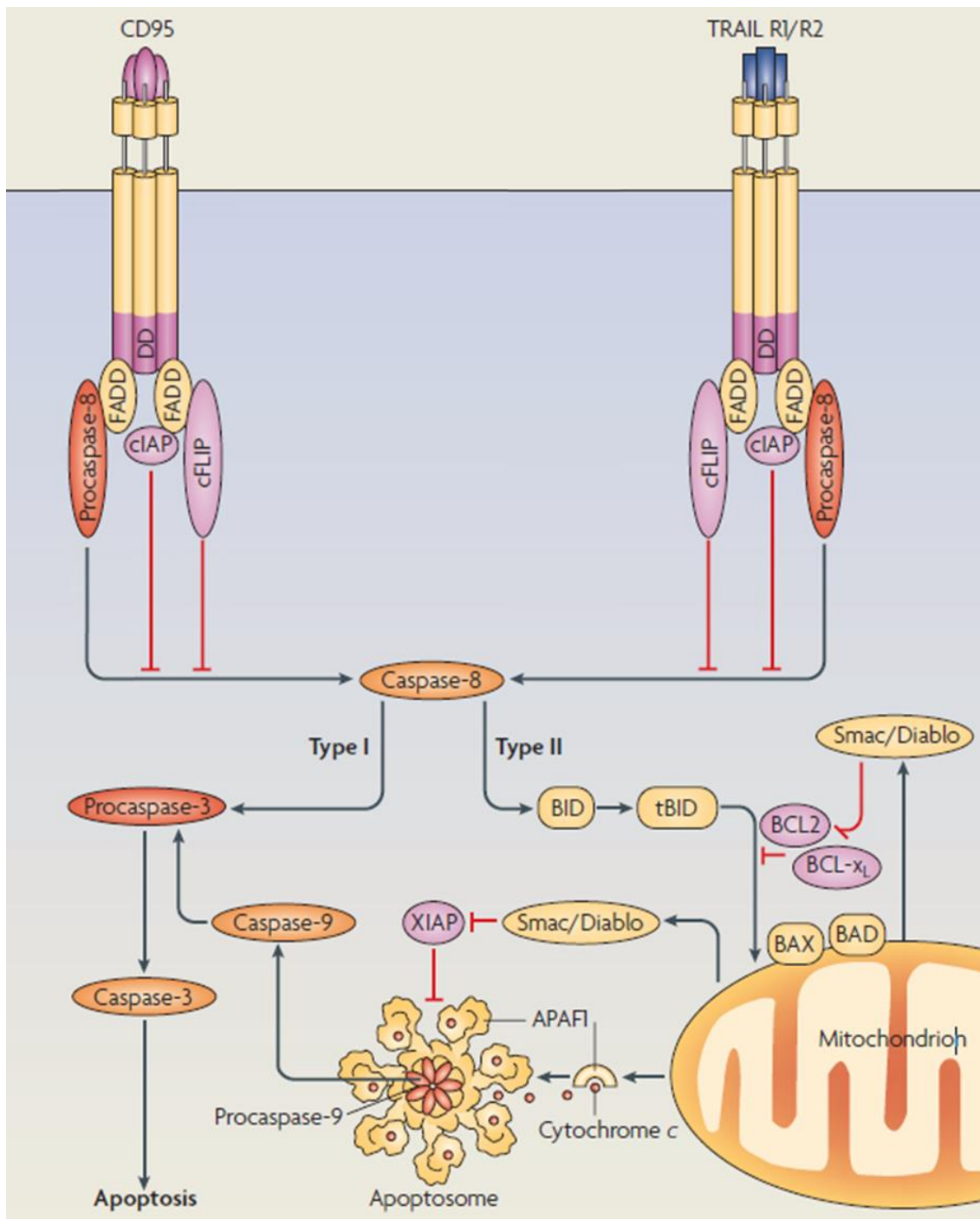


**Figure 2: Apoptosis signaling pathway of death receptor CD95 and TRAILR1/2.** Upon ligand binding, pre-assembled CD95 and TRAILR1/2 (TNF-related apoptosis inducing ligand receptor 1/2) trimerize, enabling the recruitment of the adaptor proteins FADD (FAS-associated death domain protein) and procaspase-8 to the receptors via DD (death domain) interactions forming the DISC (death inducing signaling complex). In case of high amounts of auto-activated caspase-8 mediated by dimerization, apoptosis is directly initiated by procaspase-3 cleavage (type I pathway, triggered in type I cells). In type II cells, low amounts of caspase-8 require activation of a mitochondrial amplification loop resulting in the truncation of the Bcl2 (B cell lymphoma protein-2) family protein BID (BH3-interacting domain death agonist) to tBID which translocates into the outer mitochondrial membrane, promoting MOMP (mitochondrial outer membrane permeabilization) by the pro-apoptotic Bcl2 proteins Bax and Bad. As a result, pro-apoptotic proteins such as cytochrome c, APAF1 (apoptotic protease activating factor-1) and Smac/Diablo are released from the mitochondrial intermembrane space into the cytoplasm, forming the apoptosome composed of cytochrome c, APAF1 and procaspase-9. Auto-activated caspase-9 subsequently triggers the activation of caspase-3 by proteolysis, resulting in apoptosis. These pathways can be blocked by anti-apoptotic proteins such as FLIP

## 2. Introduction

---

(FADD-like interleukin 1 $\beta$ -converting enzyme-like protease inhibitory protein) and cIAP (cellular inhibitor of apoptosis protein) preventing either the FADD recruitment or caspase-8 activation. At the intrinsic level, anti-apoptotic Bcl2 proteins such as Bcl2 and BclxL inhibit the Bid mediated formation of the transition pore by blocking Bax and Bad. The inhibitory protein XIAP (X-linked inhibitor of apoptosis) blocks apoptosis by preventing caspase-9 activation. As a counterpart, the mitochondrial proteins Smac/Diablo neutralize the inhibitory effect of XIAPs, guaranteeing caspase activation (**adopted and modified from Schütze et al., 2008**).

### 2.3 The biology of TNF

In 1975 the description of a soluble cytokine causing lysis of tumor cells in mouse models led to the identification of the then so called tumor necrosis factor (TNF) [Carswell et al., 1975]. TNF is mainly produced by cells of the immune system such as macrophages and lymphocytes but also in a broad variety of other cells such as fibroblasts, mast cells and endothelial cells. However, the hope of having found a tumor killing cytokine was destroyed when following *in vivo* studies revealed strong pro-inflammatory and immunostimulatory activities of TNF, mediating the progression of many diseases such as autoimmune diseases e.g. rheumatoid arthritis, inflammatory bowel disease and psoriasis; cardiovascular diseases like atherosclerosis and also pulmonary disease as asthma. Nowadays, TNF is known as a highly pleiotropic cytokine acting like a two-edged sword, mediating regeneration and expansion as well as destruction in tissues [Locksley et al., 2001; Wajant et al., 2003; Aggarwal et al., 2012].

The signal transducers responsible for the variety of the aforementioned biological outcome were discovered ten years later in 1985 and named as tumor necrosis factor receptor 1 and 2 (TNF-R1/2) [Aggarwal et al., 2012]. Both receptors share four cysteine-rich repeats in their extracellular domain, enabling the formation of receptor homotrimers by hemophilic interactions of the pre-ligand assembly domain in the absence of TNF. TNF-R1 became the prototypic representative of the 23 members comprising TNF-receptor superfamily including the death receptors mentioned above. Although TNF-R2 belongs to the TNF-receptor superfamily, it does not represent the death receptors due to the inability of transducing apoptosis by lacking the DD.

The reason of the huge variety of cellular processes induced by TNF such as inflammation, differentiation, control of proliferation and cell death in cells and tissues relies on the ability of TNF-R1 to induce a diametrical opposed downstream signaling which is characteristic for the family of TNF-Rs [Peter et al., 2007; Falschlehner et al., 2007; Muppidi et al., 2004].

### 2.4 Tumor necrosis factor receptor 1 signaling

After the binding of TNF to pre-formed receptor homotrimers, a struggle for the dominance of both main signal pathways begins which results in the activation of either NF- $\kappa$ B (Nuclear factor kappa-light-chain-enhancer of activated B cells) causing inflammation and survival, or effector caspases leading to apoptosis. The cell's fate is thereby determined by the selective binding of specific adaptor proteins to TNF-R1.

TNF induced TNF-R1 clustering enables the adaptor protein TRADD (TNF-R-associated death domain) to recruit to the receptor via DD interactions. TRADD itself acts with its DD as a membrane-bound scaffold, recruiting additional adaptor proteins such as RIP1 (receptor-interacting protein 1), TRAF2 (TNF R-associated factor-2) and cIAP1/2 (cellular inhibitor of apoptosis protein 1/2) forming the signaling complex I which triggers the NF- $\kappa$ B pathway [Figure 3; Micheau and Tschopp, 2003; Schütze et al., 2008; Fritsch et al., 2014; Green and Lambi, 2015].

This pathway is initiated by the TRAF2 and cIAP1/2 mediated K11 or K63 ubiquitination of RIP1 which serves as a scaffold platform for downstream proteins like LUBAC (linear ubiquitin chain assembly complex), TAK1 (transforming growth factor (TGF)- $\beta$ -activated kinase 1) and NEMO (NF- $\kappa$ B essential modulator). NEMO itself belongs to the IKK signalosome (inhibitor of I $\kappa$ B kinase) comprising additionally to NEMO (also known as IKK $\gamma$ ) also IKK $\alpha$  and IKK $\beta$ . This complex is activated by the LUBAC mediated ubiquitination of NEMO, resulting in conformational changes of the IKK signalosome which bring IKK $\alpha$  and IKK $\beta$  into more susceptible positions for phosphorylation by TAK1 or *trans*-auto-phosphorylation. This phosphorylation leads to the kinase activity of the IKK signalosome which phosphorylates the I $\kappa$ B (Inhibitor of kappa B) protein. I $\kappa$ B normally binds to NF- $\kappa$ B in the cytosol, hindering NF- $\kappa$ B to translocate into the nucleus by masking its nuclear localization sequence. This phosphorylation of I $\kappa$ B results in its K48 ubiquitination, leading to the proteasomal degradation and the release and activation of NF- $\kappa$ B. NF- $\kappa$ B thereafter translocate into the nucleus and enhances the transcription of several gene such as for cytokines, chemokines, other transcriptions factors and anti-apoptotic regulators such as Bax, BclXL, Bcl2, Bim, FLIPs (FADD-like interleukin 1 $\beta$ -converting enzyme-like protease inhibitory protein), cIAPs and XIAPs, representing a negative feedback loop by hampering apoptosis induction [Wajant and Scheurich, 2011; Ting and Bertrand, 2016; Napetschnig and Wu, 2013; Fritsch et al., 2014; Zhang et al., 2017].

On the other hand, TNF mediated activation of plasma membrane resident TNF-R1 results in the rapid recruitment of the E3-ubiquitin ligase RNF8 to TNF-R1, leading to its K63

## 2. Introduction

---

ubiquitination which initiates receptor internalization by clathrin-coated pit-mediated endocytosis. To the internalized TNF-R1 vesicles, also known as receptosomes, another E3 ligase CARP2 (caspase-8 and -10-associated RING protein-2) is recruited, promoting the termination of NF- $\kappa$ B activation by K48 ubiquitination of RIP1, leading to the dissociation of complex I proteins RIP1 and TRAF2 [Liao et al., 2008; Liao et al., 2009; Fritsch et al., 2014]. In its place complex II is assembled by the recruitment of FADD and caspase-8, forming the DISC. This step is also regulated by another anti-apoptotic protein FLIP which is upregulated by NF- $\kappa$ B mediated gene activation and represents a caspase-8 homolog, lacking the catalytic activity but blocks the recruitment of caspase-8 to FADD [Scaffidi et al., 1999]. Early receptosomes traffic and fuse along the endocytic pathway with other endosomes and trans-Golgi vesicles, containing pro-aSMase (endolysosomal acid sphingomyelinase) and pro-CTSD (cathepsin D), forming multivesicular bodies. In such late endosomes, caspase-8 mediates caspase-7 activation, resulting in aSMase maturation and generation of ceramide, a potent pro-apoptotic mediator in death receptor signaling [Dumitru and Gulbins, 2006; Thon et al., 2006]. Ceramide activates CTSD which cleaves Bid to tBid (truncated Bid), connecting the extrinsic pathway with the intrinsic pathway of apoptosis. tBid translocates then to the outer mitochondrial membrane and promotes MOMP, which activates effector caspases such as caspase-9 and caspase-3 resulting in apoptosis [Figure 3; Heinrich et al., 2004; Schütze et al., 2008].

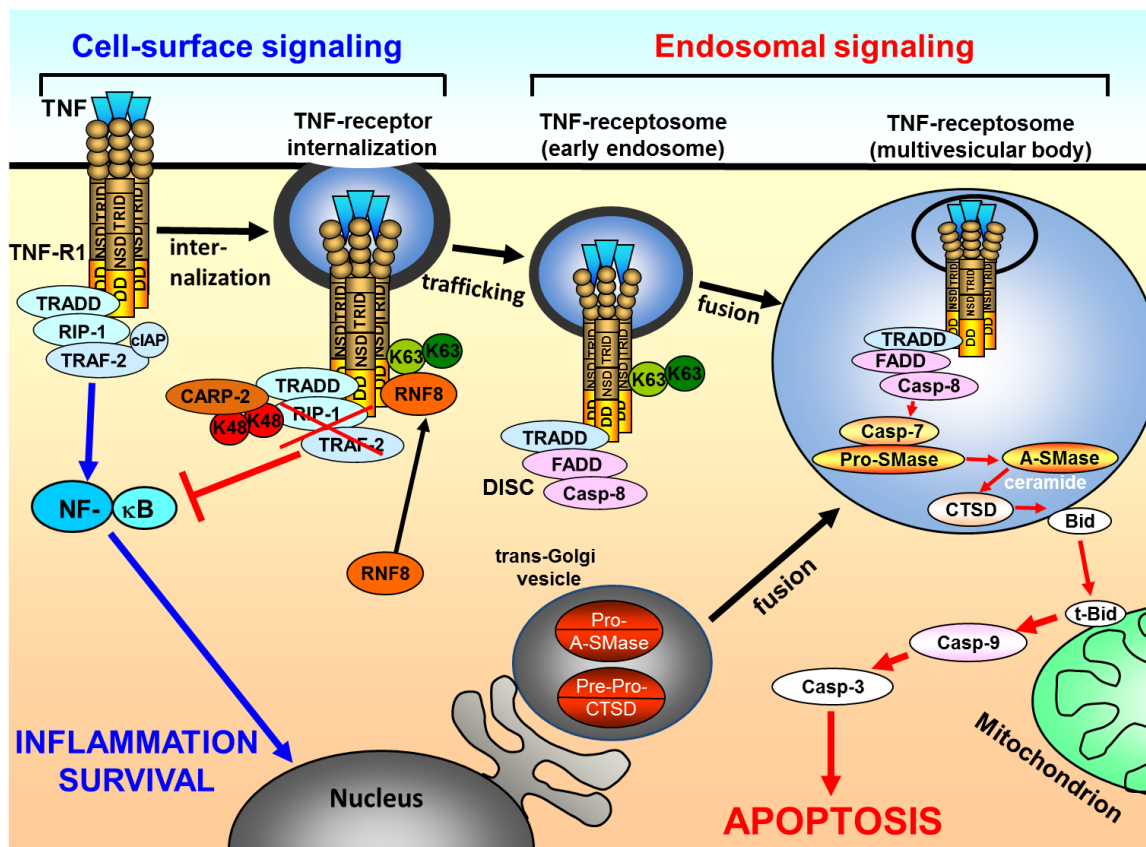


**Figure 3: Signaling pathway of TNF-R1.** After ligand binding, pre-assembled TNF-R1 (tumor necrosis factor receptor 1) trimerize enabling the assembly of the signaling complex I at the cell surface composed of TRADD (TNF-R-associated death-domain), RIP1 (receptor-interacting protein 1), TRAF2 (TNF-R-associated factor-2) and cIAP (cellular inhibitor of apoptosis protein). This complex triggers then the activation of the NF-κB (Nuclear factor kappa-light-chain-enhancer of activated B cells) pathway, resulting in inflammation and survival signals. On the other hand, K63 ubiquitination of TNF-R1 by the E3-ubiquitin ligase RNF8 leads to the internalization of complex I. After K48 ubiquitination of RIP1 catalyzed by CARP2 (caspase-8 and -10-associated RING protein-2), complex I proteins RIP1 and TRAF2 dissociate from TNF-R1, terminating the NF-κB pathway. In its place, complex II or DISC (death inducing signaling complex) is formed by the recruitment of FADD (FAS-associated death domain protein) and caspase-8 to TRADD via DD (death domain) interactions. After the fusion with other endosomes and trans-Golgi vesicles, the multivesicular body is formed where caspase-8 activates caspase-7, leading to the production of ceramide by cleaved aSMase (acid sphingomyelinase). Ceramide triggers the activation of CTSD (cathepsin D) which cleaves Bid (BH3-interacting domain death agonist) to truncated (t)Bid. tBid then translocates to the mitochondrion and promotes MOMP (mitochondrial outer membrane permeabilization) leading to the activation of the effector caspases-9 and -3, resulting in apoptosis. TRID (TNF-R internalization domain); NSD (neutral sphingomyelinase domain); (adopted and modified from Fritsch et al., 2017).

## 2.5 Post translational modification of TNF-R1 - palmitoylation

This highly complex and ingenious TNF-R1 signaling needs a tight regulation to enable the correct context-dependent cell fate decision for either inflammation and survival or cell death. Previous studies revealed that TNF-R1 itself is modified by multiple posttranslational modifications such as glycosylation, phosphorylation and ubiquitination, all influencing the apoptotic signaling of the receptor itself by changing either the affinity of ligand-receptor binding, subcellular localization or receptor internalization [Han et al.,

## 2. Introduction

---

2015; Holdbrooks et al., 2018; Corti et al., 1995; Richter et al., 2012; Van Linden et al., 2005; Cottin et al., 1999; Schütze et al., 2008; Fritsch et al., 2014].

Over the last 15 years, the generally known but hitherto difficult to study posttranslational modification of S-acylation has come into the focus of research due to more sensitive detection methods as well as the discovery of the respective enzymes catalyzing this reaction [Mitchell et al., 2006; Chamberlain and Shipston, 2015]. S-acylation, exclusively occurring posttranslational, is characterized by the attachment of mainly palmitic acid onto the thiol group of a cysteine residue forming a labile thioester linkage. Nearly three-quarters ( $\approx 74\%$ ) of S-acylated proteins were modified by palmitate while stearate (22 %) and oleate (4 %) are less common. Thus S-acylation is frequently referred to as palmitoylation [Muszbek et al., 1999]. S-acylation, once discovered in cultured cells in 1980, seems to be highly conserved since it occurs in all eukaryotic organisms from yeast to humans. Until today, it is suggested that more than 10 % of the human proteome consists of S-acylated proteins [Schlesinger et al., 1980; Roth et al., 2006; Mitchell et al., 2006; Greaves and Chamberlain, 2011; Blanc et al., 2015]. In contrast to other lipidations such as myristoylation and farnesylation where stable amide or thioether linkages are formed, S-acylation is fully reversible and thus, dynamic. This suggests its high potential for regulation and coordination of cytoplasmic and membrane bound proteins, enabling rapid cycles of de- and palmitoylation. The addition of lipids onto amino acid residues increases the proteins hydrophobicity, impacting several characteristics such as protein structure, assembly, maturation, trafficking, intracellular localization and modulate the affinity of proteins to cellular membranes or subdomains and other proteins. [Greaves and Chamberlain, 2007; Salaun et al., 2010; Linder and Deschenes, 2007; Greaves and Chamberlain, 2014; Chamberlain and Shipston, 2015].

The attachment of the palmitate onto the cysteine residue is catalyzed by the polytopic membrane protein family of protein acyltransferases (PATs). 23 different PATs have been identified in mammals which possess four to six transmembrane domains (TMD) spanning alternating through the biological membrane. The characteristic and highly conserved active site of the Asp-His-His-Cys (DHHC) tetrapeptide motif is located within a cysteine rich domain of a protein loop between two TMDs facing the cytoplasmic membrane leaflet. The cysteine residue in the active site is critical for the palmitate transfer onto the target substrate which is realized by a “ping-pong” mechanism. DHHCs are expressed ubiquitously in cell tissues localizing in intracellular membranes of the Golgi and the



## 2. Introduction

endoplasmic reticulum (ER) as well as a few at the plasma membrane [Figure 4; Jennings and Linder, 2012; Mitchell et al., 2010; Greaves and Chamberlain, 2011; Resh, 2016].

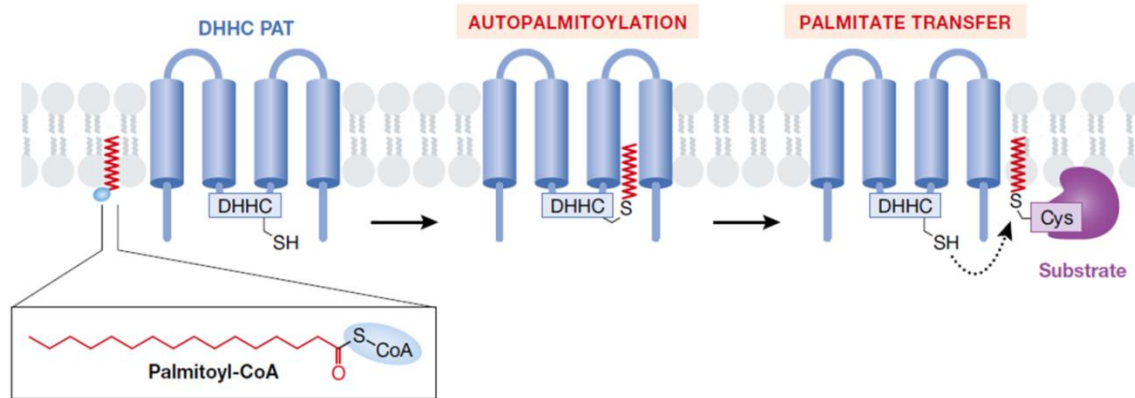


**Figure 4: Substrate palmitoylation by a protein acyltransferase PAT.** Protein acyltransferases (blue), spanning the biological membrane with their transmembrane domains four to six times, catalyze the transfer of an acetyl-CoA activated palmitate to a free thiol group (-SH) of a cysteine residue of a substrate protein by a “ping-pong” mechanism. First the PAT is autopalmitoylated at the catalytic cysteine in the DHHC tetrapeptide motif, releasing free coenzyme A (CoA) into the cytosol. Afterwards, the palmitate group is transferred to the acceptor cysteine residue of the substrate protein (purple) (**adopted and modified from Ko and Dixon, 2018**).

The detachment of fatty acids from target proteins is catalyzed by protein thioesterases (PTE) in a hydrolysis reaction releasing the fatty acids into the cytosol. The small but still growing group of known PTEs belongs to the serine hydrolase superfamily consisting of APT1 and 2 (acyl protein thioesterase 1 and 2), PPT1 and 2 (palmitoyl protein thioesterase 1 and 2), APT1-like thioesterase and the ABDH17 ( $\alpha\beta$  hydrolase-domain) family comprising ABDH17 A, B, C [Figure 5; Kong et al., 2013; Vartak et al., 2014].

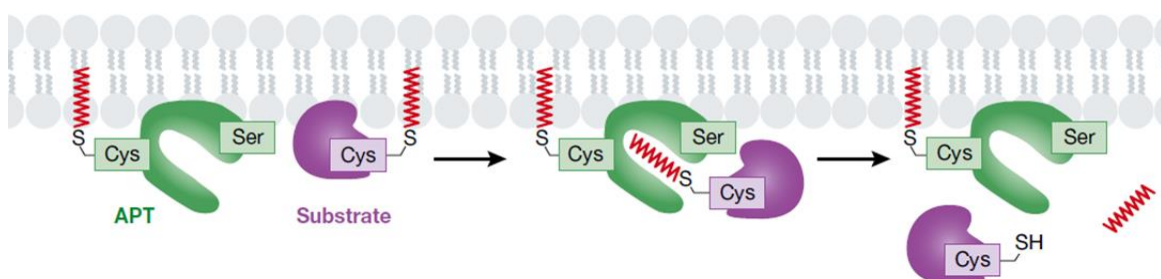


**Figure 5: Substrate depalmitoylation by a protein acylthioesterase PTE.** Acylprotein thioesterase (APT, green) is one group member of the family of protein acylthioesterases (PTE) which belong to the serine hydrolases and catalyze the removal of palmitate groups from palmitoylated proteins (purple) by a hydrolysis reaction. The removed palmitate is released into the cytoplasm. APTs itself are also described as palmitoylated which localize them to their specific membranes (**adopted and modified from Ko and Dixon, 2018**).

## 2. Introduction

---

As mentioned above, S-acylation of proteins affects diverse biological processes and the palmitoylation and depalmitoylation cycle of proteins depends on the proper function of PATs and PTEs. Previous studies revealed that mainly the activity of both S-acylation enzyme groups are crucial for the appropriate physiological function of cell tissues wherefore a disturbance links them to a diverse range of diseases such as schizophrenia, Huntington's disease, type 1 diabetes and also cancer like bladder cancer, lung cancer, colorectal cancer and to gastric adenocarcinoma [Greaves and Chamberlain, 2014; Chamberlain and Shipston, 2015; Young et al., 2012; Yamamoto et al., 2007; Kang et al., 2008; Yan et al., 2013; Oyama et al., 2000].

Due to the attachment of a saturated fatty acid, associated with an increased hydrophobicity of the protein, S-acylation is suggested as an important signal for the sequestration and lateral distribution of receptor proteins from lipid raft microdomains. First described in 1973, and despite persistent discussions and doubts, lipid rafts are nowadays characterized by a variety of scientists as a heterogeneous, ordered, detergent resistant, temporal and spatial compartmentalization of subdomains in the biological membrane [Yu et al., 1973]. This specific microdomain is enriched in cholesterol, saturated lipids, glycosylated lipids, sphingomyelin and sphingolipids which are tightly packed forming dynamic clusters of 10 to 200 nm upon protein-protein and/or protein-lipid interaction [Pike, 2006; Wang et al., 2003; Resh, 2016; Sezgin et al., 2017]. After clustering, lipid rafts are suggested to be functional platforms regulating cellular processes such as signaling and membrane trafficking of receptors and other membrane resident proteins [Brown and London, 1998; Lingwood and Simons, 2010]. Since the direct detection via microscopy is still not feasible due to the diffraction limit, the existence of lipid rafts is still a subject of debate [Klotzsch and Schütz, 2013]. However, 35 % of all plasma membrane bound proteins have been reported to be localized in ordered domains where one third is anchored by palmitoylation, another third is represented by GPI (Glycosylphosphatidylinositol)-anchored proteins and for the last third the association mechanism is still unclear [Levental et al., 2010; Sezgin et al., 2017].

### **2.6 Aims of the dissertation**

Preliminary data of the Schütze group suggested an involvement of S-acylation in the signaling of TNF-R1, affecting its biological outcome. The death receptors CD95, TRAILR1 and DR6 have been reported as being constitutively palmitoylated, triggering the rearrangement of their subcellular localization [Feig et al., 2007; Rossin et al., 2009; Klíma et al., 2009].

The primary aim of the presented dissertation was to investigate how the posttranslational modification of S-acylation contributes to the regulation of TNF-R1 signaling. To this, the following issues will be addressed: First, it will be clarified whether the palmitoylation of TNF-R1 is constitutive or inducible in response to TNF stimulation. Second, the palmitoylation sites within the TNF-R1 will be determined by mutagenesis analysis. Third, the enzymes responsible for (de)-palmitoylation such as PATs and PTEs will be identified by immunoprecipitation and knockout experiments, using the CRISPR/Cas9 technology. Furthermore, the impact of the receptor mutations and deletions as well as the knockouts of the enzymes involved in the subcellular localization of TNF-R1, on the trafficking and maturation of TNF-receptosomes as well as the differential TNF-induced signaling pathways, leading either to cell survival or cell death, will be analyzed. For this, sucrose density ultracentrifugation, Western blot analysis, nuclear fragmentation, surface staining and enzyme inhibition assays will be performed.

Additionally, intensive crosstalk between TNF-R1 and its close relative TNF-R2 has been described before, affecting the signaling outcome of both receptors respectively [Grell et al., 1998; Fotin-Mleczek et al., 2002]. Since palmitoylation also influences the relocation of transmembrane proteins within the plasma membrane and thus delivers different proteins into close proximity, also TNF-R2 S-acylation will be further analyzed. For that, it will be examined whether TNF-R2 is palmitoylated or not by the acylRAC assay. Finally, TNF-R2 will be knocked out by CRISPR/Cas9 for future palmitoylation, signaling and crosstalk experiments.

### 3. Materials and Methods

The following chapter describes the materials used, instruments, reagents and chemicals as well as the used methods in more detail. For all buffers and solutions, high purified, sterile Milli-Q water ( $R = 18.2 \text{ M}\Omega\cdot\text{cm}$ ) was utilized.

#### 3.1 Materials

**Table 1: Cell culture solutions**

Media	Company	Cat.-No
Dulbecco's Modified Eagle Medium (DMEM)	Gibco <sup>®</sup> , life technologies™	42430025
Fetal Calf Serum (FCS)	Gibco <sup>®</sup> , life technologies™	10270106
FreeStyle <sup>®</sup>	Gibco <sup>®</sup> , life technologies™	12338018
Opti-MEM	Gibco <sup>®</sup> , life technologies™	31985062
Penicillin/Streptomycin (Pen/Strep)	Merck Millipore	A2212
RPMI 1640	Gibco <sup>®</sup> , life technologies™	52400025

**Table 2: Growth media for bacteria**

Media	Composition
LB (Lysogeny Broth) medium	1 % (w/v) tryptone, 0.5 % (w/v) yeast extract, 1 % (w/v) NaCl, pH 7.0
LB agar	1 % (w/v) tryptone, 0.5 % (w/v) yeast extract, 1 % (w/v) NaCl, 1.5 % (w/v) agar, pH 7.0
SOB (Super Optimal Broth) medium	2 % (w/v) tryptone, 0.5 % (w/v) yeast extract, 10 mM NaCl, 2.5 mM KCl, 10 mM MgCl <sub>2</sub> , 10 mM MgSO <sub>4</sub> , 20 mM glucose, [pH 7.0]

**Table 3: Laboratory equipment**

Laboratory equipment	Designation	Company
Agarose gel chamber	Horizon <sup>®</sup> 58	Life technologies <sup>™</sup>
Cell sorter	Aria I	BD Biosciences
Centrifuge	Megafuge 1.0 R (rotor: BS 4402/A)	Heraeus Sepatech
Centrifuge	Micro Centrifuge IR	Carl Roth GmbH + Co. KG
Centrifuge	Minifuge RF (rotor: BS 4402/A)	Heraeus Sepatech
Centrifuge	5417R	Eppendorf
Centrifuge	Avanti <sup>™</sup> J-25I (rotor: JA-10)	Beckman Coulter <sup>™</sup>
Centrifuge	3K30 (rotor type: 12156)	Sigma <sup>®</sup>
Concentrator	SpeedVac <sup>®</sup> Plus, SC110A	Savant <sup>™</sup> Thermo Scientific
Confocal laser scanning microscope	LSM 510	Zeiss
Developer machine	CP 1000	AGFA
Freezer ( - 20 °C)	GS 5203	Liebherr
Freezer ( - 80 °C)	Kryotech KLT3085-1	Hans-S. Schröder GmbH
Freezing container	Mr. Frosty <sup>™</sup>	Nalgene
Gel Electrophoresis device	Mini PROTEAN <sup>®</sup> Tetra Cell	Bio-Rad
Haemocytometer	Neubauer Improved (0.0025 mm <sup>2</sup> )	LO-Laboroptik Ltd.
Heat block	Thermomixer comfort	Eppendorf
Humidity incubation box	HIC-1	LabScientific
Ice machine	AF 100	Scotsman
Imaging flow cytometer	ImageStream ISX MK2	Amnis/EMD Milipore
Incubator	HERAcell 150 I	Thermo Scientific
Incubator	100-800	Memmert
Injection needle	G21 gauge needle	BD Microlance <sup>™</sup>
Inverse microscope	IM	Olympus
Laminar hood	Laminair <sup>®</sup> HB2472K	Heraeus Instruments
Magnetic stirrer	Thermostat RCT basic	IKA Labortechnik

### 3. Materials and Methods

Microplate reader	Infinitive <sup>®</sup> M200	Tecan Group Ltd.
Mixer	Vortex REAX 1	Heidolph Instruments GmbH + Co. KG
pH-Meter	pH-Meter 766	Knick
pH-Sensor	pH-Sensor SE100N	Knick
Pipette	pipetus <sup>™</sup>	Hirschmann Laborgeräte
Power supply	Electrophoresis EV265P	PEQLAB
Roller mixer	SRT 1	Stuart
Scale	Micro balance, 1601A MP8-1	Sartorius
Scale	H120-*D2	Sartorius
Shaker	KS200 basic	IKA Labortechnik
Shaking incubator	3033	GFL <sup>®</sup>
Shaking incubator	3032	GFL <sup>®</sup>
Spectrophotometer	SmartSpec <sup>™</sup> 3000	Bio-Rad
Spectrophotometer	Nanodrop ND-1000.	Thermo Fisher
Test-tube rotator	34528	Snijders
Transfection device	Amaxa <sup>™</sup> Nucleofector <sup>™</sup> II	Lonza
Transfection device	Gene Pulser <sup>™</sup> X cell	Bio-Rad
Ultracentrifuge	XL-80 (rotor: SW 60 Ti)	Beckman Coulter <sup>™</sup>
Ultrasonic Homogenizer (equipped with cup resonator cooling device)	Sonifier <sup>®</sup> S-450  DLK 402	Branson  Fryka-Kältetechnik GmbH
UV system	High Performance UV Transilluminator TFM-30V	UVP
Vacuum pump	RZ6	Vaccum GmbH + Co. KG
Water bath	1003	GFL
Water purification system	Milli-Q BioCel A-10	Merck Millipore

### 3. Materials and Methods

**Table 4: Chemicals**

<b>Designation</b>	<b>Company</b>	<b>Cat-No.</b>
2-Propanol	Carl Roth GmbH + Co. KG	CP41.3
4-(2-hydroxyethyl)-1-piperazineethanesulfonic acid (HEPES)	AppliChem	A1069,0500
Acetone	PanReac AppliChem	131007.1212
Acrylamide/Bis Solution 37.5:1 (40 % (w/v))	Serva Electrophoresis	10681.01
Agar-agar	Carl Roth GmbH + Co. KG	2266.3
Agarose	life technologies™	15510-027
Ammonium persulfate	Sigma-Aldrich	A-3678
Ampicillin	Carl Roth GmbH + Co. KG	K029.2
Boric acid	Carl Roth GmbH + Co. KG	5614.2
Bovine serum albumin (BSA)	Sigma-Aldrich	A4503-50G
Bromophenol blue	Sigma-Aldrich	B-5525
Calcium chloride	Carl Roth GmbH + Co. KG	CN93.1
3-[(3-Cholamidopropyl)dimethylammonio]-1-propanesulfonate (CHAPS)	Carl Roth GmbH + Co. KG	1479.4
Dimethylsulfoxide (DMSO)	Santa Cruz Biotechnology	Sc-358801A
Dithiothreitol (DTT)	Serva Electrophoresis	20710
Ethanol 96 % denatured	Carl Roth GmbH + Co. KG	T171.4
Ethanol 99 % pure	Carl Roth GmbH + Co. KG	5054.5
Ethylenediaminetetraacetic acid (EDTA)	Sigma-Aldrich	E-5143
Glucose	Carl Roth GmbH + Co. KG	6887.1
Glycerol	Carl Roth GmbH + Co. KG	3783.1
Glycine	Serva Electrophoresis	23390.03
Glyoxal	Sigma-Aldrich	128465-100G
Hydrogen chloride	Merck Millipore	1,030,571,000
Hydroxylamine	Sigma-Aldrich	159417-100G
Imidazole	Fluka	16011

### 3. Materials and Methods

IPTG	Thermo Scientific™	R1171
Kanamycin	Carl Roth GmbH + Co. KG	T832.2
Magnesia chloride	Carl Roth GmbH + Co. KG	HN03.1
Magnesia sulfate	Carl Roth GmbH + Co. KG	0261.1
Manganese chloride	Sigma-Aldrich	221279-100G
Methanol	Carl Roth GmbH + Co. KG	8388.6
Na-deoxycholate	Sigma-Aldrich	D-5670
Nonidet-P-40	Fluka	74385
Paraformaldehyde	Carl Roth GmbH + Co. KG	0335.2
Phosphate buffered saline	BioChrom AG	L182-10
Piperazine-N, N'-bis(2-ethanesulfonic acid (PIPES)	Carl Roth GmbH + Co. KG	9156.2
Potassium chloride	Carl Roth GmbH + Co. KG	PO17.2
Puromycin dihydrochloride	Santa Cruz Biotechnology	Sc-108071A
Saponin	Sigma-Aldrich	47036-50G-F
S-Methyl methanethiosulfonate (MMTS)	Sigma-Aldrich	64306
Sodium chloride	Carl Roth GmbH + Co. KG	3957.2
Sodium dihydrogen phosphate (NaH <sub>2</sub> PO <sub>4</sub> )	Carl Roth GmbH + Co. KG	K300.1
Sodium dodecyl sulfate (SDS)	Carl Roth GmbH + Co. KG	CN30.2
Sucrose	Serva Electrophoresis	35580.03
Tetramethylethylenediamine	Merck Millipore	1.107.320.100
Tris(hydroxymethyl)aminomethane	Carl Roth GmbH + Co. KG	5429.2
Tris/2-carboxyethyl)phosphine (TCEP)	Serva Electrophoresis	36970.02
Triton X-100	Sigma-Aldrich	T-9284
Tryptone	Carl Roth GmbH + Co. KG	8952.1
Tween 20	Sigma-Aldrich	P1379-1L
Yeast extract	Carl Roth GmbH + Co. KG	2363.1



### 3. Materials and Methods

**Table 5: Reagents and utensils**

Designation	Company	Cat-No.
μ Columns	Miltenyi Biotech	130-042-701
2-Bromopalmitate (2BrP)	Sigma-Aldrich	21604
6 x loading dye	ThermoScientific™	#R0611
Avidin, AlexaFluor™ 488 conjugate	life technologies™	A21370
Biotinylated TNF	R&D systems	BT210
CellMask™ Deep Red	Invitrogen™	C10046
CL-XPosure™	Thermo Scientific	3408
cOmplete™ protease inhibitor cocktail	Roche	4693132001
desalting column PD-10	GE Healthcare	17-0851-01
DPP-2	Prof. Bryan Dickinson	-
DPP-3	Prof. Bryan Dickinson	-
ECL Western Blotting Detection Reagent	Amersham, GE Healthcare	RPN2106
EcoRI	Thermo Scientific™	FD0275
Fab fragment anti-TNF (Fab <sub>TNF</sub> , 10 mg/ml))	Prof. Daniela Männel	-
Filtropur S (0.45 μm)	Sarstedt AG & Co. KG	83.1826
Fluoro-gel	Electron Microscopy Sciences	17985010
Gene Ruler 1 Kb Plus DNA ladder	ThermoScientific™	#SM1331
GW4869	Sigma Aldrich	D1692
Hexadecylsulfonyl Fluoride (HDSF)	Santa Cruz Biotechnology	86855-26-7
HiTrap™ Protein G HP 1 ml column	GE Healthcare	29-0485-81
Hoechst stain 33258	Invitrogen™	H3569
Human Fibronectin Cellware 22 mm round coverslips	BioCoat™	354088
Instant skimmed milk powder	Frema	0203V02
Lipofectamine2000	ThermoScientific™	11668019
ML349	Tocris	5344
NotI	ThermoScientific™	FD0596

### 3. Materials and Methods

PageRuler™ Prestained Protein Ladder	Thermo Scientific	26616
Palmostatin B (PalB)	Merck Millipore	178501
Paper filter, folded, grade 595, 90 mm	GE Healthcare	WH10311642
Pefabloc® SC (AEBSF)	Roche	11429868001
Protein G Microbeads	Miltenyi Biotech	120-000-397
RedSafe™	INtRON Biotechnology	21141
Roti®-PVDF (Polyvinylidene fluoride), 0.45 µm	Carl Roth GmbH + Co. KG	T830.1
TNF (1 mg/ml)	Prof. Dr. Daniela Männel	-
Slides microscopes	Paul Marienfeld GmbH + Co. KG	1000200
T4 DNA Ligase	Invitrogen	15224041
TALON® metal affinity resin	Clontech Laboratories	635501
Thiopropyl sepharose 6B	GE Healthcare	71-7105-00 AE
Ultracentrifugation tubes Ultra-Clear™	Beckman Coulter®	344061
zDEVD-AFC	AAT Bioquest	13420
zVAD	Bachem	N-1510
Rotilabo® -Blotting Papers 1.0 mm	Carl Roth GmbH + Co. KG	CL74.1

**Table 6: Software used for documentation and analysis**

Software	Version
Amnis IDEAS software	6.0.154.0
GrapPad Prism	v. 6.07
ImageJ	v. 1.52r
Amnis inspire software	200.1.388.0
Microsoft Excel® 2010	v. 14.0.7212.5000
Microsoft Word® 2010	v. 14.0.7212.5000
Scanner Driver and EPSON Scan Utility	v3.9.2.1 DE

### 3. Materials and Methods

**Table 7 Bacterial strain**

Bacterial strain	Company	Cat-No.
Mach1 T1 <sup>R</sup>	Invitrogen <sup>TM</sup>	C862003

**Table 8: Primary antibodies**

Antigen	Dilution	Host	Cat-No	Company	Theoretical MW/kDa
$\alpha$ -tubulin	1:10000	m	HRP-66031	proteintech	50
$\beta$ -actin	1:5000	m	HRP-60008	proteintech	42
APT1	1:1000	r	PA5-28034	ThermoFisher Scientific	25
APT2	1:1000	r	LS-C158086	LifeSpan BioSciences	25
CD71 (D7G9X)	1:1000	r	#13113	Cell Signaling	90
Ceramide (15B4)	1:1000	m	ALX-804-196-T050	Enzo Life Sciences	-
cl. Caspase 3	1:1000	r	#9661S	Cell Signaling	17, 19
zDHHC20	1:1000	r	PA5-39359	ThermoFisher Scientific	42
zDHHC5	1:1000	r	A304-652-AM	Bethyl Laboratories	77
zDHHC5	1:1000	r	NBP1-81376	Novus Biologicals	77
FLAG M2	1:1000	m	F1804-200UG	Sigma-Aldrich	-
Flotillin-2 (C42A3)	1:500	r	#3436	Cell Signaling	49
GAPDH	1:10000	m	HRP-60004	proteintech	36
His <sub>6</sub>	1:1000	r	#2365	Cell Signaling	-
Integrin $\alpha$ 6	1:1000	r	#3750	Cell Signaling	150, 125
I $\kappa$ B- $\alpha$	1:1000	m	#4814	Cell Signaling	39

### 3. Materials and Methods

(L35A5)					
MLKL	1:1000	r	ab187091	abcam	54
PARP1	1:1000	r	#9542S	Cell Signaling	89, 116
PPT1	1:500	r	HPA021546	Sigma-Aldrich	34
Rab5 (A-20)	1:200	r	sc-598	Santa Cruz Biotechnology	25
TNF-R1	1:1000	r	#3736	Cell Signaling	55
(C25C1)					
TNF-R1 (H5)	1:1000	m	sc-8436	Santa Cruz Biotechnology	55
TNF-R2	1:1000	m	MAB2261	R&D systems	75
TNF-R2	1:1000	r	sc-7862	Santa Cruz Biotechnology	75
(H-202)					

**Table 9: Secondary antibodies**

Antigen	Dilution	Cat-No	Company
anti-mouse	1:10000	115-036-003	Jackson Immuno Research
anti-mouse	1:200	A21202	life technologies™
AlexaFluor™ 488			
anti-rabbit	1:10000	111-036-003	Jackson Immuno Research
anti-rabbit	1:200	A21206	life technologies™
AlexaFluor™ 488			

**Table 10: Kits**

Designation	Company	Cat-No.
BCA protein assay kit	Pierce™	23227
Mutagenesis Kit “QuickChange II XL”	Agilent Technologies	200522-5
Amaya™ Cell line Nucleofector™ kit C	Lonza	VCA-1004
QIAquick® Gel extraction kit	QIAGEN	28706
QIAprep® Spin Miniprep kit	QIAGEN	27106
Plasmid Maxi kit	QIAGEN	12163

**Table 11: Oligonucleotides** [for. forward; rev. reverse]

	Sequence (5' to 3')	Description
<b>For sequencing</b>		
	TATCCAGCCCTCACTCCTTCTCTAG	pMOWS-puro [for]
	CCACATAGCGTAAAAGGAGCAAC	pMOWS-puro [rev]
<b>For point mutations in pMOWs-puro vector</b>		
C223S	AGCAGGCTCAGCAGGCTCAGGCCAAAAAATC	TNF-R1_t667a [for]
	GATTTTTTTTTGGCCTGAGCCTGCTGAGCCTGCT	TNF-R1_t667a [rev]
C304S	AAAGTTCGGGCTATCGCCCGGGGTATAGG	TNF-R1_t910a [for]
	CCTATACCCCGGGCGATAGCCCGAACTTT	TNF-R1_t910a [rev]

## 3.2 Methods

### 3.2.1 Cell culture

The human monoblastoid suspension cell line U937 (CVCL\_0007; Sundström and Nilsson, 1976) was purchased from the DSMZ (ACC5, Braunschweig, Germany) and cultured in RPMI 1640 medium (Table 1) supplemented with 5 % (v/v) FCS (Table 1) and 1 % (v/v) penicillin/streptomycin ( $100 \frac{U}{ml}$  pen,  $100 \frac{\mu g}{ml}$  strep, Table 1) under standard cell culture conditions (37 °C, 5 % CO<sub>2</sub>).

HeLa80 cells (CVCL\_4776, Gille and Joenje, 1989) derived from the cervical cancer cell line HeLa and were obtained from H. Wajant, University hospital, Würzburg, Germany.

HEK293T cells (CVCL\_0063; Graham et al., 1977) derived from human embryonic kidney cells, transfected with fragments of the adenovirus type 5 DNA. The cells were purchased from the DSMZ (ACC635, Braunschweig, Germany) and used for the production of Fc60TNF (section 3.2.7).

Gryphon™ cells derived from HEK293T were purchased from Allele Biotechnology and used for the retroviral gene transduction (section 3.2.19). All adherent cell lines were cultured in DMEM medium (Table 1) supplemented with the same reagents as RPMI 1640 medium and incubated under standard cell culture conditions.

For cell harvesting, the cell number per ml was determined by a Neubauer improved cell counting chamber in combination with equation 1. The calculated volume was transferred into 50 ml tubes and centrifuged at 350 x g, RT, for 5 min.

$$\text{Concentration [cells/ml]} = \frac{\text{number of cells} \times 10000}{\text{number of square} \times \text{dilution}} \quad (1)$$

For freezing stocks, cells were harvested, washed once in PBS, resuspended in freezing medium (90 % (v/v) FCS, 10 % (v/v) DMSO) and slowly cooled down to – 80 °C into a cryo freezing container (Nalgene, Table 3).

### 3.2.2 Preparation of whole cell lysates

For protein based analyses,  $1 \cdot 10^6$  to  $1 \cdot 10^7$  cells were harvested by centrifugation at 450 x g, 4 °C for 5 min and washed once with PBS. Cell pellet was then resuspended in modified RIPA (Radioimmunoprecipitation assay) buffer (50 mM Tris-HCl [pH 7.5], 150 mM NaCl, 1 % (v/v) NP-40, 1 % (v/v) Triton X-100, 1 mM EDTA, 0.25 % (w/v) Na-deoxycholate) and further lysed by freezing for 20 min at -20 °C. Afterwards, lysate was centrifuged at 1,000 x g, 4 °C for 5 min, supernatant was transferred into a new 1.5 ml tubes and stored at – 20 °C.

#### 3.2.3 Protein quantification

Protein concentration was determined by the BCA (bicinchoninic acid) assay kit (Pierce™, Table 10) according to the manufacturer's instruction. BSA (bovine serum albumin) was used as a standard (concentration: 0.2; 0.4; 0.6; 0.8; 1.0 mg/ml). The absorbance was measured at 562 nm with the Infinite® M200 system (Tecan Group Ltd., Table 3) and Microsoft Excel® 2010 (Table 6) was used for data analysis.

#### 3.2.4 SDS-PAGE/Western blot

The SDS (sodium dodecyl sulfate)-PAGE (polyacrylamide gel electrophoresis) was used to separate proteins by their molecular masses in an electric field with following analysis and detection by Western blot. According to the size of the proteins of interest, discontinuous SDS- gels were cast according to the standard protocol (Laemmli, 1970), composed of either 10 % or 12.5 % separation gel and 5 % stacking gel. Gels were submerged in 1 x Tris-Glycine-SDS buffer (25 mM Tris, 192 mM Glycine, 0.1 % SDS), run at constant current of  $20 \frac{mA}{gel}$  and samples were prepared with 5 x SDS loading buffer (50 mM Tris [pH 6.8], 25 % (v/v) glycerol, 10 % (w/v) SDS, 150 mM DTT, pinch bromophenol blue) containing DTT as reductant. To determine the size of the separated proteins a molecular weight standard "PageRuler™ Prestained Protein Ladder" (Thermo Scientific, Table 5) was used. For the subsequent immunoblotting, a tank blot protocol was used (25 mM Tris, 192 mM Glycine, 20 % (v/v) Methanol; Harlow and Lane, 1988, chapter 13) at a constant potential of 110 V for 75 min, where proteins were transferred onto a methanol activated PVDF membrane (Carl Roth, Table 5). Afterwards, membrane was blocked in blocking buffer (5 % (w/v) skimmed milk and TBST (10 mM Tris [pH 7.5], 100 mM NaCl, 0.1 % (v/v) Tween-20) for 1 h at RT and then incubated shaking overnight at 4 °C with the primary antibody diluted in blocking buffer according to table 8. After a fourfold washing within TBST each for 5 min at RT, membrane was incubated for 1 h at RT in blocking buffer added with the diluted secondary antibody corresponding to the host species of the primary antibody (Table 9). Thereafter, membrane was washed fourfold with TBST each for 5 min at RT. For detection, the chemiluminescent detection reagent was prepared according to the manual of Amersham ECL (GE Healthcare, Table 5), dropped onto the membranes and emitted chemiluminescence was detected by light-sensitive films CL-XPosure™ (Thermo Scientific™, Table 5) for 10 sec to 60 min. For further analysis and quantification, films were scanned with Epson® software and evaluate by Microsoft Excel® 2010 and ImageJ (Table 6) where the relative peak intensity was calculated considered with the peak areas as a base.

#### 3.2.5 Acyl-resin-assisted capture

To determine the palmitoylation status of specific proteins the acyl resin-assisted capture (acyl-RAC) was used [Forrester et al., 2011]. Therefore,  $1 \times 10^8$  cells per sample were harvested and washed once with ice cold PBS and if needed, cells were treated with TNF, incubated on ice for 15 min and then placed in a 37 °C pre-warmed water bath for the indicated time points. The cell pellet was resuspended in 1 ml buffer A (25 mM HEPES [pH 7.5], 25 mM NaCl, 1 mM EDTA, 1 x protease inhibitor cocktail (Roche, Table 5)) and lysed by sonication (3 x 20 sec with 10 sec break in between, constant output 2.5, 4 °C). To remove nuclear debris, the cell lysate was centrifuged at 800 x g, 4 °C for 5 min. For the enrichment of membrane proteins the post-nuclear supernatant was further high-speed centrifuged at 21.000 x g, 4 °C for 60 min and the resulting crude membrane pellet was resuspended in buffer A + 0.5 % (v/v) Triton X-100. 10 µl of the resuspended fraction was sampled, mixed with 10 µl modified RIPA buffer (50 mM Tris-HCl [pH 7.5], 150 mM NaCl, 1 % (v/v) NP-40, 1 % (v/v) Triton X-100, 1 mM EDTA, 0.25 % (w/v) Na-deoxycholate), labeled as membrane fraction (MF) and stored at -20 °C. To ensure same amounts of proteins, protein concentration was measured by BCA assay (section 3.2.3). To rule out that free thiol groups are formed during the experiment and negatively interfere with the assay, all existing disulfide bonds were reduced by adding 10 mM TCEP to the crude membrane fraction and incubated shaking for 30 min at RT. For the subsequent blocking of free thiol groups 2 mg of total protein was mixed with blocking buffer (100 mM HEPES [pH 7.5], 1 mM EDTA, 2.5 % (w/v) SDS, 3 % (v/v) MMTS (Table 4)) in the ratio 1:2 and incubated shaking at 40 °C for 3 h. The removal of excess MMTS was implemented by an acetone precipitation, where proteins were precipitated by adding thrice the volume of 100 % ice-cold acetone and incubated for 20 min at -20°C. Afterwards, precipitated proteins were pelleted at 21.000 x g, 4 °C for 2 min, washed fivefold with 70 % (v/v) ice-cold acetone and dried at 40 °C. The final pellet was mixed with 400 µl binding buffer (100 mM HEPES [pH 7.5], 1 mM EDTA, 1 % (w/v) SDS) and resuspended by sonication (3 x 20 sec with 10 sec break in between, constant output 2.5, 4 °C). 0.05 g prior in binding buffer activated thiopropyl sepharose 6B beads (GE Healthcare, Table 5) were added with 200 µl of protein suspension and either treated with 2 M hydroxylamine solution [pH 7.5] for thioester cleavage or 2 M Tris-HCl [pH 7.5] as a negative control, to reach a final concentration of 0.5 M, respectively. The beads suspension was then incubated overnight on a test-tube rotator (Snijders, Table 3). On the next day, beads were washed fivefold with binding buffer and centrifuged at 1000 x g, RT for 2 min. Bound proteins were eluted by adding 60 µl SDS loading buffer (50 mM Tris [pH 6.8], 25 % (v/v) glycerol, 10 % (w/v)



SDS, 150 mM DTT, pinch bromophenol blue), incubating for 15 min at RT and subsequently for another 15 min shaking at 98 °C. Afterwards, samples were analyzed by SDS-PAGE and Western blot analysis (section 3.2.4).

#### **3.2.6 Electroporation**

HEK293T cells were transfected with 10 µg of the Fc60TNF-plasmid (provided by H. Wajant, University hospital, Würzburg, Germany) using an electroporation device Gene Pulser™ X cell (Bio-Rad, Table 3). Therefore,  $2 \cdot 10^6$  cells per electroporation were sedimented (450 x g, RT, 5 min), resuspended in 200 µl RPMI only medium and mixed with 10 µg plasmid DNA. The mixture was then transferred into a pre-warmed cuvette (0.2 µm), placed into the device and pulse (110V, pulse length 25 ms) was initiated. After pulsing, cells were rinsed in RPMI 1640 only medium, transferred into a 24-well plate, containing pre-warmed RPMI 1640 only medium and incubated under standard cell culture conditions.

#### **3.2.7 Purification of Fc60TNF**

For Fc60TNF,  $2 \cdot 10^6$  cells per transfection of HEK293T were transiently transfected with 10 µg Fc60TNF-plasmid via electroporation (section 3.2.6). Cells were transferred into antibiotic free FreeStyle® medium (Table 1), cultivated overnight under standard cell culture conditions and then treated with 1 % (v/v) penicillin/streptomycin. After the third day of transfection, supernatant was harvested (450 x g, 4 °C, 5 min), sterile filtrated (0.45 µm filter, Table 5) and 1 x protease inhibitor cocktail (Roche, Table 5) was added. Cells were refilled with fresh FreeStyle® medium (Table 1) supplemented with 1 % (v/v) penicillin/streptomycin (Table 1) and cultivated for two more days. Subsequently, supernatants were pooled and Fc60TNF was purified with a HiTrap™ Protein G HP 1 ml column (GE Healthcare, Table 5) according to the manufacturer's protocol. Afterwards, protein concentration was determined by BCA assay (section 3.2.3) and the biological activity was detected by apoptosis assay (section 3.2.20) using U937 cells.

#### **3.2.8 Immunoprecipitation via Fc60TNF**

For immunoprecipitation,  $2 \cdot 5 \cdot 10^7$  cells per sample were harvested and washed once with ice-cold PBS. After 30 min incubation, 100 ng/ml Fc60TNF which specifically binds to TNF-R1 (section 3.2.7) was added and incubated on ice for 30 min. The internalization event was initiated by the temperature shift incubating the samples for the respective time points in a 37 °C pre-warmed water bath. Afterwards, cells were immediately lysed by adding 1 ml modified RIPA buffer (50 mM Tris-HCl [pH 7.5], 150 mM NaCl, 1 % (v/v) NP-

### 3. Materials and Methods

---

40, 1 % (v/v) Triton X-100, 1 mM EDTA, 0.25 % (w/v) Na-deoxycholate) and incubated for 45 min on ice. Subsequently, cells were sheared by using a G21 gauge needle (BD Microlance™, Table 3) and cell debris was sedimented at 12,500 x g, 4 °C for 10 min. The supernatant was then mixed with 30 µl protein G Microbeads (Miltenyi Biotech, Table 5) and incubated on a test-tub rotator for 2 h at 4 °C. Next, lysate was applied to an equilibrated µ Columns (Miltenyi Biotech, Table 5), washed with 800 µl modified RIPA buffer (50 mM Tris-HCl [pH 7.5], 150 mM NaCl, 1 % (v/v) NP-40, 1 % (v/v) Triton X-100, 1 mM EDTA, 0.25 % (w/v) Na-deoxycholate) and eluted with pre-heated SDS loading buffer (50 mM Tris [pH 6.8], 25 % (v/v) glycerol, 10 % (w/v) SDS, 150 mM DTT, pinch bromophenol blue). After heat incubation at 98 °C for 5 min, eluate was used for SDS-PAGE and Western blot analysis (section 3.2.4), where 10 µl of the eluate was used.

#### **3.2.9 Nucleofection**

U937 cells were transfected with 2 µg CRSIPR/Cas9-plasmid DNA using the Amaxa™ Cell line Nucleofector™ kit C (Lonza, Table 10) according to the manufacturer's standardized manual. In brief,  $1 \times 10^6$  cells per transfection were centrifuged (250 x g, RT, 10 min), resuspended in 100 µl nucleofactor solution C +supplements, combined with 2 µg plasmid-DNA and then transferred into a pre-warmed cuvette (0.2 µm). Transfection was applied with the Amaxa™ Nucleofector™ II (Table 3) program W-001, cells were rinsed in pre-warmed RPMI 1640 only media and transferred into a 12-well plate for 5 h at 37°C. Subsequently, supplemented RPMI 1640 was added and cells were incubated for 48 h.

#### **3.2.10 Generation of U937 knockout cells by CRISPR/Cas9 plasmids**

For the CRISPR/Cas9 knockouts, CRISPR/Cas9-plasmids were either obtained from Sigma-Aldrich (TNF-R1, TNF-R2, PPT-1, zDHHC20, Table 12) or SantaCruz Biotechnology (APT2, Table 12) or were self-designed (zDHHC5, Table 12) and transfected to U937 cells using Amaxa® nucleofection (section 3.2.9). Afterwards, cells were FACS sorted (Aria I, BD Biosciences, Table 3) for GFP positive signals and single clones were isolated into 96-well plates containing conditioned media. Growing monoclonal mutants were then further characterized by SDS-PAGE and immunoblotting (section 3.2.4). For the zDHHC5 knockout, guide RNAs were designed by Pascal Meier (Institute of Cancer Research, London, UK) according to Ran et al., 2013 and cloned into the pSpCas9(BB)-2A-GFP vector (addgene, 48138).

**Table 12: CRISPR/Cas9 plasmids**

Customer	Vector	Gene	Target-ID/site	
Sigma-Aldrich	U6gRNA-Cas9- 2A-GFP	TNF-R1	HS0000079005	
			HS0000079009	
		zDHHC20	HS0000533372	
			HS0000533370	
		PPT-1	HS0000011277	
			HS0000011270	
			TNF-R2	HS0000079027
				HS0000079030
Pascal Meier	pSpCas9(BB)-2A- GFP	zDHHC5	TSAGGGGGACGGTAAAAGCGGC TSAAGGATACGTGACAGCCGTG	
Santa Cruz Biotechnology	CRISPR/Cas9 KO	APT2	not specified	

### 3.2.11 Generation of TNF-R1 constructs

For the generation of the TNF-R1 constructs, the TNF-R1 sequence was modified adding a triple FLAG-tag with enterokinase site at its C-terminus and restriction sites of EcoRI (N-terminus) and NotI (C-terminus) at its ends for cloning purposes. Furthermore, TNF-R1 sequence was shortened by deleting the death domain and the residual of the C-terminus, termed as  $\Delta$ DD. Additionally, a point mutation at cysteine 248 to serine was introduced in both WT- and  $\Delta$ DD forms and all four constructs (TNF-R1<sub>wt</sub>, TNF-R1 $\Delta$ DD, TNF-R1<sub>C248S</sub>, TNF-R1<sub>C248S $\Delta$ DD</sub>) were ordered from Invitrogen GeneArt (ThermoFisher Scientific). Constructs were cloned into the retroviral vector pMOWS-puro as described in 3.2.12 and both insertion and sequence was verified by sequencing (section 3.2.17). For further point mutations at Cysteine 223 and 304 a mutagenesis kit “QuickChange II XL” (Agilent Technologies, Table 10) and the respective primer (Table 11) were used according to the manufacturer’s instruction resulting in sixteen TNF-R1 mutants as shown in table 13. After sequence verification (section 3.2.17), constructs were transfected into Mach1 T1<sup>R</sup> competent cells (section 3.2.16) and maxi preparation was performed (section 3.2.18).

### 3. Materials and Methods

DNA plasmids were then transfected into Gryphon™ cells (Allele Biotechnology) for the generation of virus particles (see section 3.2.19).

**Table 13: TNF-R1 constructs**

Number	Designation
I	TNF-R1
II	C248S
III	TNF-R1 $\Delta$ DD
IV	C248S $\Delta$ DD
V	C223S
VI	C304S
VII	C223S $\Delta$ DD
VIII	C304S $\Delta$ DD
IX	C223S/C248S $\Delta$ DD
X	C248S/C304S $\Delta$ DD
XI	C223S/C248S
XII	C248S/C304S
XIII	C223S/C304S
XIV	C223S/C304S $\Delta$ DD
XV	C223S/C248S/C304S
XVI	C223S/C248S/C304S $\Delta$ DD

#### 3.2.12 Recloning

For recloning of the TNF-R1 constructs from the vector pMK-RQ into the retroviral vector pMOWS-puro, 2  $\mu$ g of the constructs were digested with the restriction enzymes EcoRI (ThermoScientific™, Table 5) and NotI (ThermoScientific™, Table 5) for 2 h at 37 °C according to the manufacturer's protocol. Afterwards, DNA fragments were separated by agarose gel electrophoresis (section 3.2.13) and purified from the agarose gel by the QIAquick® Gel extraction kit (section 3.2.14). Ligation of the purified insert within the pMOWS-puro vector was performed according to the manufacturer's protocol (T4 DNA Ligase, Invitrogen, Table 5). Subsequently ligation mixture was transfected into competent Mach1 T1<sup>R</sup> cells (section 3.2.16) and obtained plasmid DNA was verified by sequencing (section 3.2.17).

#### 3.2.13 Agarose gel electrophoresis

Agarose gel electrophoresis was used for the separation of DNA fragments resulting from restriction enzyme digestions. According to the size of the DNA fragments, 0.6 % to 1 % (w/v) agarose gels were produced. The appropriate amount of agarose was boiled in 1 x Tris-Borate-EDTA buffer (TBE, 89 mM Tris base, 89 mM boric acid, 2 mM EDTA [pH 8.0]), mixed with 0.5 µg/ml RedSafe™ (INtRON Biotechnology, Table 5), and poured into a horizontal gel chamber (Table 3). The samples were mixed with 6 x loading dye (ThermoScientific™, Table 5) and separated at 100 – 120 V for 60 to 90 min in 1 x TBE as running buffer. The visualization of the separated DNA fragments was completed under ultraviolet light (Table 3). In order to estimate the size of separated DNA fragments the size standard Gene Ruler 1 Kb Plus DNA ladder (ThermoScientific™, Table 5) was used.

#### 3.2.14 Isolation of DNA fragments from agarose gel

The isolation and purification of DNA fragments from agarose gels was performed with the QIAquick® Gel extraction kit (QIAGEN, Table 10). The separated DNA bands were cut out from agarose gel under ultraviolet light (Table 3), the agarose blocks were transferred into reaction vessels and the DNA was purified according to the manufacturer's protocol. The purified DNA was eluted in 25 µl ultra-pure distilled water and stored at 4 °C. DNA concentration was determined by Nanodrop (Thermo Fisher, Table 3).

#### 3.2.15 Competent cells

To generate competent Mach1 T1<sup>R</sup> cells, cells were plated on a LB agar plate (1 % (w/v) tryptone, 0.5 % (w/v) yeast extract, 1 % (w/v) NaCl, 1.5 % (w/v) agar, [pH 7.0]) and incubated overnight at 37 °C. 100 ml of a LB medium (1 % (w/v) tryptone, 0.5 % (w/v) yeast extract, 1 % (w/v) NaCl, [pH 7.0]) sub culture was inoculated with one clone of the LB agar plate and incubated shaking overnight at 37 °C, 250 rpm (Table 3). 5 ml of the sub culture was then used to inoculate 245 ml SOB medium (2 % (w/v) tryptone, 0.5 % (w/v) yeast extract, 10 mM NaCl, 2.5 mM KCl, 10 mM MgCl<sub>2</sub>, 10 mM MgSO<sub>4</sub>, 20 mM glucose, [pH 7.0]) which was incubated overnight at 18 °C and 350 rpm (Table 3). On the next day, culture was diluted until OD<sub>600</sub> ≈ 0,4 and again incubated at 18 °C until OD<sub>600</sub> ≈ 0,6 (Table 3). After that, culture was cooled down on ice for 10 min and then centrifuged at 2,500 x g, 4 °C for 10 min. The pellet was resuspended in ice-cold transformation buffer (10 mM HEPES, 15 mM CaCl<sub>2</sub>, 250 mM KCl, MnCl<sub>2</sub>, [pH 6.7]), incubated 10 min on ice and centrifuged at 2,500 x g, 4 °C for 10 min. Pellet was again cautiously resuspended on ice in 20 ml transformation buffer and DMSO was added dropwise until an end concentration of

7 % (v/v) of DMSO was reached. Mixture was incubated on ice for 10 min, aliquoted into pre-cooled vials, frozen immediately in liquid nitrogen and stored at - 80 °C.

#### **3.2.16 Transfection of Mach1 T1<sup>R</sup> competent cells**

For bacterial plasmid replication, Mach1 T1<sup>R</sup> competent cells were used (Table 7) Therefore, 50 µl of Mach1 T1<sup>R</sup> competent cells were thawed on ice and gently mixed with 100 ng plasmid-DNA. After 30 min of incubation on ice, heat-shock was initiated placing the vial for 30 sec at 42 °C without shaking. The vial was placed on ice for another 2 min and Mach1 T1<sup>R</sup> cells were transferred into a 15 ml tube containing 1 ml of SOB medium (2 % (w/v) tryptone, 0.5 % (w/v) yeast extract, 10 mM NaCl, 2.5 mM KCl, 10 mM MgCl<sub>2</sub>, 10 mM MgSO<sub>4</sub>, 20 mM glucose, [pH 7.0]). The tube was incubated for 1 h at 37 °C, 250 rpm. Meanwhile, LB agar plates (1 % (w/v) tryptone, 0.5 % (w/v) yeast extract, 1 % (w/v) NaCl, 1.5 % (w/v) agar, [pH 7.0]) were mixed with ampicillin (100 µg/ml) and air-dried under a laminar hood. After incubation, 50 µl of bacterial suspension was streaked onto the LB agar plate and incubated for 12 h in a 37 °C incubator (Memmert, Table 3). Grown colonies could be used on the next day for further analysis.

#### **3.2.17 Sequencing**

The method of Sanger sequencing was used for the validation of the accurate base sequence of the altered plasmid by restriction, ligation or point mutation. Hence, plasmids were separated (section 3.2.13), purified and concentration was determined (section 3.2.14). For sequencing by the Sanger dideoxynucleotide chain termination reaction, 250 ng DNA was mixed with 4.8 µM primer (Table 11) and sent to the Institute of Clinical Molecular Biology (IKMB) in Kiel, where capillary sequencers (Analyser 3700, Applied Biosystems) separated the samples and collected the chromatograms, which were subsequently analyzed with Microsoft Word<sup>®</sup> (v. 14.0.7212.5000) by comparison.

#### **3.2.18 Mini-/ Maxi-preparation**

Bacterial cells were lysed via the selective alkaline denaturation for purification and extraction of plasmid DNA (Birnboim and Doly, 1979) Bacteria were grown shaking (250 rpm) overnight at 37 °C in either 5 ml (mini-preparation) or 250 ml (maxi-preparation) LB medium (1 % (w/v) tryptone, 0.5 % (w/v) yeast extract, 1 % (w/v) NaCl, [pH 7.0]) with the appropriate antibiotics (50 µg/ml ampicillin, 25 µg/ml kanamycin, Table 4). For both preparations, buffers of the plasmid kits from QIAGEN were used, which were identical in their composition (Table 10). The following instruction depicts the mini-preparation. Instructions regarding the maxi-preparation are indicated in square

### 3. Materials and Methods

---

brackets. After the centrifugation of the overnight culture at 3,000 x g for 10 min at RT [5000 x g for 10 min at 4 °C], the supernatant was discarded and the bacteria were resuspended in 250 µl [10 ml] of ice-cold buffer P1 and the mixture was transferred into a 2 ml tube [50 ml tube]. In order to start the alkaline cell lysis, 250 µl [10 ml] buffer P2 was added and the tube was inverted thrice. After 5 min incubation at RT, cell lysis was stopped and the solution neutralized by adding 350 µl [10 ml] of ice-cold buffer P3 and samples were thoroughly mixed. To precipitate SDS-bound proteins and denatured bacterial chromosomal DNA, tubes were chilled for 10 min [20 min] on ice. Meanwhile, for maxi-preparation, a QIAGEN-tip was equilibrated by applying 10 ml buffer QBT. Next, either the mixture was centrifuged at 17,000 x g for 10 min at RT and the supernatant was transferred into a QIAprep<sup>®</sup> spin column (mini-preparation) or the mixture was filtered through a paper filter (GE Healthcare, Table 5) by gravity flow into the QIAGEN-column (maxi-preparation). After two washes with 0.5 ml buffer PE [30 ml buffer QC], purified DNA was eluted with 50 µl [15 ml] elution buffer QF into a clean 1.5 ml [50 ml] tube by either centrifugation at 17,000 x g for 1 min at RT (mini-preparation) or gravity flow (maxi-preparation). For maxi-preparation, plasmid DNA was precipitated with 10.5 ml isopropanol and centrifuged at 10,000 x g for 1 h at 4 °C. Thereafter, pellet was washed with 5 ml 70% (v/v) ethanol, pelleted again at 10,000 x g for 10 min at 4 °C and air-dried for 15 min. Finally, the DNA was dissolved in 200 µl Milli-Q water and concentrations were determined by the spectrophotometer Nanodrop (Thermo Fisher, Table 3).

#### **3.2.19 Retroviral gene transduction**

To ensure the production of stable transfectants, the retroviral gene transduction was used. All constructs used for transduction are listed in table 13, section 3.2.11. There, the amphotropic, retroviral packaging cell line Gryphon<sup>™</sup> (Allele Biotechnology) was plated into a T25 flask at a density of  $2 \times 10^6$  cells and incubated under standard cell culture conditions. On the next day, cells were transfected with the designed pMOWS-puro vector by Lipofectamine2000 (Table 5; Ketteler et al., 2002) according to the manufacturer's instruction. For each construct, 237.5 µl Opti-MEM (Table 1) were mixed with 12.5 µl Lipofectamine2000 and 10 µg Plasmid-DNA was mixed with Opti-MEM to reach 250 µl in total. Both mixtures were incubated for 5 min at RT and then mixed together and incubated for 20 min at RT. Afterwards, mixture was dropped onto cells and incubated overnight under standard cell culture conditions. The next day, medium was either exchanged with 2.5 ml RPMI 1640 medium (U937) or DMEM (HeLa80) and incubated overnight. For transduction, virus containing medium was harvested,

### 3. Materials and Methods

---

centrifuged at 500 x g, 4 °C for 5 min and the supernatant was sterile filtrated (0.45 µm filter, Table 5). 3 ml of the supernatant were added to  $0.5 \times 10^6$  cells to be transduced and incubated overnight under standard cell culture conditions. On the next day, medium was exchanged with fresh RPMI 1640 or DMEM. Prior to the selection of transduced cells, kill curves for the respective cell lines were implemented with increasing puromycin concentrations (0.25, 0.5, 0.75, 1.0, 1.5, 2.0, 4.0 µg/ml) to determine the minimum antibiotic concentration. 1.5 µg/ml puromycin was added to both cell lines and cells were observed for the next 3-4 weeks until stable transfectants grew. Transfectants were then further analyzed by SDS-PAGE and immunoblotting (section 3.2.4).

#### **3.2.20 Apoptosis assay**

Apoptosis was measured by nuclear DNA fragmentation via the ImageStream device (Amnis/EMD Millipore, Table 3). Therefore,  $1 \times 10^6$  cells per sample were transferred into a 24-well plate, if needed, cells were pre-incubated with inhibitors (50 µM ML349, 50 µM PalB) for 1 h at 4 °C, then treated with 100 ng/ml TNF and incubated for 20 h under standard cell culture conditions. 30 min before end Hoechst stain 33258 (Table 5) to a final dilution of 1:10,000 was added into the culture medium. Afterwards, cells were transferred into 1.5 ml tubes, centrifuged at 350 x g for 5 min at 4 °C, fixed with 2 % (v/v) PFA/PBS solution and stored on ice until analysis. At least 10,000 images per sample were acquired by the Inspire software (Table 6) and analyzed using the apoptosis wizard of the Amnis IDEAS software (Table 6).

#### **3.2.21 Detection of cleaved Caspase-3, PARP1 and phosphorylated MLKL**

$5 \times 10^6$  cells were pre-incubated for 45 min with 50 µM ML349 and 50 µM zVAD, respectively and then treated with 100 ng/ml TNF for 6 h. After sedimentation, cells were lysed in TNE buffer (1 M Tris [pH 8.0], 5 M NaCl, 1 % (v/v) NP-40, 0.5 M EDTA, 1 x protease inhibitor cocktail (Roche, Table 5)) centrifuged at 1,000 x g, 4 °C for 5 min and protein concentration was determined by BCA assay (section 3.2.3). 20 µg of total protein were then analyzed by SDS-PAGE and immunoblotting using antibodies against caspase-3, PARP1 and pMLKL (Table 8; section 3.2.4).

#### **3.2.22 IκB degradation**

For IκB degradation,  $2 \times 10^6$  cells per sample were cooled on ice for 15 min and subsequent treated with 100 ng/ml TNF for another 15 min on ice. Afterwards, cells underwent a temperature shift for the indicated time points (0, 5, 10, 15, 30, 45 min) at 37 °C and were then lysed in 100 µl modified RIPA buffer (50 mM Tris-HCl [pH 7.5], 150 mM NaCl,



1 % (v/v) NP-40, 1 % (v/v) Triton X-100, 1 mM EDTA, 0.25 % (w/v) Na-deoxycholate). Equal amounts of protein, quantified by BCA assay (section 3.2.3), were separated by SDS-PAGE with following Western blot analysis using an antibody against  $\kappa$ B (Table 8, section 3.2.4).

#### **3.2.23 Surface expression staining of TNF-R1**

The surface expression of TNF-R1 and its mutated forms were analyzed by imaging flow cytometry using an ImageStream device (Amnis/EMD Millipore, Table 3). Therefore,  $1 \times 10^6$  cells per sample were cooled on ice for 20 min. During the cooling 10  $\mu$ l biotinylated TNF (0.005  $\mu$ g/ $\mu$ l, R&D systems, Table 5) was coupled to 1  $\mu$ l Avidin, AlexaFluor™ 488 conjugate (Table 5) on ice for 20 min. Afterwards, 10  $\mu$ l of TNF-AlexaFluor488 was added to each sample, snapped cautiously and incubated again on ice for 20 min. During incubation, CellMask™ Deep Red (dilution: 1:20,000; Table 5) was prepared in PBS and cells were rinsed once in 500  $\mu$ l CellMask™ Deep Red -PBS and incubate for 5 min on ice. After another washing step with 500  $\mu$ l PBS, pellets were sedimented and fixed in 2 % (v/v) PFA/PBS and stored on ice until analysis. For each sample at least 10,000 images were acquired by the Inspire software (Table 6) and evaluated with the Amnis IDEAS software (Table 6).

#### **3.2.24 Surface expression staining of TNF-R2**

For the detection of surface expression of TNF-R2 on U937 WT cells and TNF-R2 knockout cells,  $1 \times 10^6$  cells per sample were fixed by the addition of 3 % (w/v) glyoxal/PBS for 20 min on ice. Afterwards, cells were washed twice with 0.1 % (w/v) BSA/PBS. Subsequently, the primary antibody  $\alpha$ -TNF-R2 (1:200 in 0.1 % (w/v) BSA/PBS, Table 8) was added and incubated for 20 min on ice. After another twofold washing step with 0.1 % (w/v) BSA/PBS, secondary antibody  $\alpha$ -mouse-AlexaFluor™ 488 (1:200 in 0.1 % (w/v) BSA/PBS, Table 9) was incubated for another 20 min on ice. After a final twofold washing step with 0.1 % (w/v) BSA/PBS, cells were resuspended in 0.1 % (w/v) BSA/PBS and determined by ImageStream device (Amnis/EMD Millipore, Table 3) acquiring at least 10,000 images by Inspire software (Table 6) and analyzed with the Amnis IDEAS software (Table 6).

#### **3.2.25 Internalization assay**

To analyze the internalization of TNF-R1 and its mutants after TNF stimulation an ImageStream device (Amnis/EMD Millipore, Table 3) was used for imaging flow cytometry. For this,  $1 \times 10^6$  cells per sample were pre-cooled on ice for 20 min and if needed, pre-treated with inhibitors for 1 h on ice (50  $\mu$ M ML349; 75  $\mu$ M PalB, 50  $\mu$ M

### 3. Materials and Methods

---

2BrP, 75  $\mu$ M HDSF; Table 5). Meanwhile, for each sample 10  $\mu$ l biotinylated TNF (0.005  $\mu$ g/ $\mu$ l, R&D systems, Table 5) was coupled to 1  $\mu$ l Avidin, AlexaFluor™ 488 conjugate (Table 5) on ice and after incubation, 10  $\mu$ l TNF-AlexaFluor™ 488 mixture was added to the cells and incubated for 20 min on ice. For synchronized receptor internalization, samples were then incubated in pre-heated 37 °C water bath for the indicated time points (0, 30 min). The addition of ice-cold PBS added with CellMask™ Deep Red (dilution 1:20,000; Table 5) stopped internalization and 5 min incubation on ice stained membrane. Afterwards, cells were sedimented and fixed in 17  $\mu$ l 2 % (v/v) PFA/PBS and for each samples 10,000 images were acquired by the Inspire software (Table 6) and analyzed using the internalization wizard of the Amnis IDEAS software (Table 6).

#### 3.2.26 Immunofluorescence

For immunofluorescence  $1 \times 10^6$  HeLa80 cells were seeded into a well of a 6-well plate containing a fibronectin coated coverslip (BioCoat™, Table 5) and cultivated overnight under standard cell culture condition. On the next day, cells were washed twice with PBS, incubated for 10 min with 4 % (v/v) PFA/PBS at RT and washed again thrice with PBS for 5 min, respectively. Subsequently, cells were permeabilized by adding ice-cold methanol for 10 min at – 20 °C and washed thrice for 5 min each with PBS. Next, cells were blocked for 1 h in 4 % (w/v) BSA/PBS at RT and then incubated with primary antibody (1:200, Table 8) in 1 % (w/v) BSA/PBS overnight at 4 °C in a humidity incubation box (Table 3). The next day, cells were washed thrice with PBS for 5 min respectively and incubated with the secondary antibody coupled to AlexaFluor™ 488 (1:200, Table 9) in 1 % (w/v) BSA/PBS, containing Hoechst stain 33258 (2  $\mu$ g/ml, Table 5) for 1 h at RT. After three washing steps with PBS for 5 min, cells were rinsed in Milli-Q water, embedded in Fluoro-gel (Electron Microscopy Sciences, Table 5) and sealed with clear nail polish. Slides were stored at 4 °C until immunofluorescence analysis was performed with a confocal laser scanning microscope (LSM 510, equipped with an Axiovert 100M; Zeiss, Table 3) with a 63 $\times$  objective.

#### 3.2.27 Sucrose density gradient ultracentrifugation

To determine the localization of TNF-R1 and its mutated form C248S within the (plasma) - membrane, the sucrose gradient ultracentrifugation was used, adopted from Legler et al., 2003. Therefore,  $1 \times 10^8$  cells were sedimented at 500 x g, 4 °C for 5 min, washed once in 25 ml cold PBS, transferred into 1.5 ml tube and if needed, stimulated with TNF for 20 min at 37 °C. For lysis, cell pellet was resuspended in 1.5 ml TX buffer [25 mM Tris [pH 7.5], 150 mM NaCl, 5 mM EDTA, 1 % (v/v) Triton X-100, 1 x protease inhibitor cocktail

(Roche, Table 5)], incubated for 1 h on ice and homogenized by sonication (3 x20 sec with 10 sec break in between, constant output 2.5, 4 °C). Protein concentration was determined by BCA assay (section 3.2.3) and 2 mg of the cell lysate was adjusted to a volume of 1 ml using TX buffer and mixed with the same volume of 95 % (w/v) sucrose in buffer S (25 mM Tris, 150 mM NaCl, 5 mM EDTA, [pH 7.5]) and placed into ultracentrifugation tubes Ultra-Clear™ (Beckman Coulter®, Table 5): The cell lysate mixture was overlaid sequentially with 4 ml 35 % (w/v) sucrose and 4 ml 5 % (w/v) sucrose dissolved in buffer S and centrifuged for 16 h at 175,000 x g and 4 °C using a SW 60 Ti rotor (Beckman Coulter®, Table 3). Afterwards, 11 x 1 ml fractions (I – XI) were collected from the top of the gradient and 200 µl of fractions V to XI were used for SDS-PAGE and immunoblotting using antibodies against TNF-R1 and flotillin-2 (Table 8, section 3.2.4).

#### **3.2.28 PTE activity assay**

For PTE activity, APT specific probes were used provided from Kathayat et al., 2017 which were analyzed by Imaging flow cytometry (Amnis/EMD Milipore, Table 3). Therefore,  $1 \times 10^6$  U937 cells were pre-incubated for 10 min first at RT then on ice with 5 µM DPP-2 or DPP-3 fluorescence probes. Cells were then treated with 100 ng/ml TNF and incubated for another 20 min on ice. Activation was initiated by a temperature shift to 37 °C for the indicated time points (0, 5, 10, 15 min), followed by an immediate cooling and fixation in ice-cold 2 % (v/v) PFA/PBS. Plasma membrane was stained by CellMask™ Deep Red incubation (dilution: 1:10,000 in PBS, Table 5) for 5 min on ice and after a twofold washing in PBS, images were acquired by the Inspire software (Table 6) and changes in fluorescence intensity were determined using the IDEAS software (Table 6).

#### **3.2.29 Generation of APT2 knockdown cells**

APT2 knockdown cells of U937 cells were generated by Amaxa® nucleofection (section 3.2.9) using shRNA/plasmids (Santa Cruz Biotechnology, LYPLA2 shRNA, sc-78672-sh). Afterwards, cells were isolated by limiting dilution. Growing mutants were then selected for puromycin (1.5 µg/ml) and further characterized by SDS-PAGE and immunoblotting for APT2 (Table 8, section 3.2.4).

#### **3.2.30 Generation and purification of recombinant APT2**

For the generation of recombinant APT2 (rAPT2), protocol was adapted from Kathayat et al., 2017. Competent Mach1 T1<sup>R</sup> cells were transfected with the plasmid previously described in section 3.2.16. The plasmid was provided by the group of Prof. Bryan Dickinson, Department of Chemistry, University of Chicago, Chicago, Illinois, USA. One

### 3. Materials and Methods

---

colony was used to inoculate 5 ml LB medium (1 % (w/v) tryptone, 0.5 % (w/v) yeast extract, 1 % (w/v) NaCl, [pH 7.0]) of a sub culture which was cultured at 37 °C, 250 rpm until  $OD_{600} \approx 0.6$ . After that, 500 ml of LB medium supplemented with kanamycin (50 µg/ml, Table 4) was inoculated by the sub culture and incubated at 37 °C until  $OD_{600} \approx 0.6$ . Subsequently, 1 mM IPTG (Table 4) was added and the culture incubated at 22 °C, 250 rpm for 20 h. On the next day, culture was harvested by centrifugation at 5,000 x g, 4 °C for 10 min, pellet was resuspended in 25 ml lysis buffer (50 mM  $NaH_2PO_4$ , 300 mM NaCl, 10 % (v/v) glycerol, [pH 7.5]) and the solution was sonicated (10 x 10 sec with 10 sec break in between, constant waves, output 8.0). Cell debris was discarded by sedimentation at 3,800 x g, 4 °C for 5 min and supernatant was incubated with 2 ml TALON<sup>®</sup> metal affinity resin (Clontech Laboratories, Table 5) under gentle agitation for 1 h on ice. Afterwards, His-tagged proteins were purified under standard immobilized metal affinity chromatography (IMAC) by washing the column five times with 2 ml washing buffer (50 mM  $NaH_2PO_4$ , 300 mM NaCl, 10 mM imidazole, 5 % (v/v) glycerol, [pH 7.5]). For elution, 3 ml of elution buffer (50 mM  $NaH_2PO_4$ , 300 mM NaCl, imidazole (50, 150, 250 mM), 5 % (v/v) glycerol, [pH 7.5]) with increasing imidazole concentration (50, 150, 250 mM) was applied to the column respectively and fractions were collected separately. Each fraction was then desalted on a desalting column PD-10 (GE Healthcare, Table 5) according to manufacturer's instruction and rAPT2 was stored at -80 °C in storage buffer (50 mM Tris-HCl, 300 mM NaCl, 1mM DTT, 10 % (v/v) glycerol, [pH 7.5]). Each fraction was verified by SDS-PAGE and immunoblotting for purity by using antibodies against APT2 and His<sub>6</sub> (Table 8, section 3.2.4).

#### 3.2.31 rAPT2 activity assay

To verify the catalytic activity of recombinant APT2 *in vitro*, the activity assay adapted from Kathayat et al., 2017 was applied. Four triplicates of 5 µM DPP-2 in activity buffer (20 mM HEPES [pH 7.4, 150 mM NaCl, 0.1 % (v/v) Triton X-100) were added to a 96-well black flat-bottom plate and either activity buffer alone, activity buffer containing rAPT2, rAPT2 with PalB or PalB only were added to reach a final concentration of 200 nM rAPT2 and 50 µM PalB. Fluorescence intensities ( $\lambda_{ex}$ , 490/9 nm;  $\lambda_{em}$ , 545/20 nm; Gain, 70; no. of flashes, 25; integration time, 100 µs; and Z-position; 20,000 µm) were measured at 0 and 20 min. At the end an emission spectra was obtained ( $\lambda_{ex}$ , 485 nm;  $\lambda_{em}$ , 510–700 nm; Gain, 100; no. of flashes, 25; integration time, 100 µs; and Z-position, 20,000 µm) and data were analyzed by Microsoft Excel<sup>®</sup> 2010 (Table 6).

#### **3.2.32 *In vitro* depalmitoylation of TNF-R1 by rAPT2**

To analyze whether TNF-R1 is depalmitoylated by recombinant APT2 *in vitro*, purified rAPT2 was pre-incubated with the crude membrane fraction for 2 h at 37 °C followed by an acylRAC and Western blot analysis using an antibody against TNF-R1 (Table 8, section 3.2.5 and 3.2.4).

#### **3.2.33 Caspase-3 activity assay**

$5 \times 10^6$  cells were incubated with the inhibitors ML349 (25  $\mu$ M, Tocris, Table 5) and GW4869 (2  $\mu$ M, Sigma Aldrich, Table 5) for 30 min at 37 °C, followed by a 4 h treatment with 100 ng/ml TNF under cell culture conditions. Afterwards, cells were centrifuged (450 x g, 4 °C, 5 min), lysed in CL buffer (10 mM HEPES [pH 7.4], 5 mM MgCl<sub>2</sub>, 1 mM EDTA, 0.2 % (v/v) NP-40, 2 mM Pefabloc<sup>®</sup> SC (AEBSF), 1 mM DTT (freshly added)) and protein concentration was determined by BCA assay (section 3.2.3). 5  $\mu$ g of total cell lysate was then incubated with 100  $\mu$ l assay buffer (20 mM PIPES [pH 7.2], 100 mM NaCl, 1 mM EDTA, 0.1% (w/v) CHAPS, 10% (w/v) Sucrose, 10 mM DTT (freshly added)) containing 100  $\mu$ M zDEVD-AFC (AAT Bioquest, Table 5) and fluorescence intensity (ex: 405 nm/em: 505 nm) was monitored at 10 min time interval for 70 min using an Infinite<sup>®</sup> M200 (Tecan Group Ltd., Table 3) plate reader at 37 °C.

#### **3.2.34 Ceramide detection assay**

Ceramide production was determined by Imaging flow cytometry (Amnis/EMD Milipore, Table 3) using an  $\alpha$ -ceramide antibody (clone 15B4). Therefore,  $5 \times 10^6$  cells were either incubated with ML349 (50  $\mu$ M, Tocris, Table 5) and GW4869 (10  $\mu$ M, Sigma Aldrich, Table 5) or left untreated for 30 min at RT with a subsequent 20 min incubation on ice. After pelleting (450 x g, 4 °C, 5 min) cells were treated with 100 ng/ml TNF and incubated again for 20 min on ice. Afterwards, cells underwent a temperature shift to 37 °C for 15 min and were then fixed in 2 % (v/v) PFA/PBS for 15 min on ice. After washing them twice with 0.1 % (w/v) BSA/PBS, cells were permeabilized in 0.2 % (w/v) saponin/0.1 % (w/v) BSA/PBS for 15 min on ice and subsequently washed twice with 0.1 % (w/v) BSA/PBS. Next,  $\alpha$ -ceramide antibody (1:100 in 0.1 % (w/v) BSA/PBS, Table 8) was incubated for 30 min on ice and after a twofold washing  $\alpha$ -mouse-AlexaFluor<sup>™</sup> 488 antibody (1:200 in 0.1 % (w/v) BSA/PBS; Table 9) was incubated for 30 min on ice. After another twofold washing in 0.1 % (w/v) BSA/PBS, cell images were acquired using the Inspire software (Table 6) and alterations in fluorescence intensity was evaluated by the IDEAS software (Table 6).

## 4. Results

### 4.1 Palmitoylation of TNF-R1

#### 4.1.1 Inhibition of (de)-palmitoylation interferes with TNF-R1 internalization

To investigate whether palmitoylation is connected to the TNF-R1 itself or to the signal transduction, receptor internalization assays were performed either with a palmitoylation inhibitor (2BrP) or depalmitoylation inhibitors (PalB, HDSF) under the supervision of Dr. Jürgen Fritsch. After a pre-incubation of the inhibitors of 30 min to the cell culture, cells were treated with biotinylated TNF and incubated at 37 °C for 30 min.

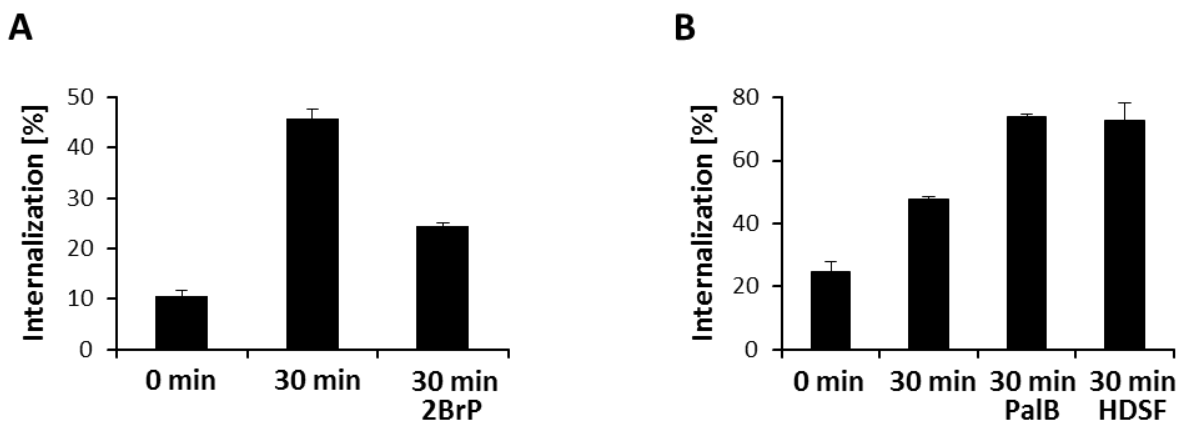
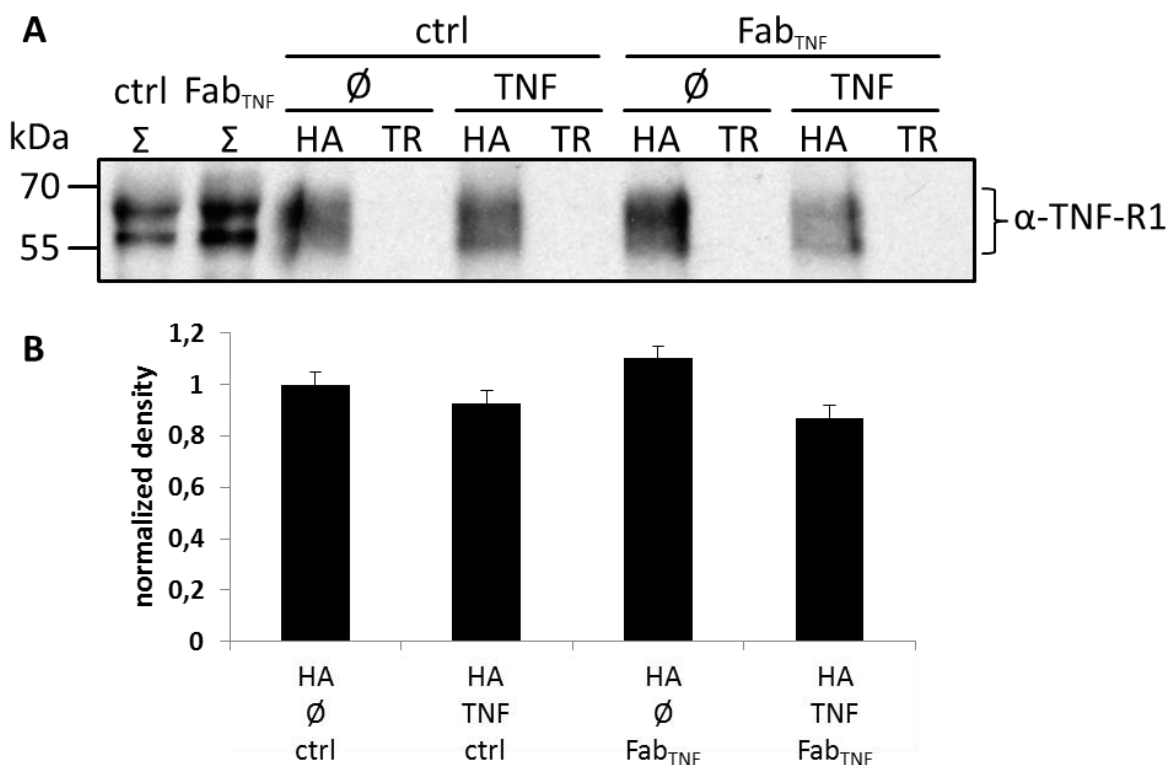


**Figure 6: Internalization of TNF-R1 in U937 cells pre-incubated with (de)-palmitoylation inhibitors.** For the analysis of the TNF-R1 internalization, cells were kept on ice and receptors were labeled with biotinylated TNF coupled to an avidin linked fluorescence dye. Internalization was initiated by temperature shift to 37 °C for 30 min. **A**, Internalization of TNF-R1 pre-treated (30 min) with palmitoylation inhibitor 2-Bromoplamate (2BrP; 50  $\mu$ M). Pre-incubation with 2BrP decreases TNF-R1 internalization approximately by half compared to untreated receptors (n=3; +/- SD). **B**, Internalization of TNF-R1 pre-treated (30 min) with depalmitoylation inhibitor Palmostatin-B (PalB; 75  $\mu$ M) or Hexadecylsulfonyl Fluoride (HDSF, 75  $\mu$ M). Blocking depalmitoylation by either PalB or HDSF increase TNF-R1 internalization by third compared to non-inhibitor treatment (n=3; +/- SD).

As shown in figure 6, A, TNF treatment increased internalization by 4 times (30 min) compared to untreated cells (0 min), whereas samples pre-treated with palmitoylation inhibitor (2BrP) showed only a twofold increase of internalization compared to untreated cells. In contrast, internalization of the depalmitoylation inhibitor treated cells (PalB, HDSF, Figure 6, B) revealed a higher internalization rate as the TNF treated cells approximately by third. Both experiments showed that palmitoylation modulates the TNF-R1 signal transduction.

#### 4.1.2 Long term Fab<sub>TNF</sub> stimulation revealed a constitutively palmitoylation of TNF-R1

To clarify the question whether TNF-R1 is palmitoylated itself and if so whether it is either constitutively or inducibly palmitoylated, the following experiments were implemented together with Vinzenz Särchen: U937 cells were treated for 2 weeks with an anti-TNF Fab fragment, which captures endogenous TNF from the cell culture supernatant. After the long term incubation, normal cultivated U937 cells and Fab<sub>TNF</sub> treated cells were stimulated with TNF for 10 min and acylRAC was performed. Figure 7, A, shows the Western blot of this experiment, probed against TNF-R1. In the cell lysates which serve as an input control, the typical pattern of TNF-R1 can be seen in equal intensities, consisting of two bands, one at ≈55 kDa and the other at ≈60 kDa. In the hydroxylamine (HA) treated samples, palmitate is cleaved resulting in a reactive thiol group which can bind to the thiopropyl sepharose beads. There, the signal for TNF-R1 could be detected between 55 and 70 kDa, indicating TNF-R1 is palmitoylated. The Tris (TR) treated samples serve as negative control since no reactive group is formed and the lanes were devoid of any signal. The comparison of the HA signal intensities of untreated U937 cells and Fab<sub>TNF</sub> treated cells with or without TNF stimulation revealed no significant difference, which was further corroborated by the densitometric quantification of Western blots (Figure 7, B), indicating that TNF-R1 is palmitoylated even in the absence of TNF. Interestingly, TNF treated fractions showed a slight decrease in signal intensity compared to the untreated HA fraction.



## 4. Results

**Figure 7: AcylRAC of untreated U937 and Fab<sub>TNF</sub> treated U937 cells.** U937 cells were either cultured with Fab<sub>TNF</sub> (0.5 µg/ml) for two weeks or left untreated (U937 ctrl) and were then either stimulated with TNF for 10 min (TNF) or left unstimulated (∅). **A**, AcylRAC was performed using 2 mg of total protein. Western blots were performed from 25 µl of acylRAC eluates and probed for TNF-R1. Comparison of the hydroxylamine fraction (HA) bands, signal intensities showed no significant change between untreated U937 and Fab<sub>TNF</sub> treated cells. Cell lysate (Σ) served as input control. Tris fractions (TR) served as a negative control and were devoid of signal. **B**, Densitometric quantification of the Western blots of acylRAC HA bands, normalized to the unstimulated HA sample (∅) of U937 ctrl. In comparison to the U937 ctrl no significant change in the Fab<sub>TNF</sub> incubated U937 cells was observed. However, signal in TNF treated cells of both cell cultures showed a slightly decrease compared to unstimulated cells. (n=3; +/- SD).

### 4.1.3 Generation of TNF-R1 knockout U937 cells

To further study TNF-R1 palmitoylation, TNF-R1 knockout U937 cells were generated by CRISPR/Cas9. In figure 8, A, three clones (#17, #9 and #22) of the CRISPR/Cas9 knockout are shown, all lacking the typical TNF-R1 band at approximately ≈55 kDa (red arrow head in U937 lane). This was verified by two different antibodies against TNF-R1 (C25C1, H5). Tubulin served as loading control. To functionally validate the knockout in the clones, apoptosis assays were performed (Figure 8, B), showing that TNF induced apoptosis induction was prevented in these cells. In WT U937 cells, the apoptotic rate increased up to 50 % after TNF treatment. To further confirm the TNF-R1 knockout, palmitoylation of possibly still existing TNF-R1 residues were determined by acylRAC, probing for TNF-R1 (Figure 8, C, showing only #22). In clone #22 no bands in all three lanes (MF, ∅ and TNF) could be detected for TNF-R1. CD71 blot served as a loading control, interestingly, showing stronger signals in the lanes of clone #22. For clones #17 and #9, TNF-R1 signal was lost at the molecular weight of 55 kDa but smaller bands appeared at 40 kDa (data not shown).



## 4. Results

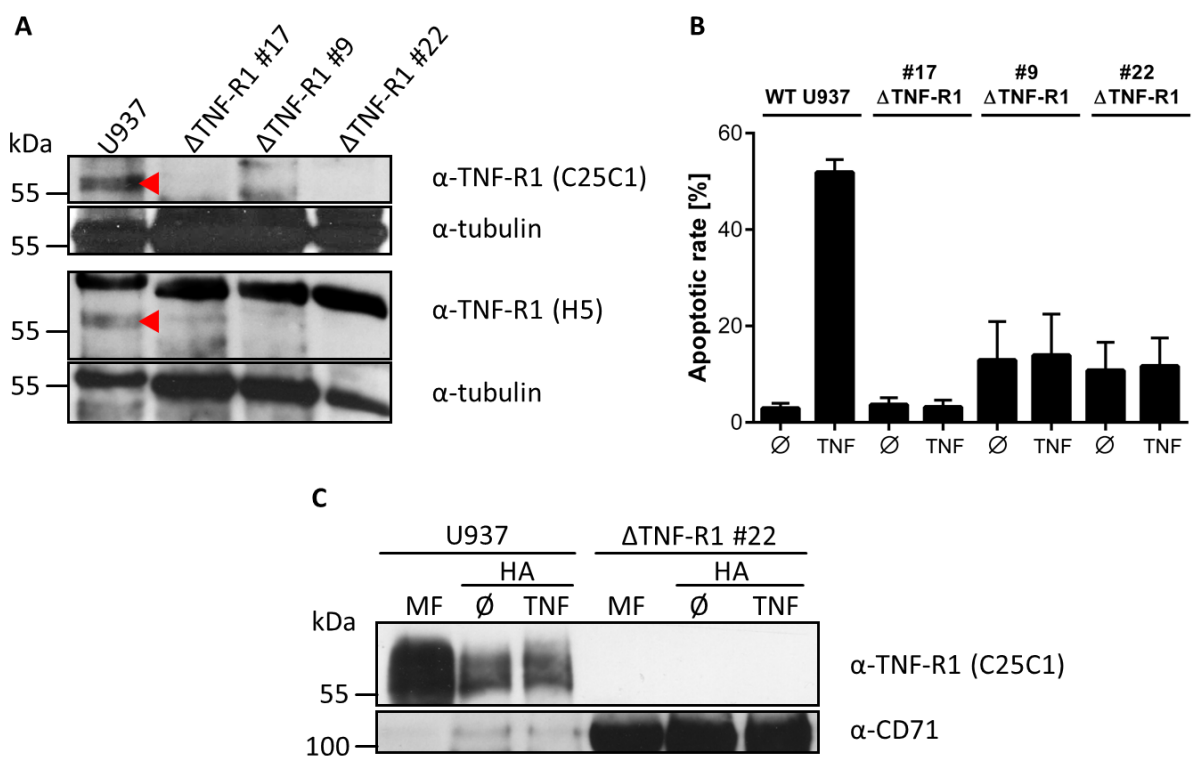


**Figure 8: Generation of TNF-R1 knockout U937 cells.** **A**, Western blot analyses of whole cell lysates from WT U937 cells and CRISPR/Cas9 clones (#17, #9 and #22, 25  $\mu$ g/lane) were performed. Blots were probed using two different TNF-R1 antibodies (C25C1, H5) to determine the deficiency of TNF-R1 in the generated clones. In all three candidates the signal for TNF-R1 at 55 kDa was absent. Detection of tubulin served as a loading control. **B**, For the apoptosis assay, cells were treated with 100 ng/ml TNF over a time course of 20 h to induce cell death. Untreated cells served as a negative control. In comparison to the WT U937 cells where TNF induced cell death in up to 50 % of the cells, the TNF-R1 knockout clones showed no apoptosis induction (n=3; +/- SD). **C**, AcylRAC of WT U937 cells and TNF-R1 knockout clone #22. For both cell lines, cells were either treated with 100 ng/ml TNF (TNF) for 60 min or left unstimulated ( $\emptyset$ ) before implementing the acylRAC with 2 mg of total protein. Western blots were performed from 25  $\mu$ l of acylRAC eluate and probed for TNF-R1 and CD71. Membrane fractions (MF, 30  $\mu$ g of total protein) served as input controls. Compared to WT fractions, lanes of clone #22 were completely devoid of signal. CD71 blot served as a loading control.

### 4.1.4 Determination of putative cysteines responsible for TNF-R1 palmitoylation

To determine the TNF-R1 palmitoylation site, six putative cysteines in the cytoplasmic domain of the receptor could be found (Figure 9, A). Based on an algorithm, predicting the putative palmitoylation sites of TNF-R1 and on previous reports of other TNF receptor superfamily members such as CD95 and DR4, where the palmitoylation site is in close proximity to the transmembrane domain, three cysteines (C223, C248, and C304) close to the TMD were chosen for mutagenesis experiments (Figure 9, B; Ren et al., 2008; Charollais and van der Goot, 2009; Blaskovic et al., 2013). Since the sheer presence of the DD can already cause apoptosis in some cell lines such as U937, a shorter form of TNF-R1 lacking the DD was generated termed as  $\Delta$ DD (Figure 9, C). Additionally, a triple FLAG tag was added to the C-terminus of the receptor for better detection. The three juxta-membranous cysteines were then mutated to serine, cloned into a retroviral transfer

## 4. Results

vector and transduced into the TNF-R1 knockout U937 clone #22. There, expression of mutated TNF-R1 could be detected in 9 out of 16 mutants by Western blots probed for TNF-R1 (Figure 10, 11). Rescue of WT TNF-R1 in U937 cells appeared lethal, since all cells died within two days in several attempts, even without selection for puromycin. The remaining other six mutant TNF-R1 expressing cells grew in the selection medium in several attempts, but never showed signals for TNF-R1 in WB.

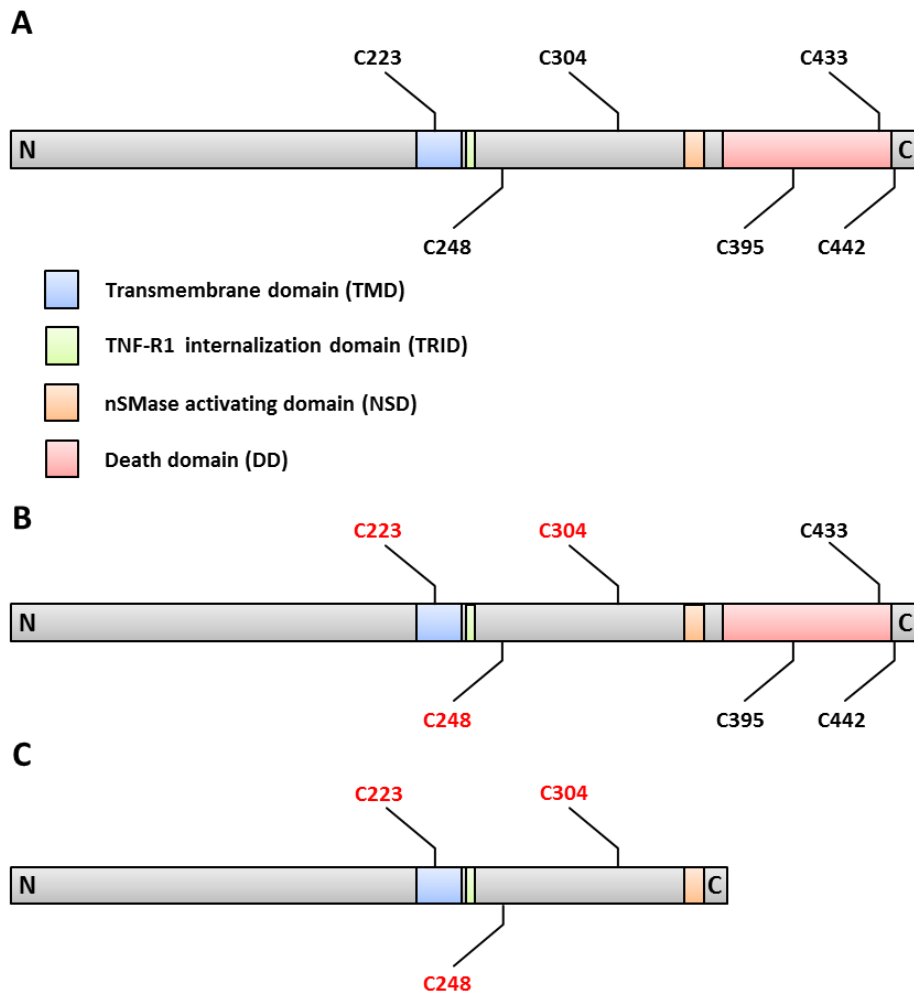


**Figure 9: Topology model of Tumor Necrosis Factor Receptor-1.** **A**, Topology of TNF-R1 from N to C-terminus. The respective cysteines in the cytoplasmic domain are labeled. Specific domains are highlighted in different colors, such as the transmembrane domain in blue, TNF-R1 internalization domain in green, nSMase domain in orange and death domain in red. **B**, Topology model showing the three putative palmitoylation sites of TNF-R1, highlighted in red front. **C**, Topology model of the short form of the TNF-R1 lacking the death domain.

### 4.1.5 Expression of mutant TNF-R1 in TNF-R1 knockout U937 cells

Figure 10 and 11 depict the Western blots showing whole cell lysates of the generated mutants probed against TNF-R1 and FLAG. In the first lane, lysate of WT U937 cells served as a positive control and shows the typical band pattern for TNF-R1 in the TNF-R1 blot (top), whereas the anti-FLAG blot (bottom) was devoid of signal, as expected. TNF-R1

#### 4. Results

knockout U937 cells served as a negative control and lack any signal for the receptor in both blots. In the other lanes, signals at the predicted molecular weight for TNF-R1 could be detected and are marked with red arrow heads. Three mutant receptors (C248S, C223S/C248S and C248S/C304S) represent the WT receptor length at 55 kDa (Figure 11), whereas the short form mutants could be detected at 39 kDa. However, several bands at other molecular weights could be detected as well (Figure 10, 11).

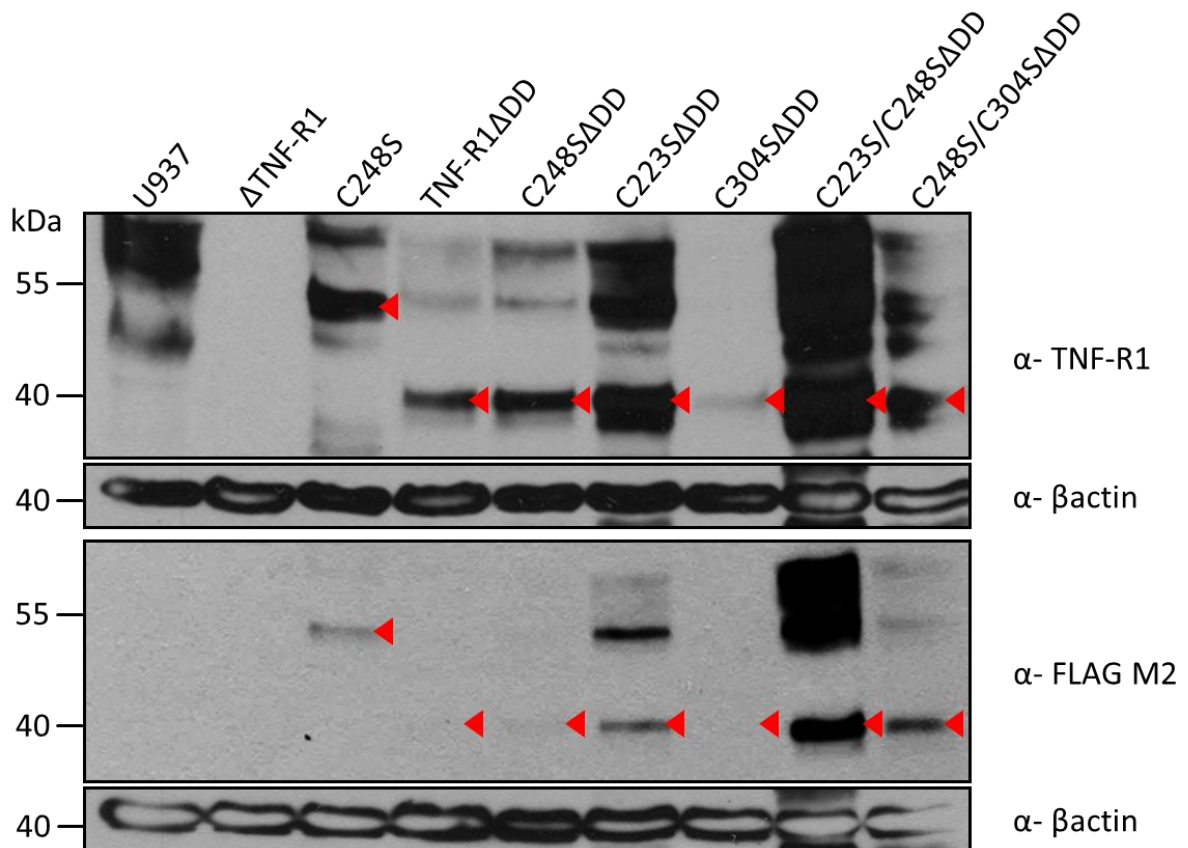


**Figure 10: Western blot for TNF-R1 mutants in TNF-R1 knockout U937 cells.** **Top**, Western blot was performed of whole cell lysates (80  $\mu$ g/lane). The blot was probed for TNF-R1. Endogenous WT receptor served as a positive control with the typical band pattern at 55 kDa. TNF-R1 knockout U937 cell lysate served as a negative control and was devoid of signal. Indicated TNF-R1 mutants show the predicted size of the receptor at 55 kDa for WT length or at 39 kDa for  $\Delta$ DD (red arrow heads). Detection of actin served as a loading control. **Bottom**, Western blot was performed of whole cell lysates (80  $\mu$ g/lane). The blot was probed for FLAG using the M2 antibody. WT U937 and TNF-R1 knockout U937 cells are devoid of signal. Transduced TNF-R1 mutants show the same band pattern as in the TNF-R1 blot (top) at 55 kDa or 39 kDa for WT length or  $\Delta$ DD forms (red arrow heads). Detection of actin served as a loading control.

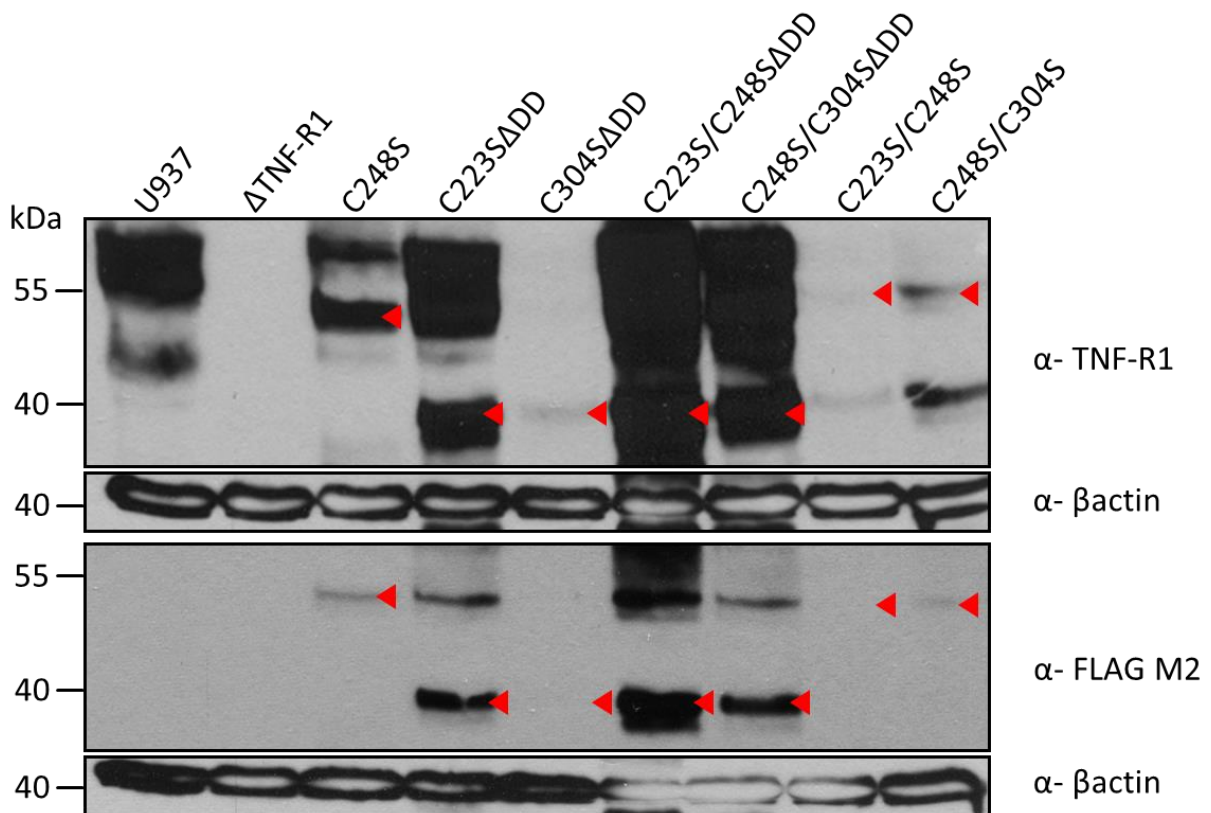


**Figure 11: Western blot of for TNF-R1 mutants in TNF-R1 knockout U937 cells.** **Top**, Western blot was performed from whole cell lysates (80  $\mu$ g/lane). The blot was probed for TNF-R1. Endogenous WT receptor served as a positive control with the typical band pattern at 55 kDa. TNF-R1 knockout U937 cell lysate served as a negative control and was devoid of signal. Indicated TNF-R1 mutants show the predicted size of the receptor at 55 kDa for WT length or at 39 kDa for  $\Delta$ DD (red arrow heads). Detection of actin served as a loading control. **Bottom**, Western blot was performed of whole cell lysates (80  $\mu$ g/lane). The blot was probed for FLAG using the M2 antibody. WT U937 and TNF-R1 knockout U937 are avoid of signal. Transduced TNF-R1 mutants show the same band pattern as in the TNF-R1 blot (top) at 55 kDa or 39 kDa for WT length or  $\Delta$ DD forms (red arrow heads). Detection of actin served as a loading control.

#### 4.1.6 AcylRAC of mutant receptor expressing cells revealed double or triple palmitoylation of TNF-R1

To verify the palmitoylation sites in the TNF-R1 overexpressing cells, acylRACs were performed, shown in figure 12. WT receptor served as a positive control, where the receptor specific signal in the HA fraction at 55 kDa confirmed palmitoylation. TNF-R1 knockout U937 cells served as a negative control showing no signal for TNF-R1 in all fractions. In all other mutant receptor expressing cells, the receptor specific signal in the HA fractions revealed that palmitoylation still occurs. Since all three single mutants showed a signal in the HA fraction, it can be assumed that TNF-R1 is either double or triple palmitoylated.

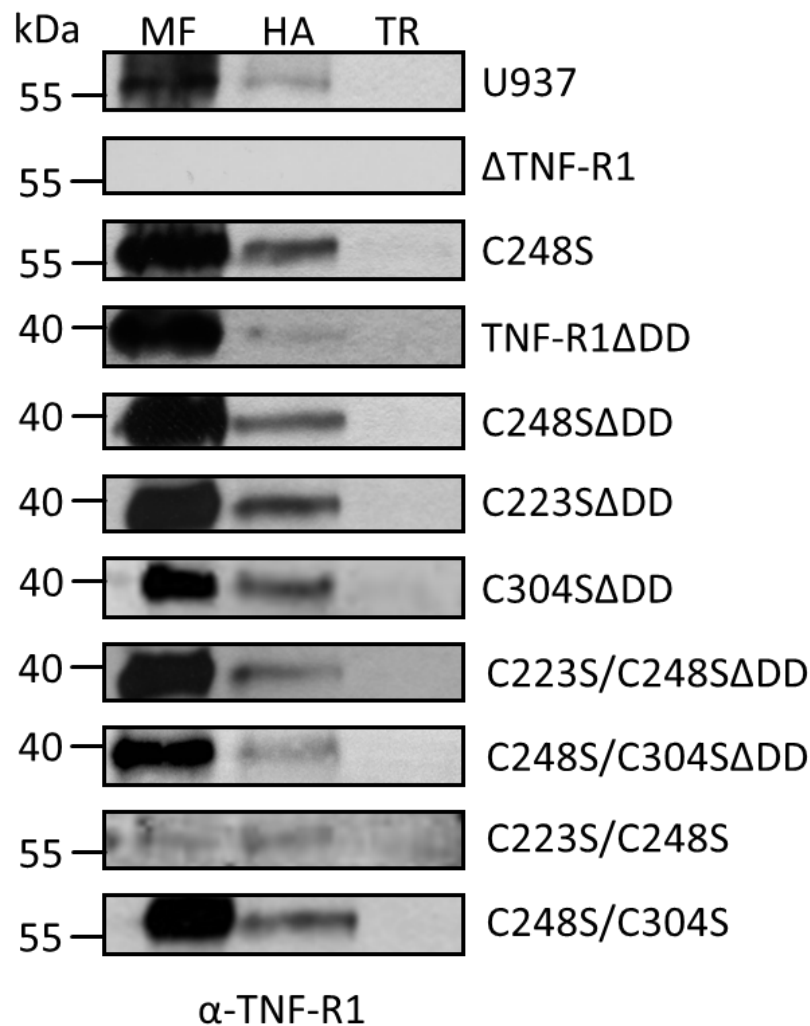


**Figure 12: AcylRAC of WT U937,  $\Delta$ TNF-R1 and mutant TNF-R1 expressing cells.** AcylRAC was performed using 2 mg of total protein. Western blots were performed from 25  $\mu$ l of acylRAC eluate and probed for TNF-R1. Membrane fraction (MF, 30  $\mu$ g of total protein) served as an input control. Lysate from cells expressing WT receptor served as a positive control and confirmed TNF-R1 palmitoylation. TNF-R1 knockout U937 cells served as a negative control and show no signal in all three fractions. Cells expressing the different mutant forms of TNF-R1 also show signal in the hydroxylamine (HA) fraction which demonstrates receptor palmitoylation. Tris (TR) fraction served as a negative control and was devoid of signal.

#### 4.1.7 Mutant receptor C248S reveals apoptosis rescue

To investigate if transfection results in an apoptosis phenotype resembling the WT TNF-R1, apoptosis assays were performed with all mutant receptor expressing cells as well as WT U937 and TNF-R1 knockout U937 cells. Figure 13 shows the apoptotic rate of each receptor mutant compared to WT and TNF-R1 knockout U937 cells. TNF treatment of WT U937 cells lead to an increase of apoptotic cells up to approximately 50 %, whereas TNF-R1 knockout U937 cells showed no response to TNF. For all cells expressing the long form mutant receptor (C248S, C223S/C248S and C248S/C304S), only C248S cells showed a partial rescue by an increase of apoptosis by half of the WT with approximately 22 %. The two other long form expressing cells (C223S/C248S and C248S/C304S) show no difference in apoptosis compared to unstimulated cells. Although short form receptors are unable to

## 4. Results

induce apoptosis due to the lack of the DD, nevertheless they were screened for verification and assumption was confirmed as there was no increase in apoptosis.

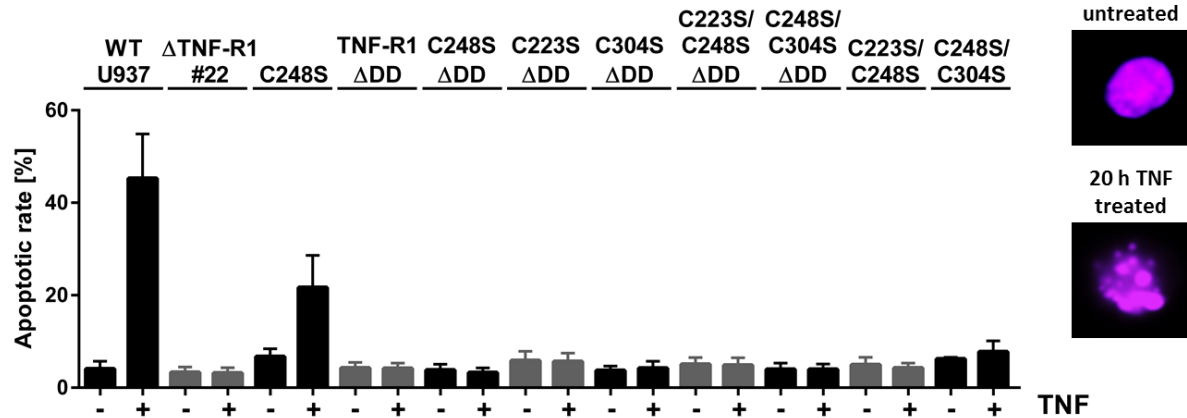


**Figure 13: Apoptosis assay of mutant TNF-R1 expressing cells.** For apoptosis induction, cells were treated with 100 ng/ml TNF for 20 h and nuclear fragmentation was determined. WT U937 cells serve as a positive control, showing apoptosis induction in approximately 50 % of the cells. TNF-R1 knockout U937 cells serve as a negative control and show no response to TNF. For long form receptors, only C248 showed an increase in apoptosis by half of WT with approximately 22 %. The two other long form receptors C223S/C248S and C248S/C304S show no response to TNF. Short form receptors (ΔΔΔ) showed no difference in apoptosis after TNF treatment compared to unstimulated cells. On the right side, pictures of the cell nucleus are shown either untreated (top) or TNF treated (bottom), visualizing the nuclear fragmentation. TNF treatment is visualized by highlighting samples either as untreated (-) or TNF treated (+), (n=13; +/- SD).

### 4.1.8 Mutagenesis of putative cysteines affects NF-κB activation in U937 cells

Since apoptosis appears to be impaired due to the mutation of specific cysteines in the TNF-R1 sequence, NF-κB activation was investigated next analyzing IκBα-degradation. Figure 14 depicts the IκBα blots with their respective tubulin control blot. For WT TNF-R1, the signal for IκBα decreases within 30 min after TNF treatment until a faint band is left and signal started to recover after 45 min. In the TNF-R1 knockout cells, a constant signal for IκBα can be detected without any change at the indicated time points. For mutant C248S the signal is slightly decreased within 15 min of TNF treatment and restored afterwards. For the other two long form receptors C223S/C248S and C248S/C304S, no change in signal intensity of IκBα could be detected. For all other short form mutants, no significant decrease in the signal intensities of IκBα could be distinguished as expected due to the lack of the DD. All tubulin blots show a consistent loading with same amounts of protein for each lane.

## 4. Results

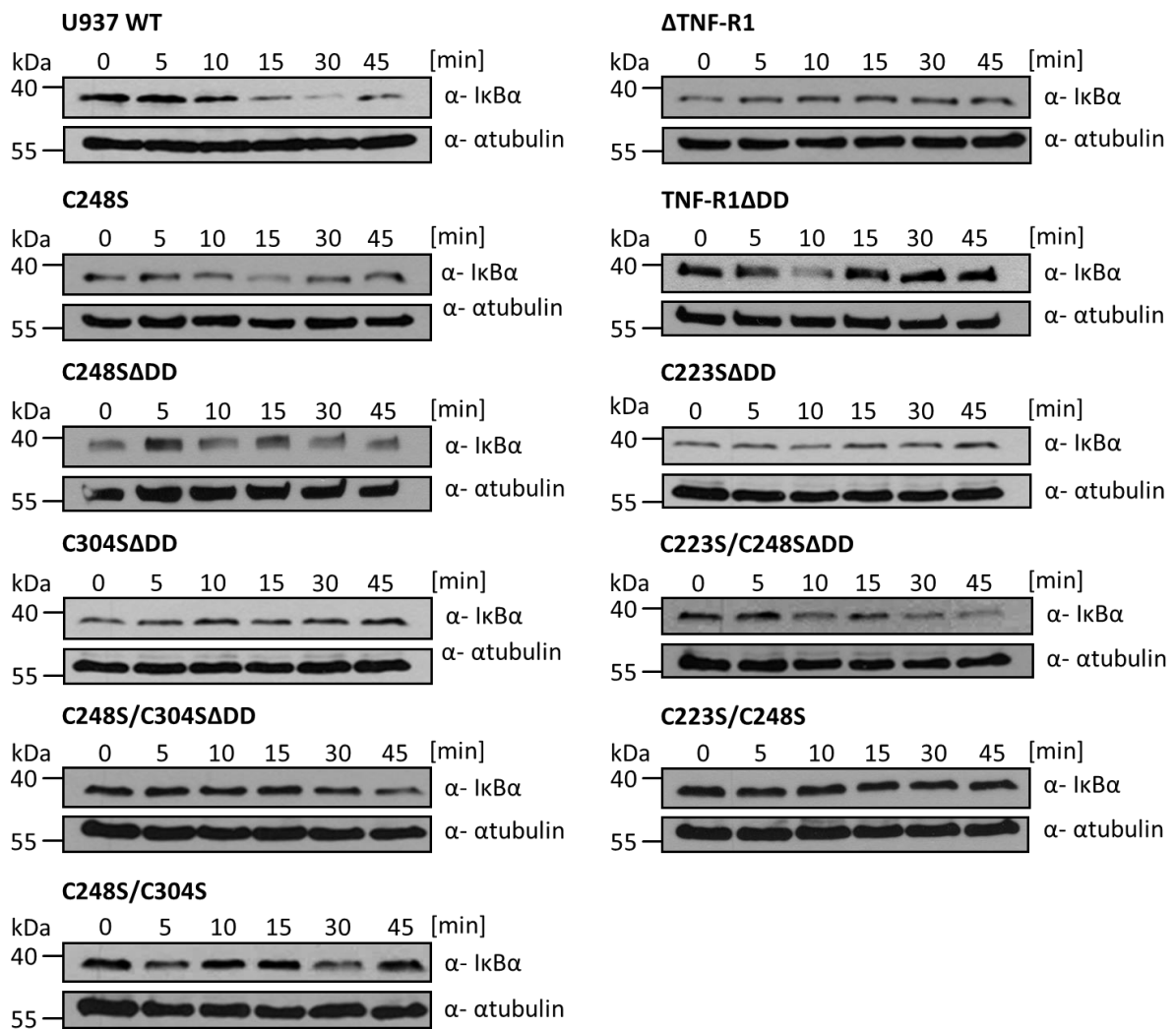


**Figure 14: IκBα degradation of WT U937, ΔTNF-R1 and mutated TNF-R1 expressing cells.** IκBα degradation was initiated by treating the respective cells with 100 ng/ml TNF for the indicated time points at 37 °C. Western blots were performed of whole cell lysates (40 μg/lane) and probed for IκBα. WT U937 cells served as a positive control for IκBα degradation where the signal decreased within 30 min of TNF stimulation. TNF-R1 knockout U937 cells served as a negative control and show no change in signal intensity during incubation time. C248S expressing cells show a slight decrease in signal intensity of IκBα at 15 min. Two other long form receptors (C223S/C248S, C248S/C304S) show no change in signal intensities. As expected, short form receptors show no alteration in signal intensities. Detection of tubulin served as a loading control.

### 4.1.9 Mutagenesis of cysteines alters surface expression but not the ability for internalization

To examine whether the signaling or the TNF-R1 presence at the cell surface is responsible for the altered outcome of apoptosis and NF-κB activation after TNF treatment, surface expression and internalization of the receptors were further analyzed. Surface expression of WT and mutant receptors is shown in figure 15 where the normalized frequency is plotted against the fluorescence intensity. Therefore, cells were kept on ice and plasma membrane receptors were labeled with biotinylated TNF coupled to an avidin conjugated fluorescence dye. TNF-R1 knockout U937 cells served as a

#### 4. Results

---

negative control (red graph), showing no signal for TNF-R1. WT receptor served as a positive control (bright green graph) whereof mutant receptors were compared. To exclude unspecific binding of the avidin conjugated fluorescence dye to the plasma membrane, WT U937 cells were incubated with the avidin conjugated fluorescence dye alone, showing the same fluorescence intensity pattern as the TNF-R1 knockout U937 cells but in a reduced frequency (blue graph). The comparison of WT receptor to the mutant receptors revealed that none of the mutant receptors gained the same fluorescence intensity of the WT receptor, except for C223S/C248S $\Delta$ DD. All other mutant receptors show diminished fluorescence intensity, suggesting a lower expression of mutant receptors at the cell surface.



## 4. Results

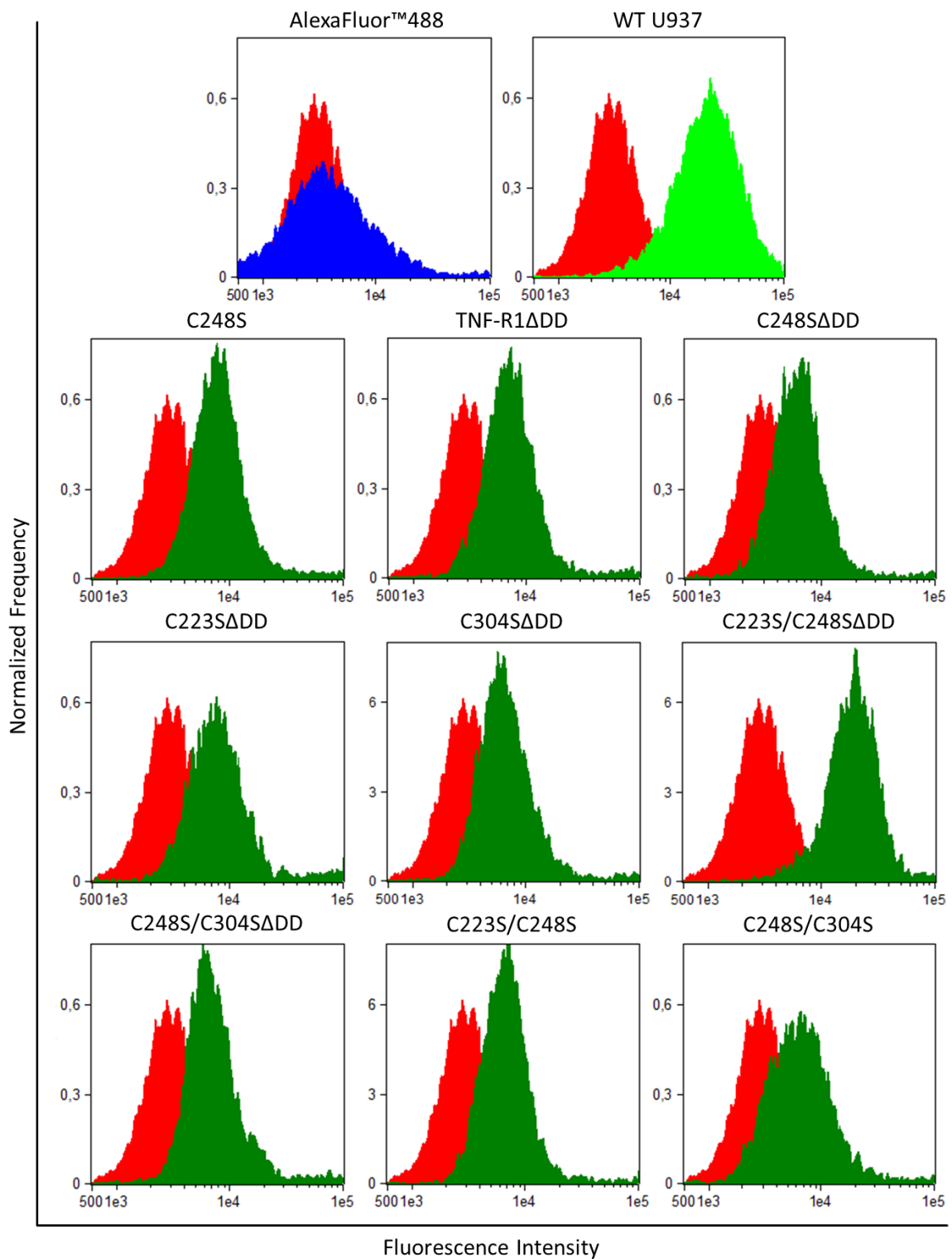


**Figure 15: Surface expression of WT and mutant TNF-R1 in U937 cells.** For the analysis of the TNF-R1 surface expression, cells were kept on ice and receptors were labeled with biotinylated TNF coupled to an avidin linked fluorescence dye. For each sample at least 10,000 images were acquired by the Inspire software (Amnis) and evaluated with the Amnis IDEAS software. The normalized frequency is plotted against the fluorescence intensity. TNF-R1 knockout U937 cells served as a negative control (red graph) and show no significant fluorescence intensity for TNF-R1. Sample only incubated with fluorescence dye is shown as blue graph and excludes unspecific binding of the fluorescence dye to the plasma membrane. WT receptor is shown in bright green, indicating a strong surface expression due to higher fluorescence intensity. Mutant receptors (dark green graphs) show lower fluorescence intensity compared to the WT receptor, except for C223S/C248S $\Delta$ DD which is similar to WT receptor. One representative experiment is shown (n=5).

## 4. Results

For the internalization assay, cells were labeled in the same manner as for surface expression, however, after ligand binding, an additional temperature shift to 37 °C initiated internalization. Figure 16 depicts the internalization potential of WT and mutant receptors. As seen in figure 16, all cells are able to internalize the receptor from its cell surface, since no significant change in the internalization behavior after TNF treatment appeared in mutant receptors compared to WT receptor.

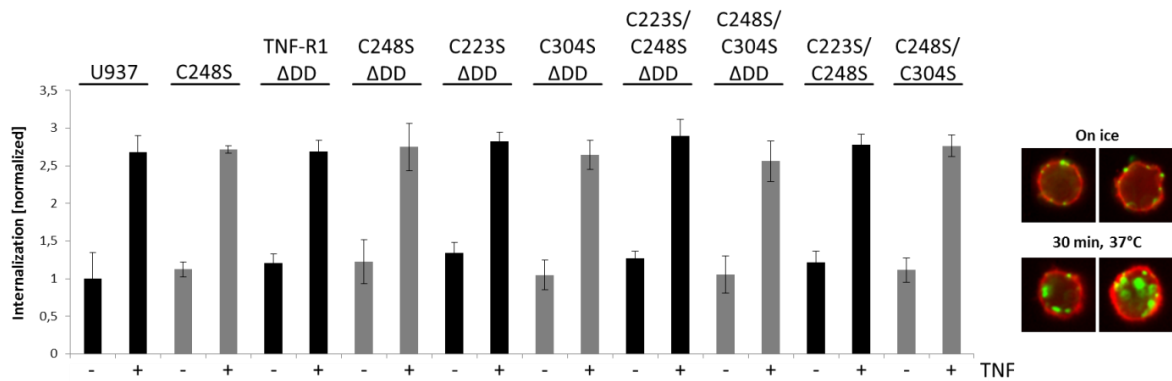


**Figure 16: Internalization of WT and mutant TNF-R1 in U937.** **Left**, For the analysis of the TNF-R1 internalization, cells were kept on ice and receptors were labeled with biotinylated TNF coupled to an avidin linked fluorescence dye. Internalization was initiated by temperature shift to 37 °C for 30 min. Normalized internalization score is shown for each receptor and internalization is represented by the treatment with TNF (bottom line, TNF +). The diagram shows comparable internalization scores of all mutant receptors to WT receptor (n=3; +/- SD). **Right**, two representative cell images of internalization in response to activation by TNF either kept on ice (top) or after 30 min internalization at 37 °C (bottom), TNF/TNF-R1: green, plasma membrane: red.

### 4.1.10 Verification of TNF-R1 knockout HeLa80 cells

Knockout cells of TNF-R1 in HeLa80 cells were provided by H. Wajant, university of Würzburg, Germany. Western blot of TNF-R1 knockout HeLa80 cells approved knockout using different TNF-R1 antibodies (C25C1, H5, Figure 17, A). Additionally, immunofluorescence of HeLa80 WT and  $\Delta$ TNF-R1 HeLa80 validated the knockout, since only a weak background signal from TNF-R1 in HeLa80 knockouts could be detected, compared to WT HeLa80 cells where TNF-R1 was strongly expressed (Figure 17, B).

## 4. Results

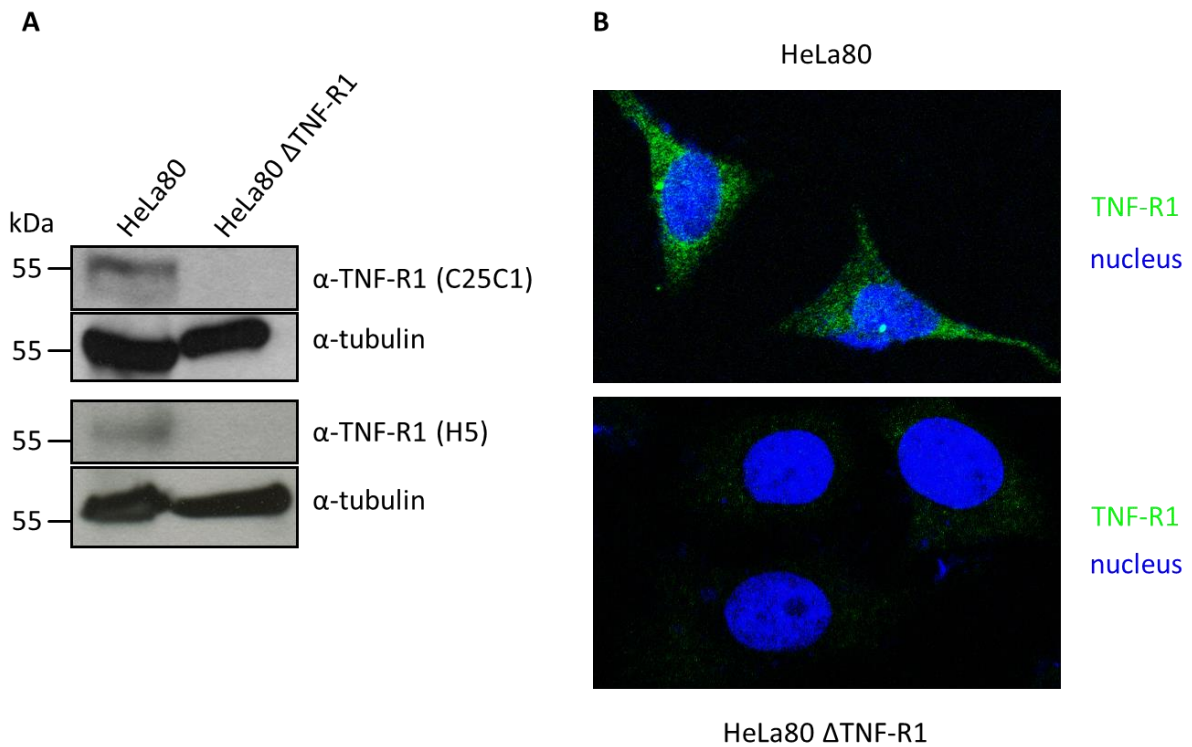
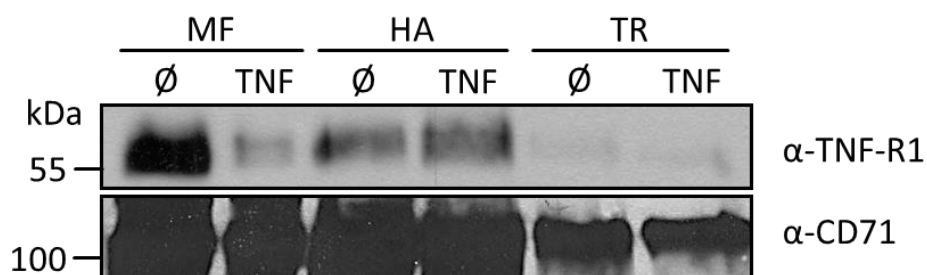


**Figure 17: Verification of TNF-R1 deficiency in HeLa80 cells by Western blot and immunofluorescence.** **A**, Western blot analyses were performed of whole cell lysates from WT HeLa80 and TNF-R1 knockout HeLa80. Blots were probed using two different TNF-R1 antibodies (C25C1, H5) to determine the lack of TNF-R1. In TNF-R1 knockout HeLa80 cells signal for TNF-R1 at 55 kDa was absent. Detection of tubulin served as a loading control. **B**, Immunofluorescence of WT HeLa80 (top) and TNF-R1 knockout HeLa80 cells (bottom). TNF-R1 is stained in green by fluorophore coupled antibody staining. Cell nucleus is stained in blue by Hoechst staining. In comparison to WT HeLa80 where TNF-R1 was strongly detectable at the cell's surface, TNF-R1 knockout HeLa80 cells show a weak signal for TNF-R1.

### 4.1.11 TNF-R1 palmitoylation also occurs in HeLa80

To ensure that the current results from U937 cells are consistent within other cell lines, HeLa80 cells were used for the aforementioned palmitoylation experiments of TNF-R1. To verify the palmitoylation status of TNF-R1 also in HeLa80 cells, acylRAC was performed with untreated and 90 min TNF treated cells, shown in figure 18. Palmitoylation of TNF-R1 was confirmed in HeLa80 cells, since signal with same intensity in the untreated and TNF treated HA fractions were detectable whereas TR was devoid of signal.

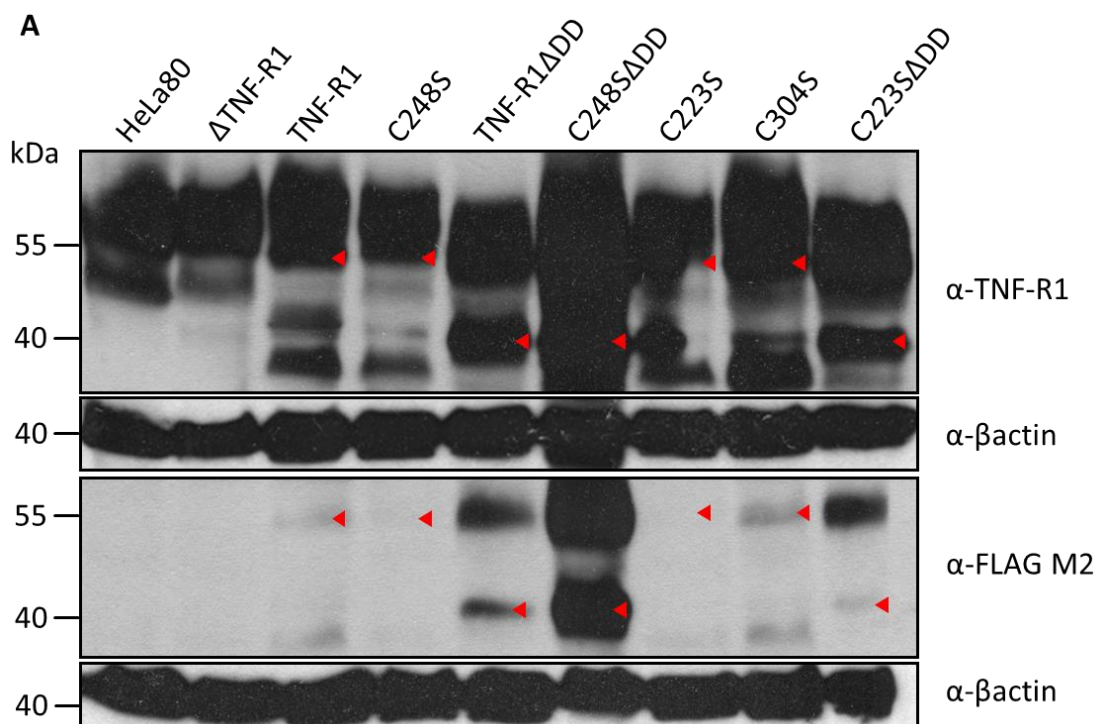


## 4. Results

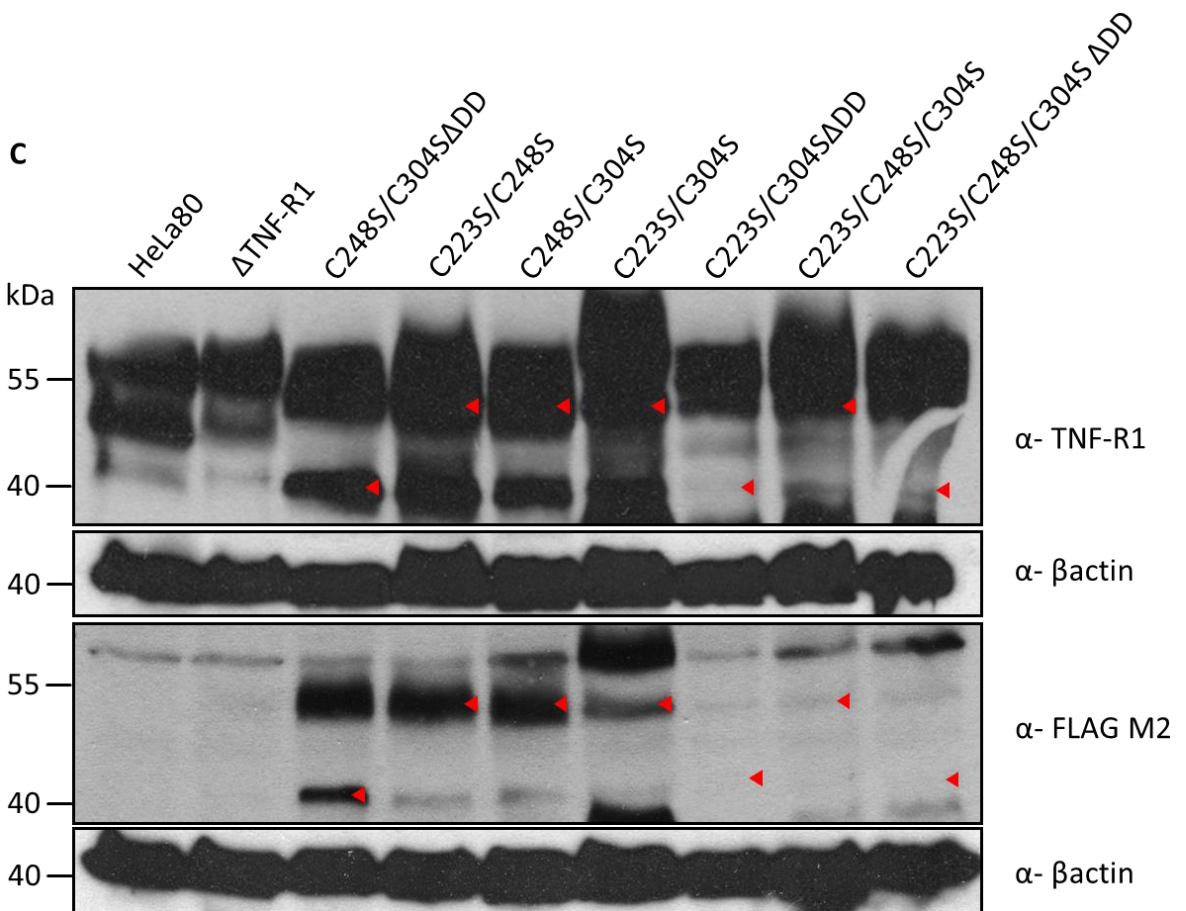
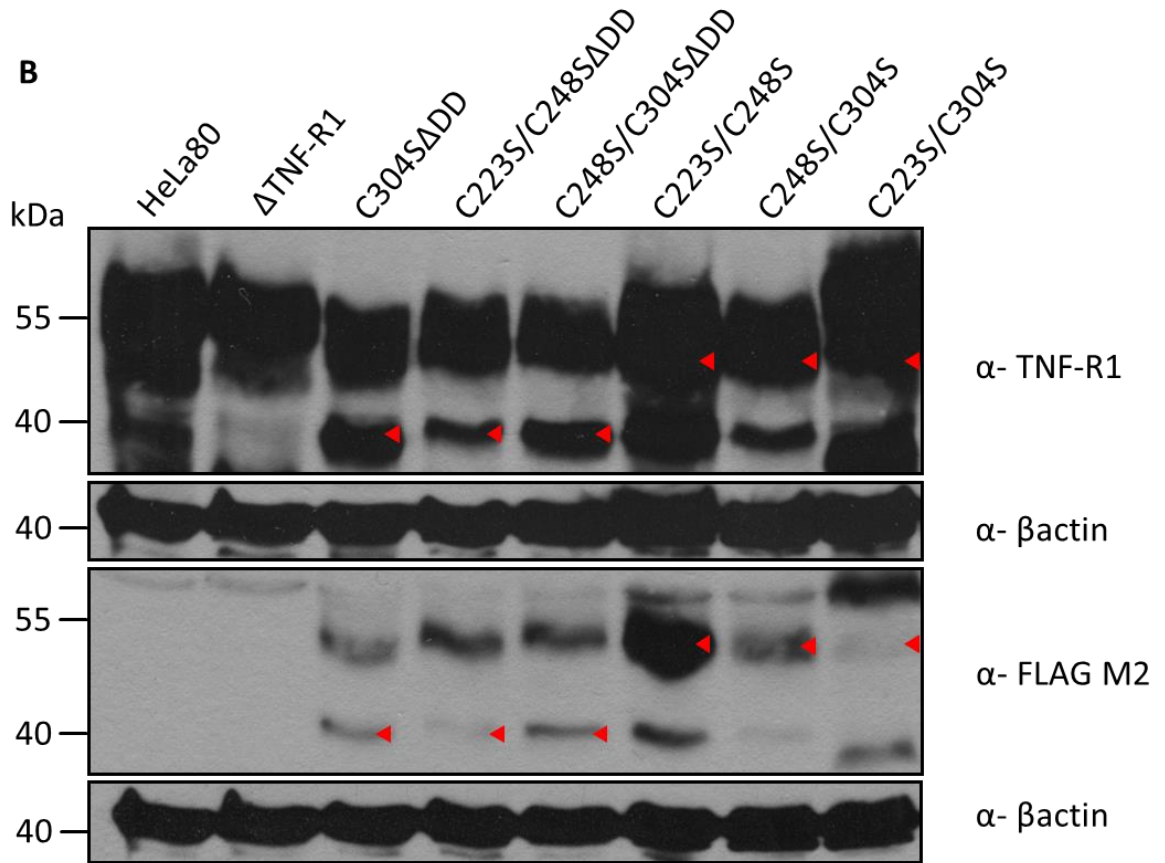
**Figure 18 AcylRAC of HeLa80 cells.** HeLa80 cells were either treated with 100 ng/ml TNF (TNF) for 90 min or left unstimulated ( $\emptyset$ ) before performing the acylRAC using 2 mg of total protein. Western blot was performed from 25  $\mu$ l of acylRAC eluate and probed for TNF-R1 and CD71. Membrane fraction (MF, 30  $\mu$ g of total protein) served as input control. Hydroxylamine fraction (HA) of untreated and TNF treated cells showed equal signals, verifying TNF-R1 palmitoylation in HeLa80. Tris fraction (TR) served as a negative control and was devoid of signal. CD71 blot served as a loading control.

### 4.1.12 Expression of mutant TNF-R1 in TNF-R1 knockout HeLa80 cells

Overexpression of mutant TNF-R1 in TNF-R1 knockout HeLa80 cells showed that all sixteen TNF-R1 could be expressed and detected in Western blot probing against TNF-R1 and FLAG (Figure 19, A, B, C). The WT appeared at the typical molecular weight of 55 kDa in the TNF-R1 blot, whereas the blot probed for FLAG was devoid of any signal. Surprisingly,  $\Delta$ TNF-R1 revealed also a signal at the height of 55 kDa albeit weaker than the WT, indicating that at higher protein concentration receptor is still detectable. However, FLAG blot of TNF-R1 knockout HeLa80 cells was devoid of signals. For all sixteen cell lines growing in the selection medium, signals in the TNF-R1 blot can be detected for both long and short form receptors (labeled with red arrow heads). However, as it was already seen in U937 cells (Figure 10, 11), after transduction of mutant receptors several other unpredicted band signals appeared in the lanes of the TNF-R1 and FLAG blots.



4. Results



## 4. Results

**Figure 19: Western blot of mutant receptors in TNF-R1 knockout HeLa80 cells.** Western blots were performed of whole cell lysates (140 µg/lane). The blots were probed for TNF-R1 and FLAG using TNF-R1 and M2 antibodies. Cells expressing endogenous WT receptor served as a positive control with the typical band pattern at 55 kDa in the TNF-R1 blots whereas FLAG blots were devoid of signal. TNF-R1 knockout HeLa80 served as a negative control, however, faint signal for TNF-R1 was still detectable in the TNF-R1 blots which was absent in the FLAG blots. Indicated mutant receptors show the predicted size of the receptor at 55 kDa for WT length or at 39 kDa for ΔDD (red arrow heads) in both TNF-R1 and FLAG blots. Detection of actin served as a loading control.

### 4.1.13 AcylRAC reveals triple palmitoylation of TNF-R1

To determine the TNF-R1 palmitoylation site in HeLa80 cells, acylRAC of all sixteen receptor expressing cells as well as WT HeLa80 and ΔTNF-R1 HeLa80 was performed. Samples of WT HeLa80, ΔTNF-R1 HeLa80 and weakly receptor expressing cells (C223S, C223S/C248SΔDD, C248S/C304SΔDD, C223S/C248S, C248S/C304S and C223S/C304SΔDD) were probed for TNF-R1 (Figure 20, A), whereas stronger receptor expressing cells were probed for FLAG (Figure 20, B). Receptor of WT HeLa80 cells served as positive control, showing the receptor specific signal in the HA fraction. TNF-R1 knockout HeLa80 served as negative control, however, also in the acylRAC signals at the molecular weight for TNF-R1 appeared, albeit much weaker than for the WT, suggesting that TNF-R1 knockout HeLa80 cells are not a complete knockout. All weakly expressed mutant receptors showed a signal in their respective HA fraction. Nevertheless, due to the incomplete TNF-R1 knockout in the HeLa80 cells, no conclusion on the palmitoylation of the long form receptors (C223S, C223/C248S and C248/C304S) can be drawn, because signals are indistinguishable from endogenous WT TNF-R1. For the short form receptors, palmitoylation can be assumed which correlates with the results from U937 cells (C223S/C248SΔDD, C248S/C304SΔDD, Figure 12).

Stronger expressed receptors were analyzed by FLAG blots due to the better distinction of long form receptors to endogenous TNF-R1 (Figure 19, B). All remaining mutant receptors show a signal in the HA fraction, indicating their palmitoylation, except for triple mutant receptors C223S/C248S/C304S and C223S/C248S/C304SΔDD. This suggests that TNF-R1 is triple palmitoylated at these three cysteines C223, C248 and C304.

## 4. Results

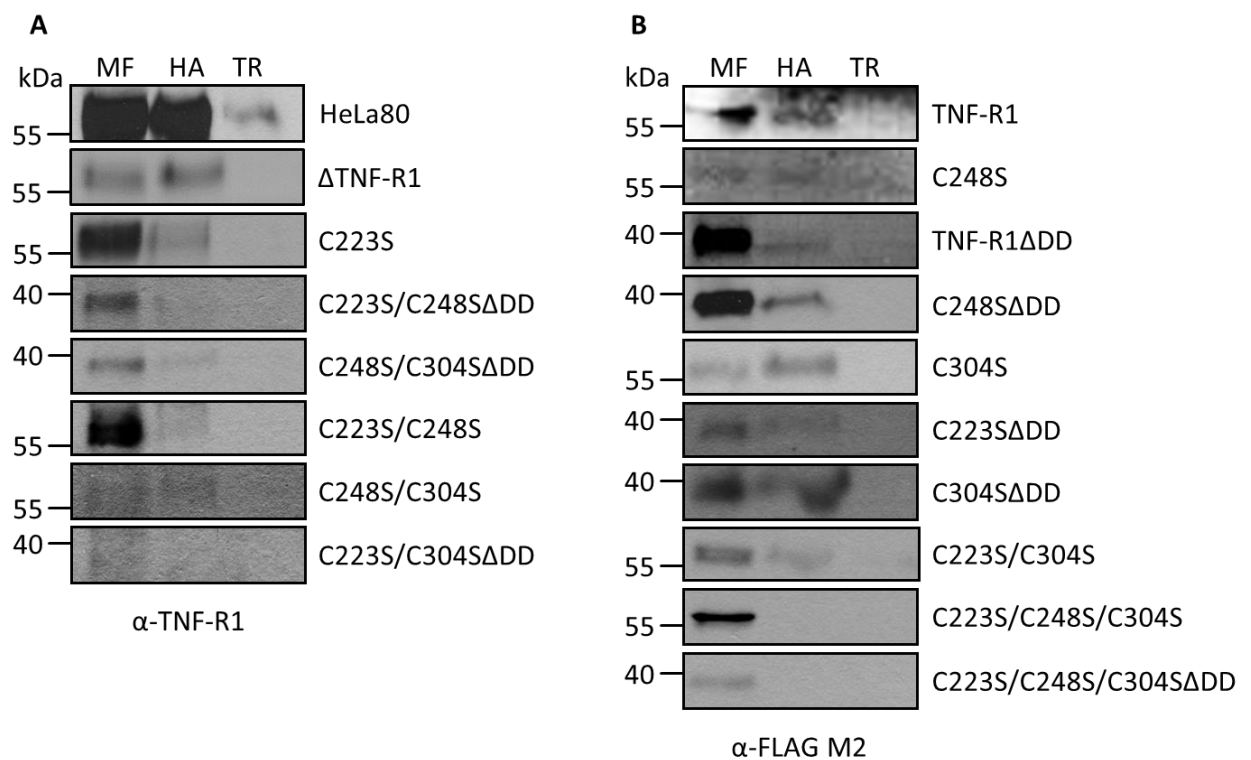


**Figure 20: AcylRAC of WT HeLa80,  $\Delta$ TNF-R1 HeLa80 and mutant TNF-R1 expressing cells.** AcylRAC was performed using 2 mg of total protein. Western blots were performed from 25  $\mu$ l of acylRAC eluate and probed for TNF-R1 and FLAG using TNF-R1 and M2 antibodies. Membrane fraction (MF, 30  $\mu$ g of total protein) served as input control. Lysate of WT receptor expressing cells served as positive control and confirmed TNF-R1 palmitoylation in HeLa80. TNF-R1 knockout HeLa80 cells served as negative control. Nevertheless, signal was detectable in MF and HA fraction, indicating an incomplete knockout. Cells expressing the different mutant forms of TNF-R1 also show signal in the hydroxylamine (HA) fraction which demonstrate receptor palmitoylation except for triple mutant receptors. Lack of the signal in the HA fraction of receptors C223S/C248S/C304S and C223S/C248S/C304S $\Delta$ DD lead to the assumption that TNF-R1 is triple palmitoylated. Tris (TR) fraction served as a negative control.

### 4.1.14 Mutagenesis of putative cysteines affects NF- $\kappa$ B activation in HeLa80 cells

I $\kappa$ B $\alpha$  degradation was used to examine how putative changes in the receptor palmitoylation due to mutagenesis affect NF- $\kappa$ B activation. In figure 21, I $\kappa$ B $\alpha$  degradation in sixteen mutant receptors expressing cells as well as the WT HeLa80 and TNF-R1 knockout HeLa80 cells is shown. In WT cells, I $\kappa$ B $\alpha$  degradation occurred within 15 min after TNF stimulation, followed by restoration of the signal. In contrast, TNF-R1 knockout HeLa80 cells showed a consistent signal throughout TNF treatment. In cells expressing the transduced WT TNF-R1, I $\kappa$ B $\alpha$  signal slightly decrease after 15 min of TNF stimulation, indicating a partial rescue. For all other mutant receptors, no alteration of the I $\kappa$ B $\alpha$  signal was observable, indicating that NF- $\kappa$ B activation is impaired by altering of the palmitoylation status of the TNF-R1. This confirms the results in U937 cells.

#### 4. Results

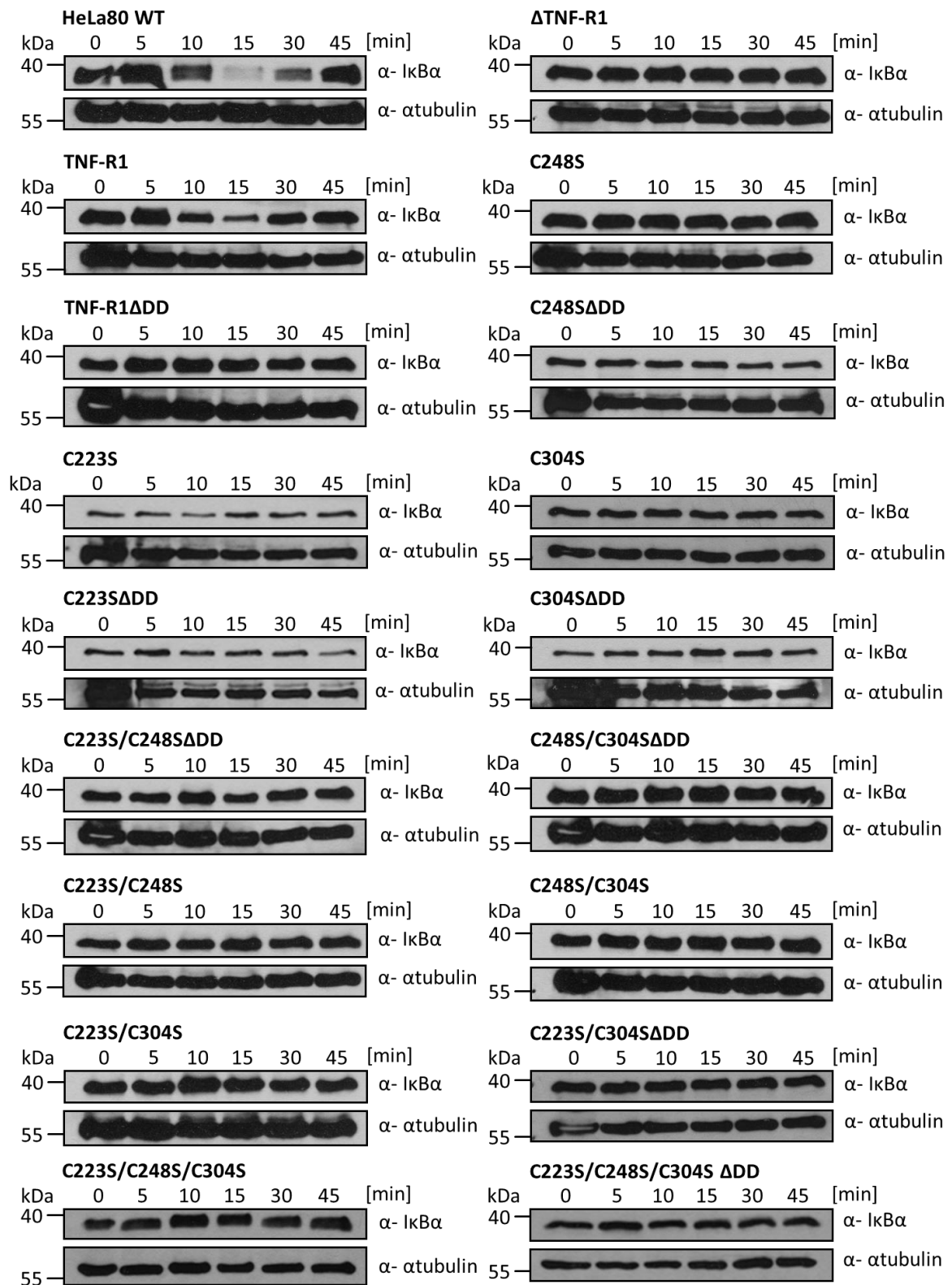


**Figure 21: IκBα degradation of WT HeLa80, ΔTNF-R1 HeLa80 and mutated TNF-R1 expressing cells.** IκBα degradation was initiated by treating the respective cells with 100 ng/ml TNF for the indicated time points at 37 °C. Western blots were performed of whole cell lysates (40 μg/lane) and probed for IκBα. WT HeLa80 cells served as a positive control for IκBα degradation where the signal decreased within 15 min of TNF stimulation. TNF-R1 knockout HeLa80 cells served as a negative control and shows no change in signal intensity during incubation time. Transfected WT TNF-R1 expressing cells show a slight decrease in signal intensity of IκBα at 15 min. As expected, none of the short form receptors but also all long form receptors show no change in their IκBα signal intensity. Detection of tubulin served as a loading control.



## 4.2 Depalmitoylation of TNF-R1

### 4.2.1 Long term TNF stimulation reveals TNF-R1 depalmitoylation

In a previous experiment of receptor palmitoylation (Figure 7) a decrease in signal intensity after TNF treatment was observed. Therefore, an approach investigating the long term kinetics of receptor palmitoylation at different time points (0, 5, 10, 20, 30, 60 min) after TNF stimulation with acylRAC was conducted together with Vinzenz Särchen (University of Kiel, Germany). The Western blot analysis of the acylRAC is shown in figure 22, A. There, an initial increase of the TNF-R1 signal in the first two time points (0, 5 min) after TNF treatment is observable. Afterwards, signal intensity progressively declines during 60 min of TNF stimulation even to a lower level as the output value of unstimulated receptors. The lightning red staining, shown in figure 22, B confirms the uniform loading of the gel with same amounts of proteins. Quantification of the Western blot is depicted in figure 22, C which visualizes and confirms the significant depalmitoylation of TNF-R1 within 60 min of TNF treatment in U937 cells.

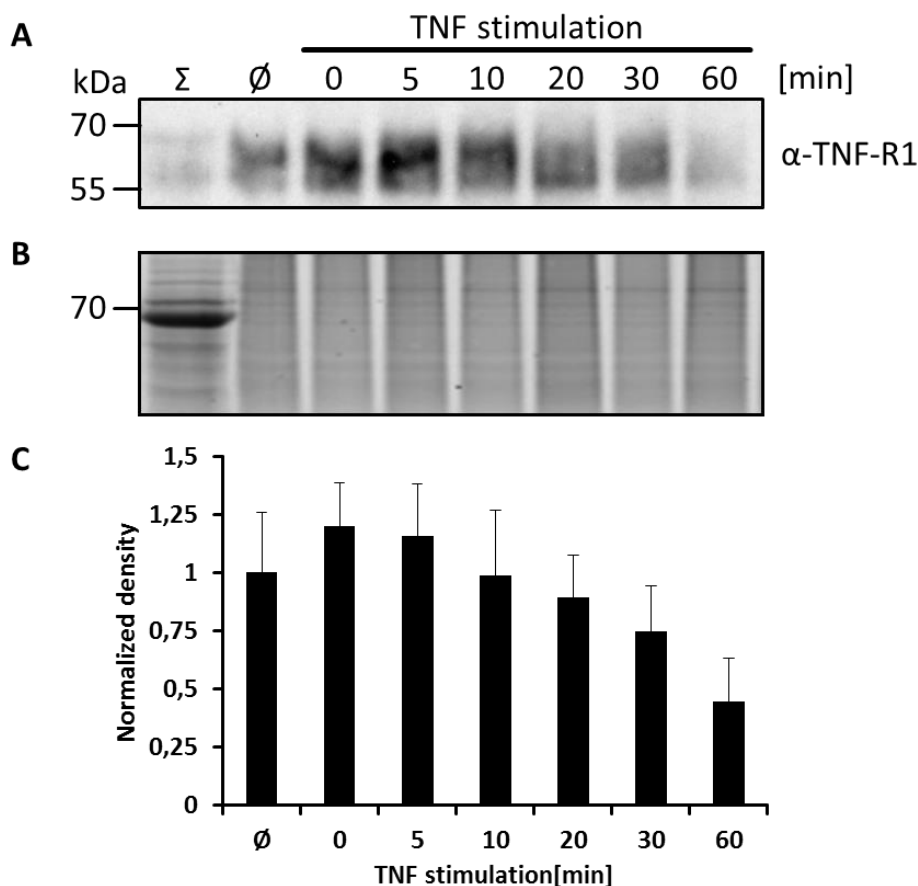


**Figure 22: AcylRAC of a TNF treated kinetic for different points of stimulation in U937 cells.** U937 cells were either treated with 100 ng/ml TNF for indicated time points (0, 5, 10, 20, 30, 60 min) or left unstimulated ( $\emptyset$ ) before implementing the acylRAC with 1.5 mg of total protein. **A**, Western blot was performed from 25  $\mu$ l of acylRAC eluate of hydroxylamine fractions for the specific time point and probed for TNF-R1. Total cell lysate ( $\Sigma$ , 20  $\mu$ g of total protein) served as an input control. After an initial increase of

## 4. Results

signal intensity up to 5 min, the signal progressively decreases during 60 min of TNF treatment. **B**, Lightning red staining of Western blot (A) as a loading control showed equal amounts of proteins per lane. **C**, Quantification of the Western blots of acylRAC hydroxylamine bands. Normalized to the unstimulated sample ( $\emptyset$ ), (n=8; +/- SD).

### 4.2.2 Analysis of TNF-R1 palmitoylation in HeLa80 cells upon TNF stimulation

Since the acylRAC from experiment of figure 18 showed no reduction of the TNF-R1 signal intensity after 90 min of TNF incubation in HeLa80 cells, the approach was repeated pre-incubated HeLa80 cells with cycloheximide (CHX) before TNF treatment. CHX is a protein synthesis inhibitor, sensitizing cells for apoptosis. Figure 23 depicts the obtained Western blot, showing a decrease of signal intensity from HA 0 min to HA 90 min. However, membrane fraction (MF) signal of the 90 min sample is weaker compared to MF 0 min, thus, no clear conclusion about the depalmitoylation of TNF-R1 in HeLa80 cells can be drawn. Therefore, it is assumed that under these conditions TNF-R1 of HeLa80 is not depalmitoylated after TNF stimulation. Nevertheless, this experiment has been performed once needing repetition also at different time points.

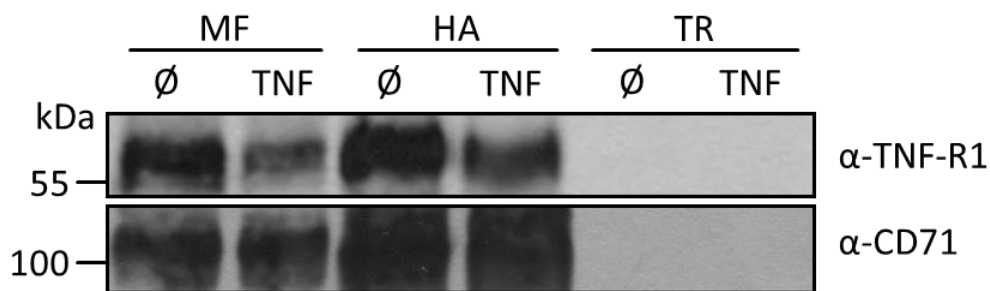


**Figure 23: AcylRAC of HeLa80 cells pre-treated with cycloheximide (CHX).** HeLa80 cells were treated with 2.5  $\mu\text{g}/\text{ml}$  CHX for 1 h. Afterwards, cells were either treated with 100  $\text{ng}/\text{ml}$  TNF (TNF) for 90 min or left unstimulated ( $\emptyset$ ) before performing acylRAC using 2 mg of total protein. Western blot was performed from 25  $\mu\text{l}$  of acylRAC eluate and probed for TNF-R1 and CD71. Membrane fraction (MF, 30  $\mu\text{g}$  of total protein) served as an input control. Hydroxylamine fraction (HA) of untreated and TNF treated cells showed a slight decrease in signal intensity after stimulation. However, due to unequal signal intensity of MF, no conclusion about depalmitoylation could be drawn. Tris fractions (TR) served as negative controls and were devoid of signal. CD71 blot served as loading control.

### 4.2.3 Detection of several putative Acyl-protein thioesterases

As TNF-R1 was depalmitoylated in U937 cells our efforts were to identify the responsible thioesterase catalyzing this reaction. In previous experiments, Dr. Jürgen Fritsch performed proteome analyses of isolated receptosomes at different time points, by which a data set of different proteins putatively involved in the TNF-R1 signaling was created. These data were screened for known thioesterases co-isolated with receptosomes. The mass spectrometry data revealed two known thioesterases APT1 and PPT1 in the 5 and 15 min receptosome fractions (Figure24, A). Immunoprecipitation via Fc60TNF confirmed the mass spectrometry data by co-precipitation of APT1 and PPT1 but also APT2 which is

## 4. Results

a close relative of APT1 (Figure 24, B). As shown in figure 24, B, TNF-R1 blot shows an expected increase in signal intensity and molecular weight shift after TNF stimulation due to receptor ubiquitination. For APT1, signal is initially strong and progressively decreases within time. For APT2, the signal appears in the first 3 min of TNF binding, increases up to 5 min and decrease again at 10 min. On the other hand, signal for PPT1 is continuously the same at all indicated time points. Input material of all four proteins showed a consistent loading of the gels.

**A**

Protein	Accession no	MW	T <sub>5min</sub>	T <sub>15min</sub>
APT1 / Lypla1	LYPA1_HUMAN	24 kDa	X	X
PPT1	PPT1_HUMAN	34 kDa	X	X

**B**

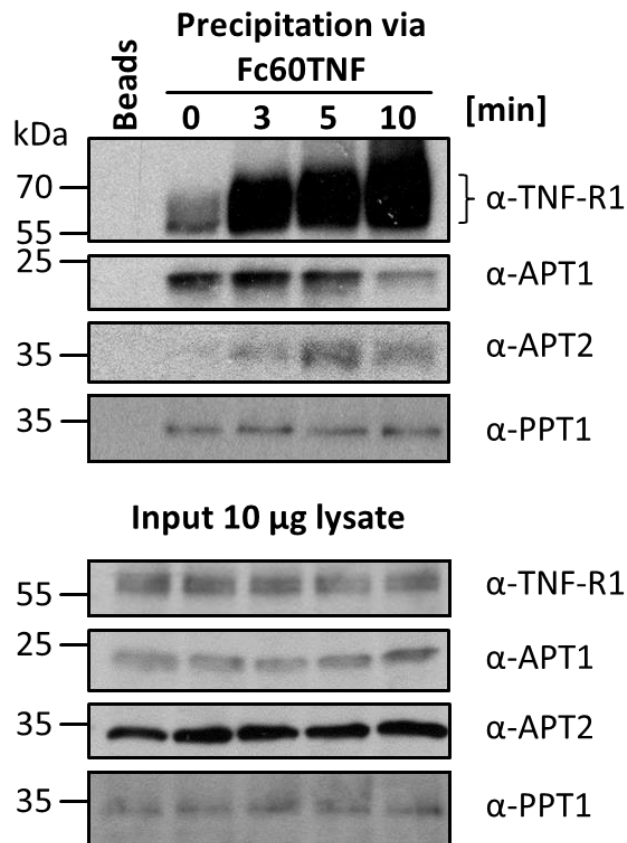


**Figure 24: Mass spectrometry data and immunoprecipitation via Fc60TNF of thioesterases APT1, APT2 and PPT1.** **A**, Table of mass spectrometry data show that APT1 and PPT1 are present in the 5 and 15 min fraction of isolated receptorosomes after TNF stimulation. **B**, For immunoprecipitation, TNF-R1 was labeled with Fc60TNF and internalization was initiated by temperature shift for the indicated time points (3, 5, 10 min). Western blots were performed using 10 µl eluate of the immunoprecipitate for the specific time point and probed either for TNF-R1, APT1, APT2 or PPT1. TNF-R1 blot show an increase in signal intensity and molecular weight shift after TNF stimulation due to receptor ubiquitination. The APT1 signal progressively decreases after temperature shift, while the signal for APT2 increases within 5 min and declines after 10 min. Signal for PPT1 is constant over time. Bead fractions served as negative controls and were devoid of any signal. 10 µg of cell lysates served as input controls (bottom) and showed consistent loading.

#### 4.2.4 Acyl-protein thioesterase activity assay disclose APT2 activation upon TNF stimulation

Based on these results of the immunoprecipitation, APT2 appeared as candidate for TNF-R1 depalmitoylation. Furthermore, the time point of transient interaction of APT2 to the receptor complex (5 min, Figure 24, B) correlates well with the start of depalmitoylation of the receptor after TNF treatment (10 min, Figure 22, A, C). To differentiate and prove which thioesterase is responsible for TNF-R1 depalmitoylation, next, TNF treated cells were analyzed by measuring the enzyme activity in living cells using fluorescent depalmitoylation probes (DPPs) and imaging flow cytometry. Depalmitoylation probes have different preferences: while DPP-2 reports on global thioesterase activity, DPP-3 is more specific for APT1 (Kathayat et al. 2017). Figure 25, A, shows the result for U937 cells pretreated with DPP-3 before TNF was added. In the upper part representative images before and after TNF treatment are depicted, showing no changes in both samples. This is in line with the histogram in the lower part showing the normalized frequency plotted against the fluorescence intensity. There, after TNF stimulation and temperature shift no significant increase in fluorescence intensity could be observed. This suggests that APT1 is not activated after TNF treatment. In contrast, U937 cells pretreated with DPP-2 a signal increase of the green fluorescent dye after TNF treatment was observed as shown in figure 25, B. This was further substantiated by the histogram in the lower part where the cells kept on ice and co-incubated with DPP-2 and TNF are represented by the green graph. After temperature shift, fluorescence intensity increase within the first 5 min (red graph) and progressively decline from 10 (orange graph) to 15 min (blue graph). U937 cells co-incubated with DPP-3 and either PalB (black graph) or ML349 (dashed red graph) before TNF stimulation serve as a negative control and showed the same graph pattern as the non-temperature shifted sample (green graph), indicating that the inhibition of APTs in general or specific for APT2 suppress thioesterase activity. Based on the fact that the global thioesterase activity was increased but APT1 was unaffected suggests that APT2 is activated after TNF stimulation.

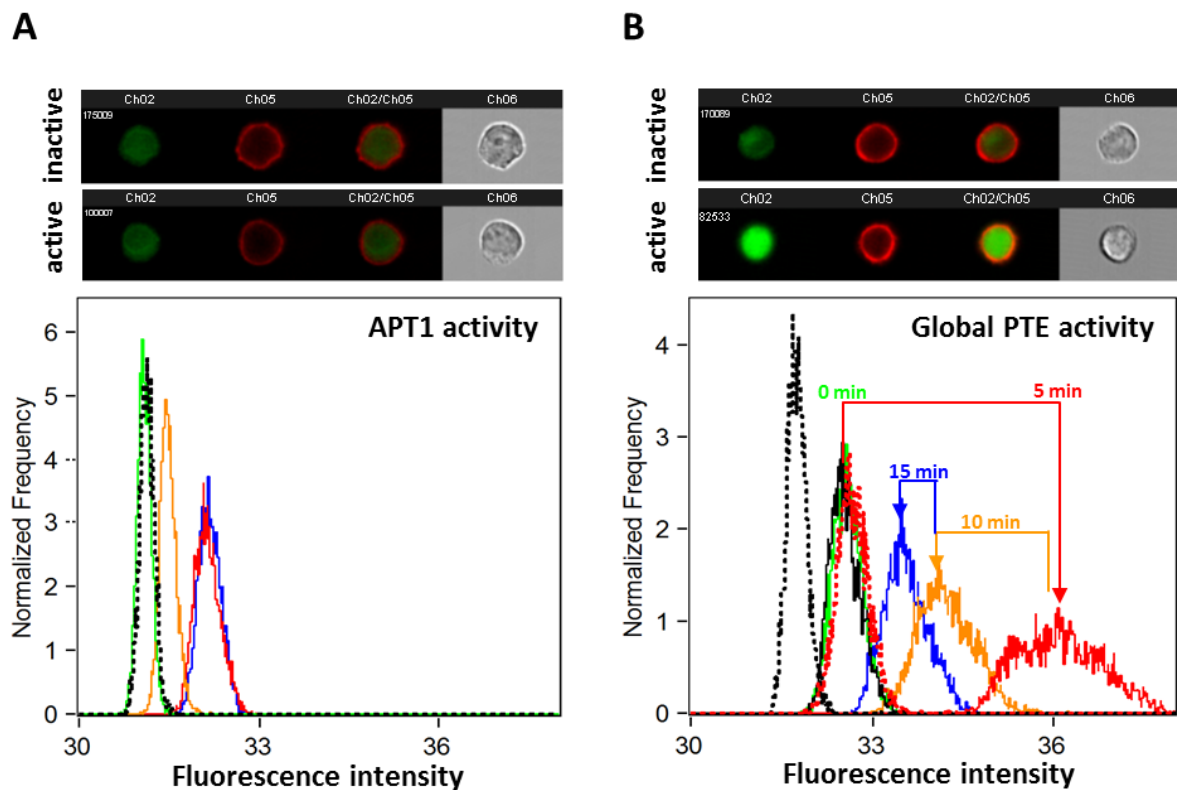


**Figure 25: Thioesterase activity assay of U937 pre-incubated with fluorescent depalmitoylation probes.** U937 cells were pre-incubated with 5  $\mu$ M of either DDP-3 (A) or DPP-2 (B) and then treated with 100 ng/ml TNF on ice. After temperature shift, U937 cells were fixed and analyzed by imaging flow cytometry. **A, Top** panels, representative cell images before (inactive) and after TNF stimulation (active) shows no activation of APT1. Plasma membrane is stained in red. **Bottom**, histogram of normalized frequency plotted against fluorescence intensity representing enzyme activity. After addition of TNF and temperature shift no change in fluorescence intensity was observable, indicating that APT1 is not activated upon TNF stimulation. One representative experiment is shown (n=3). **B, Top** panels, representative cell images before (inactive) and after TNF stimulation (active) shows activation of APTs due to signal increase of green fluorescent dye. Plasma membrane is stained in red. **Bottom**, histogram of normalized frequency plotted against fluorescence intensity representing enzyme activity. After addition of TNF and temperature shift fluorescence intensity increased within 5 min (red graph) and progressively declined from 10 min (orange graph) to 15 min (blue graph). Dashed black graph: untreated U937 cells. Green graph: U937 cells kept on ice and co-incubated with TNF and DPP-2. Black graph: U937 cells co-incubated with DDP-3 and PalB. Dashed red: U937 cells co-incubated with DPP-3 and ML349. One representative experiment is shown (n=3).

#### 4.2.5 Inhibition of APT2 blocks TNF-R1 depalmitoylation

For further corroboration and with the help of the MD student Lotta Caning (University to Kiel, Germany), acylRACs were performed suppressing APT2 activity by an APT2 specific inhibitor (ML349). Therefore, U937 cells were either left untreated or incubated with either TNF, ML349 or co-incubated with TNF and ML349. Figure 26, A, top, shows the Western blot of one representative acylRAC probed for TNF-R1. In figure 26, B, the Western blot quantification by densitometry is shown. As seen in previous blots (Figure 7, 22), TNF treatment of U937 leads to a decrease of signal intensity for TNF-R1 (Figure 26, A, B). However, U937 cells co-incubated with ML349 and TNF partially retained the signal for TNF-R1 whereas incubation of ML349 alone led to an increase of TNF-R1 signal which

## 4. Results

exceeds initial signal of unstimulated U937 cells, demonstrating a role of APT2 in TNF-R1 depalmitoylation. Western blot of PPT1 and its respective quantification blot (Figure 26, A, bottom, C) served as a negative and loading control, showing that signal intensity of PPT1 was not affected.

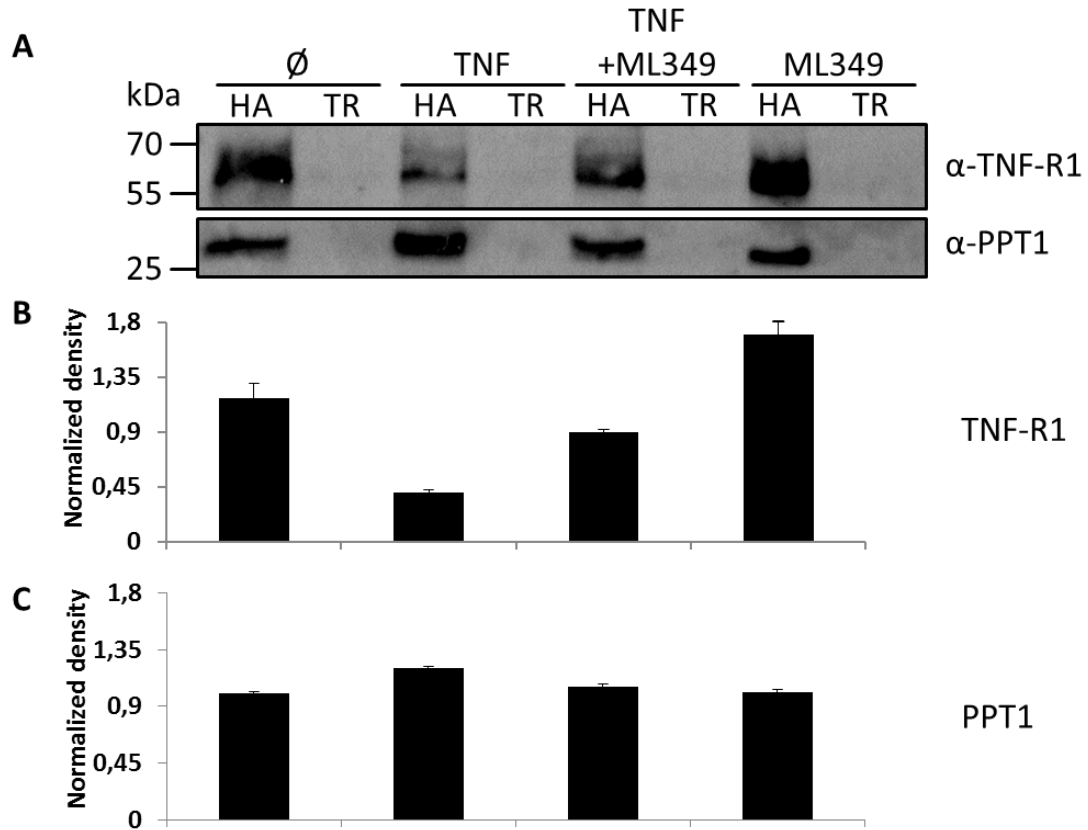


**Figure 26: AcylRAC of APT2 inhibited U937 cells.** For APT2 inhibition, U937 cells were treated with 75  $\mu$ M ML349 for 1 h. Afterwards, cells were either treated with 100 ng/ml TNF for 60 min (TNF;TNF + ML349) or left unstimulated ( $\emptyset$ ; ML349) before performing the acylRAC using 2 mg of total protein. **A**, Western blot was performed from 25  $\mu$ l of acylRAC eluate and probed for TNF-R1 (top) and PPT1 (bottom). After TNF treatment, signal for palmitoylated TNF-R1 decreased. U937 co-incubated with TNF and ML349 show maintenance in signal intensity for TNF-R1. U937 cells treated with ML349 alone show an increase in signal intensity which exceeds the initial value of unstimulated U937. PPT1 blot (bottom) served as a negative and loading control and was not affected by both TNF and ML349 incubation. Tris fractions (TR) served as a negative control and were devoid of signal. **B**, Densitometric quantification of hydroxylamine fractions (HA) of acylRACs Western blots probed for TNF-R1, normalized to the unstimulated ( $\emptyset$ ) sample (n=3, +/- SD). Quantification confirms result from figure 26, A (top) that TNF treatment of U937 cells decrease signal for TNF-R1. Co-incubation of TNF and ML349 retained signal intensity for TNF-R1. For U937 cells treated with ML349 alone, signal increased and exceeded intensity of unstimulated U937 cells. **C**, Densitometric quantification of hydroxylamine fractions (HA) of acylRACs Western blots probed for PPT1, normalized to the unstimulated ( $\emptyset$ ) sample (n=3, +/- SD). PPT1 served as a negative and loading control and confirmed results of A bottom that PPT1 is not affected by both TNF and ML349 incubation.

### 4.2.6 Purification of active recombinant APT2

Since the attempt to knockout APT2 in U937 cells with CRISPR/Cas9 failed due to mortality of the cells, no rescue experiments could be performed. Instead, recombinant APT2 (rAPT2) was overexpressed in bacteria and tested for its activity. Figure 27, A shows

## 4. Results

the purified recombinant His<sub>6</sub>-tagged APT2. As predicted, rAPT2 could be detected at 28 kDa in the 150 mM imidazole eluate, approved by two different antibodies, recognizing APT2 itself and the His<sub>6</sub>. rAPT2 was then used for an activity assay (Figure 27, B), using the global thioesterase fluorescence depalmitoylation probe DPP-2 in four different approaches: 1. DPP-2 alone; 2. DPP-2 co-incubated with rAPT2; 3. DPP-2 co-incubated with rAPT2 and PalB and 4. DPP-2 co-incubated with PalB. Within 20 min the signal of DPP-2 co-incubated with rAPT2 raised compared to other approaches, implying that rAPT2 is active under the tested conditions. The approach of DPP-2 co-incubated with rAPT2 and PalB completely blocked rAPT2 activity, since the signal was on the same level as DPP-2 alone and DPP-2 co-incubated with PalB.

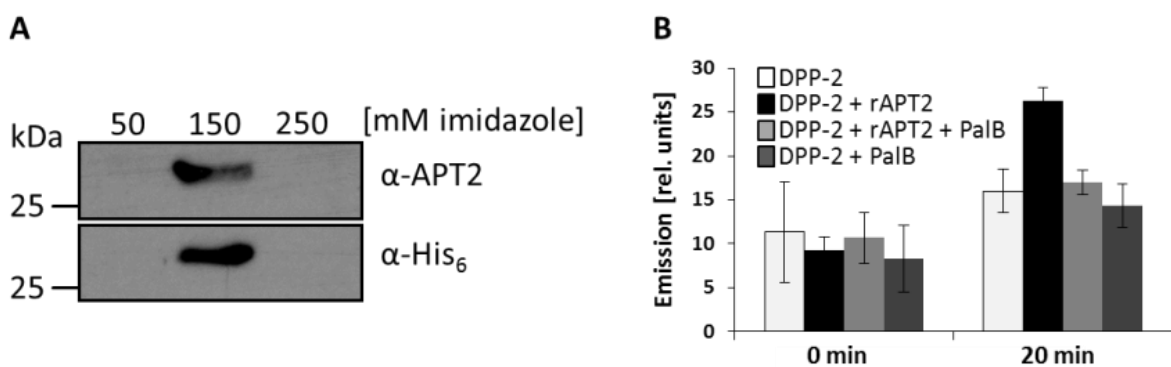


**Figure 27: Purification and activity of recombinant APT2.** Recombinant APT2 was overexpressed in *E.coli* and purified by IMAC. **A**, Western blots were performed of eluates from IMAC and probed for APT2 and His<sub>6</sub>. Purified rAPT2 was present in the 150 mM imidazole eluate fraction, approved by two different antibodies (APT2 and His<sub>6</sub>). **B**, rAPT2 for the activity assay of four different approaches were used: 1. U937 cells incubated with DPP-2 (white bar); 2. DPP-2 co-incubated with rAPT2 (black bar); 3. DPP-2 co-incubated with rAPT2 and PalB (grey bar); 4. DPP-2 co-incubated with PalB (dark grey bar). After 20 min fluorescence was measured, revealing that rAPT2 is active due to significant increase of fluorescence signal compared to control samples, (n=3; +/- SD).

### 4.2.7 Recombinant APT2 depalmitoylates TNF-R1 *in vitro*

To investigate if rAPT2 depalmitoylates TNF-R1 *in vitro*, rAPT2 was incubated with a crude membrane fraction prior to acylRAC and Western blot analysis. As shown in figure 28, A, the signal intensity for TNF-R1 in the rAPT2 pre-incubated fraction decreased compared to the untreated fraction, whereas control proteins such as CD71, Integrin α6, PPT1 and Rab5 remained unaffected in their intensity. This was further visualized in figure 28, B, which confirms the signal decrease after rAPT2 incubation. Thus, rAPT2 depalmitoylates TNF-R1 *in vitro*.

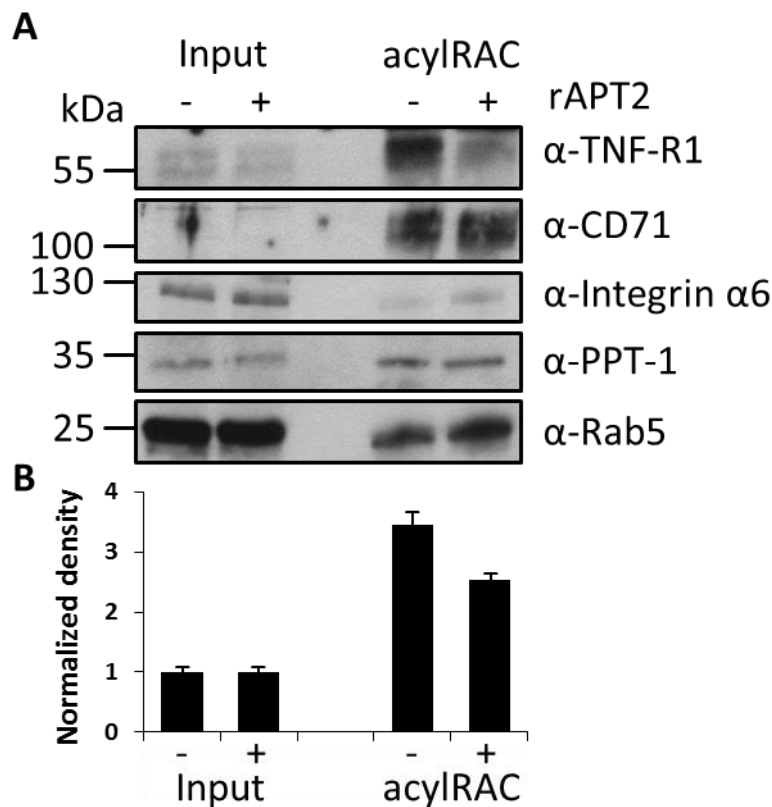


**Figure 28: AcylRAC of U937 cells pre-incubated with APT-2. A,** The membrane fraction of U937 cells was pre-incubated with 30  $\mu$ M rAPT2 for 2 h at 37  $^{\circ}$ C before implementing the acylRAC with 2 mg of total protein. Western blots were performed from 25  $\mu$ l of the acylRAC eluate of hydroxylamine fraction and probed for TNF-R1, CD71, Integrin  $\alpha$ 6, PPT1 and Rab5. Membrane fractions (20  $\mu$ g of total protein) of APT2 pre-incubated and non-incubated U937 cells served as an input control. Signal for TNF-R1 in the APT2 pre-incubated fraction show a slight decrease compared to the non-incubated fraction, indicating TNF-R1 depalmitoylation is conducted by APT2. All other control proteins (CD71, Integrin  $\alpha$ 6, PPT1 and Rab5) were not affected by rAPT2 pre-incubation. **B,** Densitometric quantification of hydroxylamine fractions of acylRAC Western blots probed for TNF-R1, normalized to the input samples (n=3; +/- SD). Quantification verifies decrease of TNF-R1 plamitoylation in rAPT2 pre-incubated fractions compared to non-incubated fraction.

#### 4.2.8 Inhibition of APT2 alters TNF-R1 internalization and apoptosis induction

To investigate the *in vivo* role of APT2 in the TNF signaling, cells were pre-incubated with increasing concentration (6.35  $\mu$ M; 12.5  $\mu$ M; 25  $\mu$ M and 50  $\mu$ M) of the inhibitors ML349 and PalB before TNF stimulation was initiated and internalization was measured (Figure 29, A). In comparison to the WT receptor internalization which increased up to approximately 70 % after TNF stimulation, pre-incubation with the inhibitor ML349 showed an irregular change of internalization where at 50  $\mu$ M and 12.5  $\mu$ M internalization decreased down to 40 % or 60 % but at 25  $\mu$ M and 6.35  $\mu$ M internalization was unaffected. In contrast the inhibition with PalB where lower concentrations of 6.35  $\mu$ M and 12.5  $\mu$ M did not affect receptor internalization but higher concentrations of 25  $\mu$ M and 50  $\mu$ M decreased receptor internalization down to 60 % or 40 %.



## 4. Results

The same setup of inhibitors compared to WT U937 cells was then used to analyze TNF induced apoptosis (Figure 29, B). WT cells showed the typical apoptotic response of approximately 50 % cell death. However, samples co-treated with TNF and 50  $\mu$ M ML349 revealed an enhanced apoptosis induction of approximately 80 %, whereas co-incubation of TNF with 12.5  $\mu$ M PalB led to a negligible decreased of apoptosis to nearly 45 %. Both inhibitors pre-incubated alone with U937 cells served as controls.

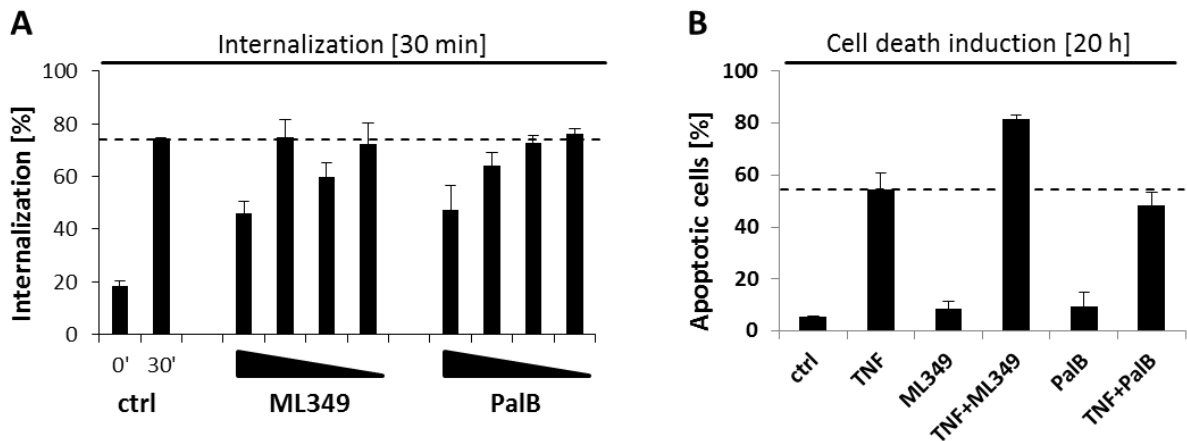


**Figure 29: Internalization and apoptosis in U937 cells pre-treated with depalmitoylation inhibitors.** **A**, For the analysis of the TNF-R1 internalization, cells were kept on ice and receptors were labeled with biotinylated TNF coupled to an avidin linked fluorescence dye. Internalization was initiated by temperature shift to 37  $^{\circ}$ C for 30 min. Prior to that, cells were pre-incubated with different inhibitor concentrations (I, 50  $\mu$ M; II, 25  $\mu$ M; III, 12.5  $\mu$ M; IV, 6.35  $\mu$ M) of ML349 and PalB. After the temperature shift, WT receptor internalization increased up to 70 % (ctrl). Pre-incubation with ML349 at 50  $\mu$ M and 12.5  $\mu$ M decreased internalization whereas 25  $\mu$ M and 6.35  $\mu$ M did not affect internalization. Pre-incubation with PalB at 50  $\mu$ M and 25  $\mu$ M decreased internalization but 12.5  $\mu$ M and 6.35  $\mu$ M showed no alteration (n=4; +/- SD). **B**, Cells were incubated with either 50  $\mu$ M ML349 or 12.5  $\mu$ M PalB and for apoptosis induction 100 ng/ml TNF was added. 20 h TNF treatment increased apoptotic cells in WT U937 up to approximately 50 % (ctrl). Incubation with ML349 increased apoptosis up to nearly 80 % while incubation with PalB decreased apoptosis negligibly down to 45 %. (n=5; +/- SD).

### 4.2.9 Inhibition of APT2 increases apoptosis induction

To verify these findings also on the protein level, Western blot analysis of cell lysates co-incubated with TNF and ML349 were performed together with Carina Saggau (University to Kiel; Germany) probing against PARP1, pMLKL and cleaved caspase-3 (Figure 30). For untreated WT U937 no PARP1 and caspase-3 cleavage was detectable since PARP1 showed just one band at 116 kDa and cleaved caspase-3 blot was devoid of signal. On the other hand, U937 cells treated with TNF showed PARP1 and caspase-3 cleavage indicated by the appearance of additional bands, one in the PARP1 blot at 89 kDa and two more in the cleaved caspase-3 blot at 17 kDa and 19 kDa, revealing the induction of apoptosis. The sample co-incubated with TNF and ML349 confirmed the results of the apoptosis assay, since cleavage and thus signals of both proteins were stronger than in merely TNF treated samples.

## 4. Results

To investigate possible effects on other types of programmed cell death such as necroptosis, the apoptosis induction was shifted towards necroptosis by adding the caspase-8 inhibitor zVAD and cells were either co-treated with TNF and ML349 or TNF alone. In both fractions a band for the necroptosis indicator phospho-MLKL appeared at 54 kDa, indicating that necroptosis was not affected by the inhibition of APT2.

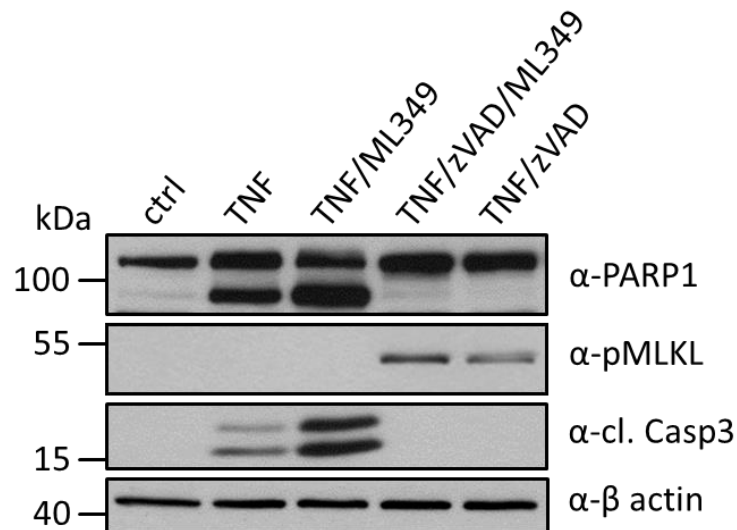


**Figure 30: Analysis of apoptosis and necroptosis in ML349 treated U937 cells.** Before U937 cells were either treated with 100 ng/ml TNF or left unstimulated, cells were either pre-incubated with 50  $\mu$ M ML349, 50  $\mu$ M zVAD or in combination. Western blots were performed of whole cell lysates (20  $\mu$ g/lane) and blots were probed for PARP1, pMLKL, cl. Casp3. Control sample (ctrl) showed one band for PARP1 at 116 kDa and pMLKL and cl. Casp3 blots were devoid of signal. U937 treated with TNF show an additional band for PARP1 at 89 kDa and in the cl. Casp3 blot two bands at 17 kDa and 19 kDa appeared, indicating apoptosis induction. U937 cells co-incubated with TNF and ML349, signal for PARP1 and cl. Casp3 increased by two compared to TNF alone treated U937 cells. Pre-treatment with zVAD and in co-incubation with TNF and ML349 showed no PARP1 and cl. Casp3 cleavage but in the blot for pMLKL a band at 50 kDa appeared which was similar to U937 pre-treated with zVAD and TNF only, demonstrating necroptosis is not affected by depalmitoylation. Detection of actin served as a loading control.

### 4.2.10 Blocking of TNF-R1 depalmitoylation triggers ceramide formation by nSMase

To elucidate the discrepancy of the receptors reduced internalization but increased apoptosis by the inhibition of APT2, earlier studies showed an activation of plasma membrane resident nSMase in response to TNF, resulting in an enhanced ceramide formation and apoptosis induction [Krut et al., 2006; Neumeyer et al., 2006; Philipp et al., 2010]. Thus, ceramide production of U937 cells was determined after incubating cells with TNF, ML349 and GW4869, an nSMase inhibitor. Figure 31, A, shows the relative ceramide production for the indicated samples. After TNF treatment of WT U937 cells ceramide production is slightly increased, but in co-incubation with ML349 ceramide production is enhanced. In contrast, co-incubation of TNF, ML349 with GW4869 blocks ceramide production similar to the level of U937 cells treated with ML349 alone, TNF co-incubated with GW4869 or untreated cells.

#### 4. Results

To validate that apoptosis is induced by ceramide formation, activity of caspase-3 was determined under the same treatment condition as mentioned for ceramide production. Relative units of activated caspase-3 were measured every 10 min for 70 min (Figure 31, B). No caspase-3 activation was detected for untreated U937 cells (rectangle) as well as for U937 cells treated alone with GW4869 (dotted line) and ML349 (triangle dotted line). TNF treated U937 cells showed a slight activation of caspase-3 within 1 h (diamonds). In contrast, TNF and ML349 co-incubated U937 cells showed an enhanced activity of caspase-3 within 1 h (triangle) which could be reduced by the co-treatment with GW4869 (crossed line).

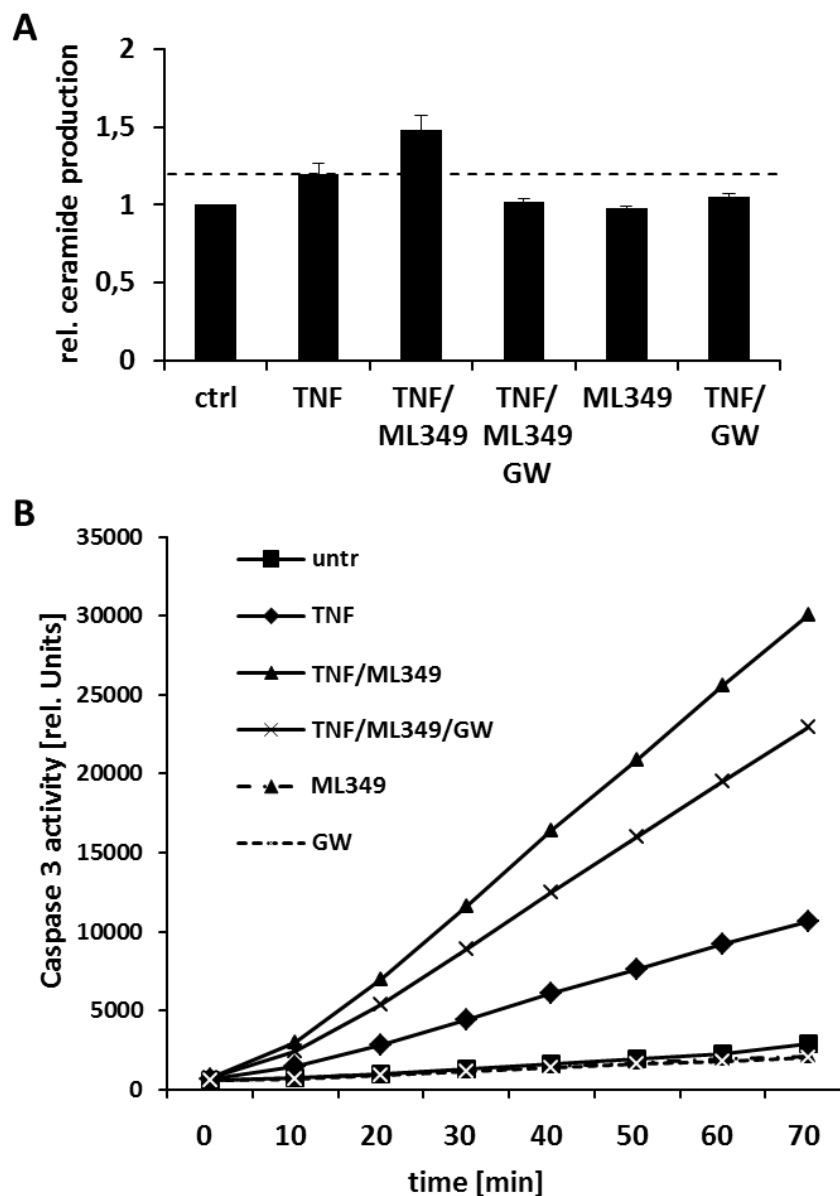


**Figure 31: Ceramide formation and caspase-3 activation in response to TNF co incubated with ML349.** A, For ceramide production, U937 cells were pre-incubated with 50  $\mu$ M ML349 and/or 10  $\mu$ M GW4869 and stimulated with 100 ng/ml TNF. Untreated U937 cells served as a control sample where relative ceramide production was normalized (n=3; +/- SD). After TNF treatment, ceramide production increased which was enhanced by co-incubation of TNF with ML349. In contrast, co-incubation of TNF and ML349 with GW4869

## 4. Results

---

decreased ceramide production to the level of untreated U937 cells. ML349 alone and GW4869 co-incubated with TNF also showed no ceramide production. **B**, For caspase-3 activation, U937 cells were pre-incubated with 25  $\mu$ M ML349 and/or 2  $\mu$ M GW4869 and stimulated with 100 ng/ml TNF. Fluorescence intensity was measured every 10 min for 70 min. Untreated U937 cells (rectangles), ML349 (triangles dotted line) and GW4869 (dotted line) alone showed no caspase-3 activation whereas TNF treatment (diamonds) increased caspase-3 activity within 70 min. Increase was enhanced by co-incubation with TNF and ML349 (triangles). Inhibition of nSMase by GW4869 co-incubated with TNF and ML349 (crossed line) decreased activity of caspase-3. A representative of three measurements in duplicates is shown.

### 4.2.11 Lipid raft isolation revealed altered receptor localization and translocation

As a final experiment the distribution of WT receptor and mutant TNF-R1 in the plasma membrane was further characterized. As the lower apoptosis response of C248S cells seems to be consistent with the decreased surface expression of mutant receptors, this does not explain the reduced NF- $\kappa$ B activation. Previous studies revealed that upon TNF stimulation, translocation of TNF-R1 into lipid rafts is crucial for the activation of NF- $\kappa$ B [Veldman et al., 2001; Legler et al., 2003]. Therefore, a lipid raft extraction based on sucrose density gradient ultracentrifugation was used to examine the localization of the mutant C248S receptor in comparison to the WT receptor within the biological membrane. As shown in figure 32, A, unstimulated WT receptor is mainly present in the more dense fraction (IX, X, XI) and less located in the lipid raft fraction, indicated by flotillin-2 detection (VII, VIII; red arrow head). However, after TNF stimulation for 20 min (Figure 32, B), WT receptor translocates into fractions with higher buoyancy, mainly in the flotillin-2 positive fractions (VII, VIII, red arrow head). Strikingly, the unstimulated receptor C248S (Figure 32, C) already seems to be partially located in the flotillin-2 fractions and even lighter fractions (V, VI, VII, red arrow head). On the other hand, down regulation of APT2 in U937 cells showed that the WT receptor is still located in higher dense fraction (X, XI; Figure 32, D), despite TNF treatment for 20 min which is completely the opposite from the results of figure 32, B.

#### 4. Results

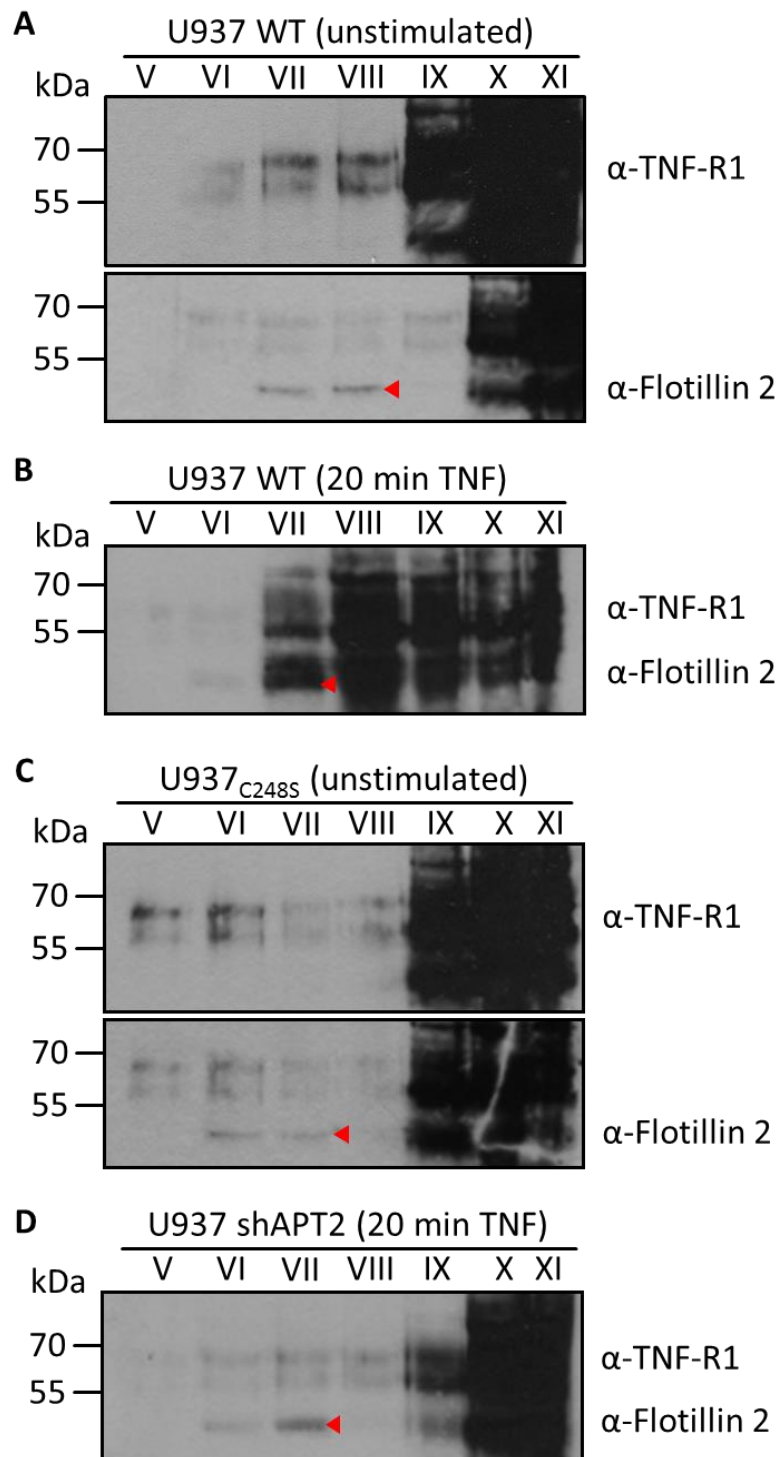


**Fig 32. Plasma membrane fragmentation by sucrose density gradient ultracentrifugation in WT U937, C248S and shAAPT2 U937 cells.** WT U937 and shAAPT2 U937 cells were treated with 100 ng/ml TNF for 20 min. 2 mg of total protein was used for the sucrose density gradient ultracentrifugation. Western blots were performed with 200  $\mu$ l of each fraction and probed for TNF-R1 and flotillin-2; V: light floating fraction; XI: heaviest fraction at gradient bottom. **A**, TNF-R1 and flotillin-2 blot of unstimulated WT U937. Top, TNF-R1 blot shows that WT receptor is mainly present in dense fractions IX, X, XI and slightly present in VI and VII. Bottom, flotillin-2 re-blot indicate existence of flotillin-2 in fraction VII and VIII (red arrow head); **B**, TNF-R1 and flotillin-2 blot of TNF stimulated U937 cells reveal shift of TNF-R1 into fractions VII and VIII where flotillin-2 is also present (red arrow head). **C**, top, TNF-R1 blot of unstimulated U937<sub>C248S</sub> shows broad distribution of receptor from fraction V to XI. Bottom, flotillin-2 blot shows flotillin-2 signal in fraction VI and VII (red arrow head). **D**, TNF-R1 and flotillin-2 blot of TNF stimulated shAAPT2 U937 cells show TNF-R1 signal mainly in fraction X and XI, weaker in VI to IX. Flotillin-2 signal appears in fraction VI and VII.

### 4.3 zDHHC5 interferes with TNF-R1 signaling

#### 4.3.1 Interaction of the protein acyltransferase 5 (zDHHC5) with the TNF-receptor complex

By searching the receptosomes proteome database for thioesterases, further proteins related to palmitoylation were analyzed too. Two protein acyltransferases zDHHC5 and zDHHC20 which are known as mainly plasma membrane bound DHHCs could be found in the 5 and 15 min fractions (Figure 33, A; Ohno et al., 2006). To examine their interaction with TNF-R1, immunoprecipitation via TNF-R1 specific Fc60TNF was performed for the indicated time points. The signal for zDHHC5 increases in the first minutes after TNF addition, peaks at 3 min and progressively decreases at 5 and 10 min. The same manner showed zDHHC20 where signal increased up to 5 min and then decreased within 10 min. Lysates served as input control and showed consistent signals for the respective proteins.

**A**

Protein	Accession no	MW	T <sub>5min</sub>	T <sub>15min</sub>
zDHHC5	ZDHC5_HUMAN	77 kDa	X	X
zDHHC20	ZDH20_HUMAN	42 kDa	X	

**B**

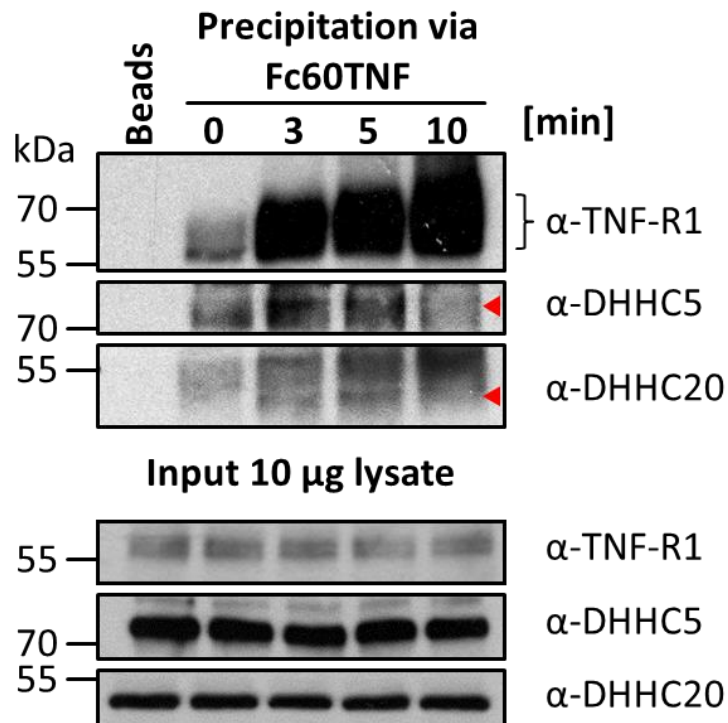


**Figure 33: Mass spectrometry data and immunoprecipitation via Fc60TNF of protein acyltransferases zDHHC5 and zDHHC20.** **A**, Table of mass spectrometry data show that zDHHC5 and zDHHC20 are present in the 5 min fraction of isolated receptosomes after TNF stimulation and zDHHC5 also in the 15 min fraction. **B**, For immunoprecipitation, TNF-R1 was labeled with Fc60TNF coupled to magnetic beads and internalization was initiated by a temperature shift for the indicated time points (3, 5, 10 min). Western blots were

## 4. Results

---

performed using 10  $\mu$ l eluate of immunoprecipitation for the specific time points and probed either for TNF-R1, zDHHC5 or zDHHC20. TNF-R1 blot show an increase in signal intensity after TNF stimulation. zDHHC5 signal peaks at 3 min and progressively decreases. Signal for zDHHC20 increases within 5 min and declines after 10 min. Bead fractions served as negative controls and were devoid of any signal. 10  $\mu$ g of cell lysates served as input controls (bottom) and showed consistent loading.

### 4.3.2 Generation of zDHHC5 knockout U937 cells

As zDHHC5 and zDHHC20 appear to interact with the TNF-receptor complex at the beginning of receptor internalization, we attempted to knock out zDHHC5 and zDHHC20 by CRISPR/Cas9 in U937 cells. In multiple attempts, knockout of zDHHC20 was not successful due to lethality.

However, zDHHC5 could be knocked out by CRISPR/Cas9 and was further validated by Western blot analysis probing with two different zDHHC5 antibodies (Figure 34, A). As shown in figure 34, A, in both zDHHC5 antibody blots (top and bottom, red arrow heads) no signal could be detected in clone #B14 compared to WT or #A8. Since zDHHC5 itself is also palmitoylated, knockout was further validated by performing acylRAC of WT U937 and  $\Delta$ zDHHC5 #B14 cells probing for zDHHC5 (Figure 34, B) and TNF-R1 (Figure 34, C). As shown in figure 34, B, signal for zDHHC5 could be detected in all fractions of WT U937 cells whereas in zDHHC5 knockout #B14 fractions were completely devoid of signal, confirming the successful knockout. Figure 34, C, shows an acylRAC of both cell lines probing for TNF-R1, where a similar signal pattern is observable, revealing that zDHHC5 is not responsible for TNF-R1 palmitoylation.

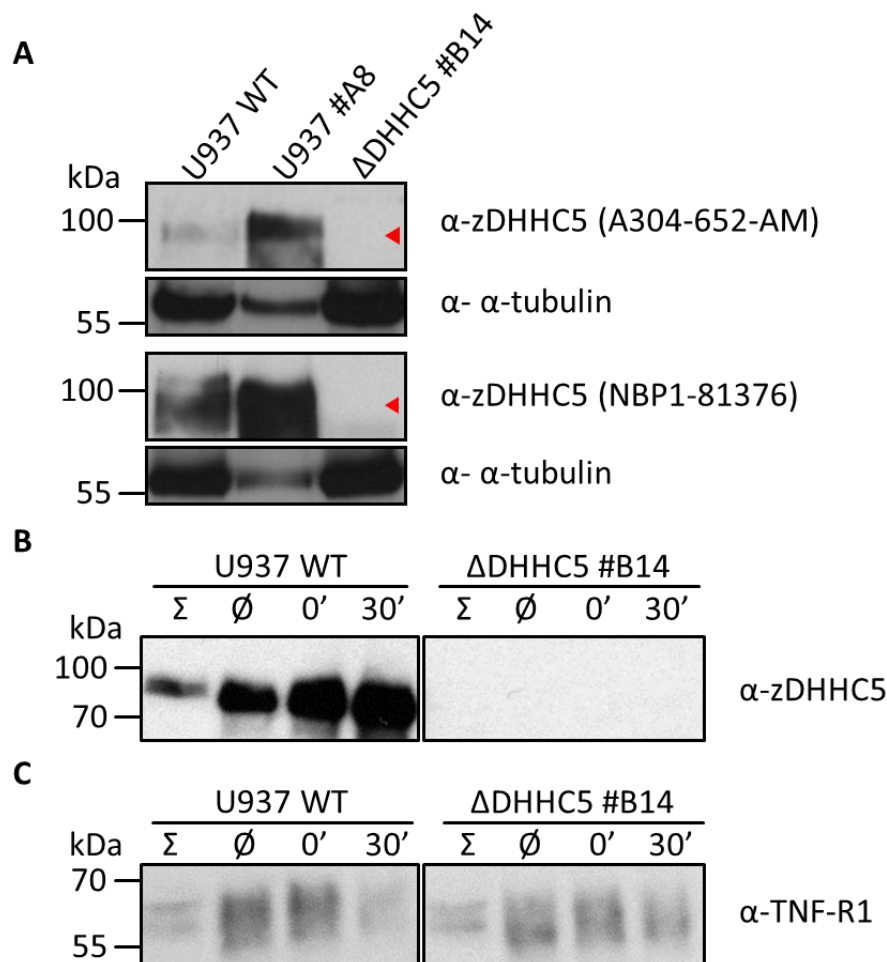


**Figure 34: Verification of the knockout of zDHHHC5 in U937 cells by Western blot analysis and acylRAC.** **A**, Western blot analyses were performed of whole cell lysates from WT U937 cells and CRISPR/Cas9 clones (#A8 and #B14, 25  $\mu$ g/lane). Blots were probed with two different zDHHHC5 antibodies (A304-652-AM, NBP1-81376) to determine the deficiency of zDHHHC5 of the generated clones. In clone #B14 signal for zDHHHC5 at 77 kDa was absent. Detection of tubulin served as a loading control. **B**, AcylRAC of WT U937 cells and zDHHHC5 knockout clone #B14 probing for zDHHHC5. For both cell lines, cells were either treated with 100 ng/ml TNF for 30 min (30') or left unstimulated ( $\emptyset$ ) before implementing the acylRAC with 2 mg of total protein. Western blots were performed from 25  $\mu$ l of acylRAC eluate and probed for zDHHHC5. Total cell lysate ( $\Sigma$ , 20  $\mu$ g of total protein) served as an input control. Compared to WT fractions, lanes of clone #B14 were completely devoid of signal, demonstrating the successful knockout. **C**, AcylRAC of WT U937 cells and zDHHHC5 knockout clone #B14 probing for TNF-R1. For both cell lines, cells were either treated with 100 ng/ml TNF for 30 min (30') or left unstimulated ( $\emptyset$ ) before implementing the acylRAC with 2 mg of total protein. Western blots were performed from 25  $\mu$ l of acylRAC eluate and probed for TNF-R1. Total cell lysate ( $\Sigma$ , 20  $\mu$ g of total protein) served as input control. Signal pattern for TNF-R1 in WT U937 coincides with pattern of zDHHHC5 knockout cells, indicating, zDHHHC5 is not the responsible protein acyltransferase for TNF-R1 palmitoylation.

#### 4.3.3 Characterization of zDHHHC5 knockout U937 cells regarding apoptosis and internalization of TNF-R1

To further characterize the zDHHHC5 knockout clone #B14 regarding TNF-R1 signaling, apoptosis and internalization was measured, shown in figure 35. Compared to the effects on WT U937 cells, the zDHHHC5 knockout clone revealed a diminished induction of apoptosis after TNF treatment (Figure 35, A), indicating that zDHHHC5 seems to be a pro-apoptotic protein. In contrast, internalization as shown in figure 35, B was unaffected by



the knockout of zDHHC5, since no significant change in the receptor internalization was measured compared to the WT.

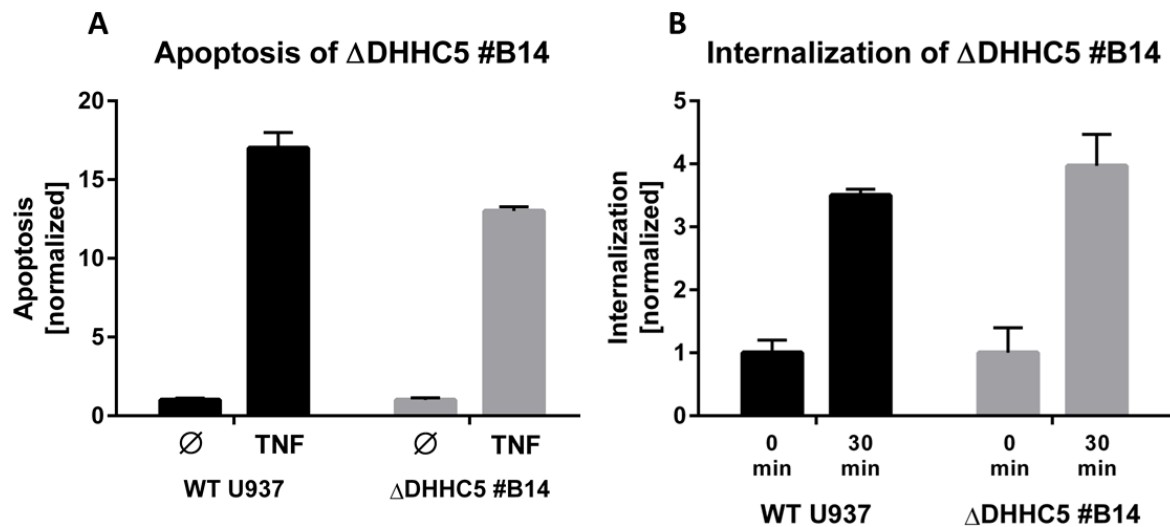


**Figure 35: Apoptosis and internalization of zDHHC5 knockout U937 cells.** **A**, For apoptosis, WT U937 and zDHHC5 knockout U937 cells were treated with 100 ng/ml TNF over a time course of 20 h to induce cell death. Untreated cells served as a negative control and values were normalized to that. In comparison to the WT where TNF induced cell death up to the factor 15, zDHHC5 knockout U937 cells show a slight decrease in apoptosis induction down to factor 12. (n=3; +/- SD). **B**, For the analysis of TNF-R1 internalization, cells were kept on ice and receptors were labeled with biotinylated TNF coupled to an avidin linked fluorescence dye. Internalization was initiated by temperature shift to 37 °C for 30 min. Internalization was normalized to cells kept on ice. After the temperature shift, WT receptor internalization increased compared to cells on ice up to the factor of 3.5. zDHHC5 knockout U937 cells showed no significant change in their internalization potential compared to WT U937. (n=3; +/- SD).

#### 4.3.4 Kinetic of zDHHC5 palmitoylation upon TNF stimulation

Although the protein acyltransferase zDHHC5 is not responsible for TNF-R1 palmitoylation, previous palmitoyl-proteome studies performed by Vinzenz Särchen as well as aforementioned immunoprecipitation and knockout studies unveiled zDHHC5 impact in receptor signaling. With the help of Vinzenz Särchen, acylRAC was performed at different time points, uncovering the palmitoylation status of zDHHC5 itself during TNF stimulation. As shown in figure 36, A, zDHHC5 signal changes during the time of TNF stimulation, after an initial increase up to 20 min, signal diminishes later on but never reaches basal level. Consistent loading of the gel was confirmed by the lightning red blot (Figure 36, B). The quantification of four independent Western blots (Figure 36, C) also approved the alternating palmitoylation status of zDHHC5, showing again an initial increase at 5 and 10 min followed by a progressive decrease within 60 min to a level which is even lower than the untreated fraction.

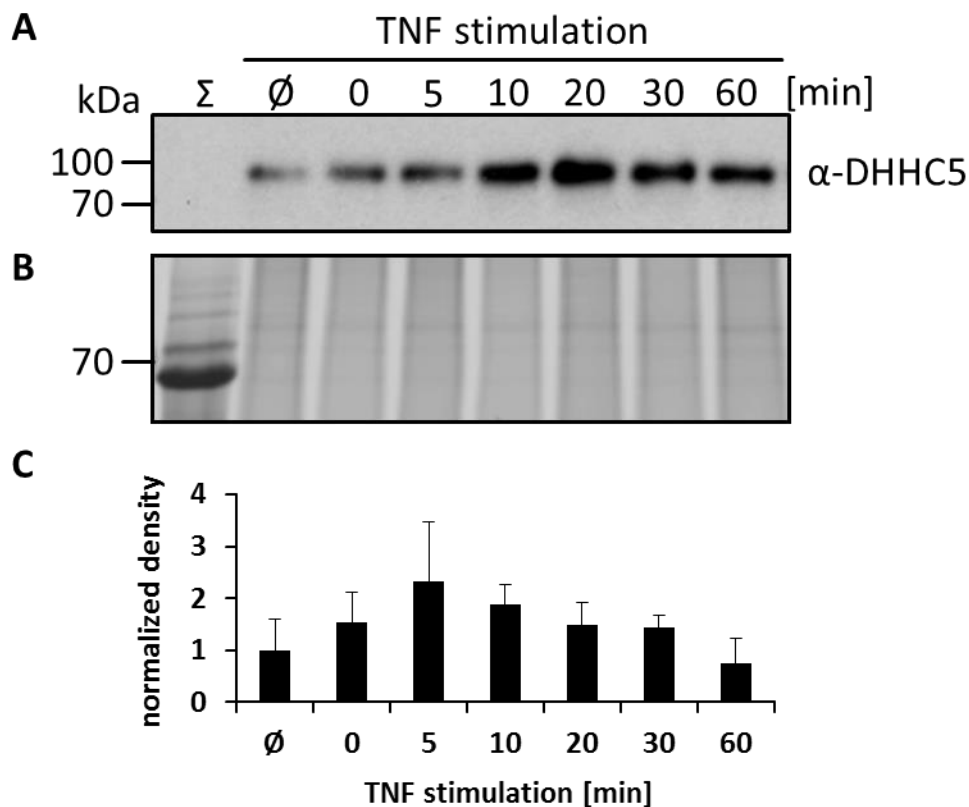


**Figure 36: Analysis of zDHHHC5 palmitoylation in response to TNF stimulation.** U937 cells were either treated with 100 ng/ml TNF for indicated time points (0, 5, 10, 20, 30, 60 min) or left unstimulated ( $\emptyset$ ) before implementing the acylRAC with 1.5 mg of total protein. **A**, Western blot was performed from 25  $\mu$ l of eluate of acylRACs hydroxylamine fractions for the specific time point and probed for zDHHHC5. Total cell lysate ( $\Sigma$ , 20  $\mu$ g of total protein) served as an input control. After an increase of signal intensity up to 20 min, signal progressively decreases during 60 min of TNF treatment. **B**, Lightning red staining of Western blot (A) as a loading control showed equal amounts of proteins per lane. **C**, Densitometric quantification of the Western blots of acylRAC hydroxylamine bands, normalized to the unstimulated sample ( $\emptyset$ ). The zDHHHC5 signal increases during the first 5 min and progressively decreases during 60 min of TNF treatment. (n=3; +/- SD).

#### 4.4 (De)-palmitoylation of TNF-R2

##### 4.4.1 Kinetic of TNF-R2 palmitoylation upon TNF stimulation

Since previous palmitoyl-proteome studies performed by Vinzenz Särchen uncovering a dynamic TNF-R2 palmitoylation upon TNF treatment. As TNF-R2 is the closest relative of TNF-R1 in the TNF superfamily and crosstalks between both receptors upon TNF binding has been reported [Fotin-Mleczek et al., 2002], palmitoylation of TNF-R2 was also further examined. In collaboration with Vinzenz Särchen, acylRAC was performed at different time points to investigate the kinetic of TNF-R2 palmitoylation after TNF treatment. In figure 37, A, the kinetic of TNF-R2 palmitoylation is depicted, showing a biphasic signal enhancement after TNF stimulation at 5 min and 20 min followed by a progressive decrease within 60 min. Figure 37, B confirms the consistent loading of the gel since all lanes show the same signal pattern. In the Western blot quantification of three

## 4. Results

independent experiments (Figure 37, C), a slight biphasic course of TNF-R2 palmitoylation could be confirmed. There, signal intensity for TNF-R2 peaks at 5 min but considering the error bars, signal progressively decrease within 60 min of TNF stimulation. In sum, the results show that TNF-R2 is also palmitoylated probably in a biphasic manner upon TNF stimulation.

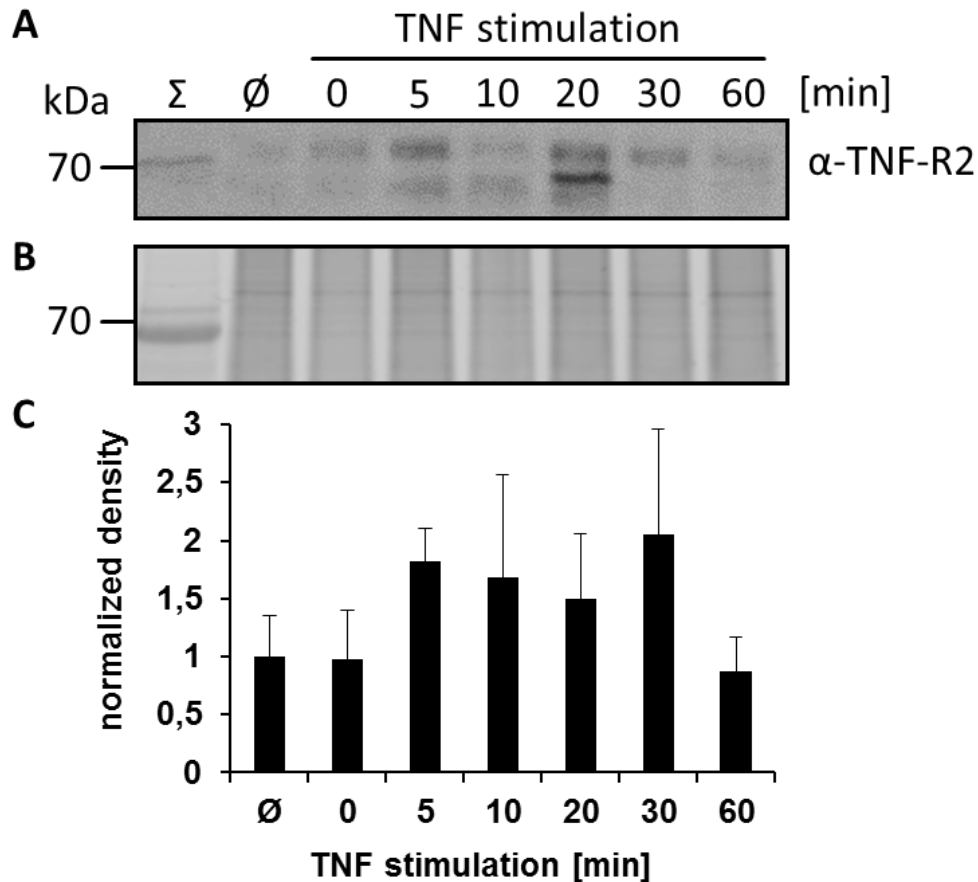


**Figure 37: AcylRAC of a TNF treated kinetic for different points of stimulation in U937 cells probing for TNF-R2.** U937 cells were either treated with 100 ng/ml TNF for indicated time points (0, 5, 10, 20, 30, 60 min) or left unstimulated ( $\emptyset$ ) before implementing the acylRAC with 1.5 mg of total protein. **A**, Western blot was performed from 25  $\mu$ l of eluate of acylRAC hydroxylamine fractions for the specific time point and probed for TNF-R2. Total cell lysate ( $\Sigma$ , 20  $\mu$ g of total protein) served as an input control. After a biphasic increase of signal intensity at 5min and 20 min, signal progressively decreases during 60 min of TNF treatment. **B**, Lightning red staining of Western blot (A) as a loading control showed equal amounts of proteins per lane. **C**, Quantification of the Western blots of acylRAC hydroxylamine bands. Normalized to the unstimulated sample ( $\emptyset$ ). TNF-R2 signal increases during the first 5 min and progressively decreases during 60 min of TNF treatment. (n=3; +/- SD).

### 4.4.2 Generation of TNF-R2 knockout U937 cells

TNF-R2 knockout cells were generated by employing the CRISPR/Cas9 system. Figure 38, A shows three putative TNF-R2 knockout clones #E2, #F8 and #H11, where no signal for TNF-R2 compared to WT is detectable. This was further corroborated by an acylRAC probing for TNF-R2 (Figure 38, B). There, hydroxylamine fractions of the TNF-R2 knockout clones were devoid of any signal whereas control blot showed signals for CD71,

## 4. Results

demonstrating equal loading. Surface staining with a TNF-R2 antibody of WT and TNF-R2 knockout U937 cells finally confirmed these results. The fluorescence intensity of the TNF-R2 knockout U937 cells was shifted towards the negative control (CellMask) while WT U937 displayed strong fluorescence intensity for TNF-R2 (Figure 38, C).

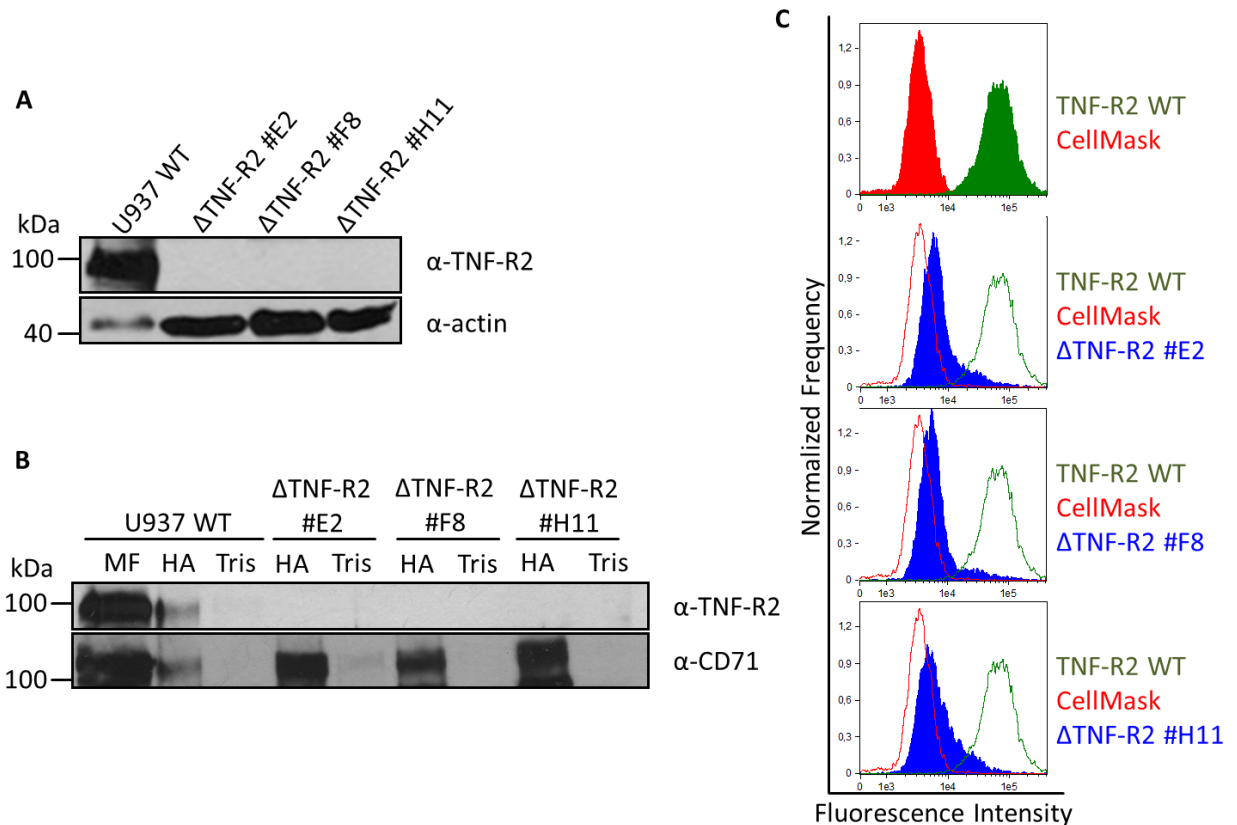


**Figure 38: Verification of the knockout of TNF-R2 in U937 cells by Western blot analysis, acylRAC and surface expression.** **A**, Western blot analyses were performed of whole cell lysates from WT U937 cells and CRISPR/Cas9 clones (#E2, #F8 and #H11, 25  $\mu$ g/lane). Blots were probed for TNF-R2 to determine the deficiency of TNF-R2 of the generated clones. In all three clones signals for TNF-R2 at 75 kDa was absent. Detection of actin served as a loading control. **B**, AcylRACs of WT U937 cells and TNF-R2 knockout U937 clones were implemented with 2 mg of total protein. Western blots were performed from 25  $\mu$ l of acylRAC eluate and probed for TNF-R2 and CD71. Membrane fraction (MF, 30  $\mu$ g of total protein) served as an input control. Compared to WT fractions, lanes of TNF-R2 knockout clones were completely devoid of signal, demonstrating the successful knockout. Tris fractions (TR) served as negative controls and were devoid of signal. CD71 blot served as a loading control. **C**, For surface expression, WT U937 and TNF-R2 knockout U937 cells were labeled with a TNF-R2 antibody coupled to a secondary antibody/fluorescent dye. The normalized frequency is plotted against the fluorescence intensity. Plasma membrane staining (CellMask) only served as a negative control (red graph) and shows no significant fluorescence intensity. WT receptor is shown as green graph indicating a surface expression based on the high fluorescence intensity compared to the controls. TNF-R2 knockout U937 clones (dark blue graphs) show low fluorescence intensity similar to plasma membrane stain, demonstrating the successful knockout of TNF-R2 in all three clones. One representative experiment is shown (n=4).

## 5. Discussion

### 5.1 Identification of TNF-R1 palmitoylation and its effect on subcellular localization and signaling

The cytokine TNF is a pleiotropic molecule with a broad biological spectrum, ranging from pro-inflammatory, proliferative and differentiation to various forms of programmed cell death. Based on the reports from the group of Stefan Schütze and others it became clear that the duality of the opposed biological signaling outcome of TNF depends primarily on the subcellular localization of its main signaling receptor: TNF-R1. It triggers either survival from membrane bound receptors or death of the cell, mediated by receptor internalization [Schneider-Brachert et al., 2004; Schütze et al., 2008; Cendrowski et al., 2016; Fritsch et al., 2017]. To avert any damage to cells and tissues from excessive cell growth or death, the physiological outcome mediated by TNF-R1 signaling needs to be tightly regulated which is assured by various dynamic posttranslational modifications. Previous studies revealed multiple modifications of TNF-R1 such as receptor phosphorylation [Cottin et al., 1999; Cottin et al., 2002; van Linden et al., 2005], glycosylation [Corti et al., 1995; Han et al., 2015; Holdbrooks et al., 2018] and ubiquitination [Draber et al., 2015; Fritsch et al., 2014; Wagner et al., 2016], altering the ligand affinity to TNF-R1, the subcellular localization, internalization and thus, signaling capacity. Despite the discovery of multiple signal pathways and their biological effects, it is still enigmatic how the intracellular trafficking and maturation of TNF-R1-receptosomes are regulated and how TNF-R1 localizes to different subdomains in the biological membranes or subcellular compartments enabling differentiated signal transduction at the right time upon TNF stimulation.

In the last decade, S-acylation became a rapid growing field of interest in the research of posttranslational modifications of proteins. Due its reversible and dynamic alteration of protein hydrophobicity it promotes the interaction of proteins with other proteins, lipids and membranes [Blaskovic et al., 2013; Resh, 2016]. S-acylation has also been described as a mechanism to redirect proteins into specific subdomains of membranes such as lipid rafts or caveolae [Charollais and van der Goot, 2009; Maguy et al., 2006]. Such associations of TNF-R1 with lipid rafts have been reported as being essential for proper NF- $\kappa$ B regulation and activation, where palmitoylation seems to be involved in [Legler et al., 2003; Doan et al., 2004; Orzechowska et al., 2011]. Caveolae-like structures which represent another subgroup of lipid rafts seem to be associated with TNF-R1 induced cell death [Ko et al., 1999; D'Alessio et al., 2010; Dargelos et al., 2018]. Two relatives of TNF-

R1, TRAILR1 and CD95 are reported to be palmitoylated where palmitoylation triggers the localization of the receptor into lipid rafts and is required for DISC formation inducing apoptotic cell death [Feig et al., 2007; Chakrabandhu et al., 2007; Rossin et al., 2009].

Rossin and colleagues claimed that TNF-R1 is not palmitoylated examining the palmitoylation status of transiently expressed death receptors by metabolic labeling with radioactive palmitate [Rossin et al., 2009]. However, in this dissertation a constitutive palmitoylation of TNF-R1 was identified using the acyl-RAC approach inspecting the palmitoylation status of endogenously expressed TNF-R1 under TNF and Fab<sub>TNF</sub> treatment as well as in untreated U937 cells. Since other death receptors also have been described as being constitutively palmitoylated (CD95, TRAILR1, DR6), this seems as a characteristic in the death receptor family [Feig et al., 2007; Chakrabandhu et al., 2007; Rossin et al., 2009; Klíma et al., 2009; Gonzalez and Ashkenazi 2010; Rossin et al., 2015].

Moreover, TNF-R1 palmitoylation was validated in the Schütze group by metabolic labeling using the clickable palmitate analog 17-ODYA. Since the detection of 17-ODYA labeled TNF-R1 was very weak, we assumed that the turnover for a strong labeling of endogenous TNF-R1 is too low, despite the short half-life of TNF-R1 of less than 3 hours. Furthermore, in comparison with other endogenously expressed death receptors presented at the cell surface, TNF-R1 expression is with 300 - 1000 receptors per cell less prominent than e.g. CD95 with 10.000 - 100.000 receptors per cell. This facilitates the detection of the respective receptor by metabolic labeling [Martin, 2013; D'Alessio et al., 2010; Pfizenmaier et al., 1987; Richter et al., 2012; Meng et al., 2011]. We assumed that TNF-R1 palmitoylation is needed for PM transport. Thus, we initially depleted TNF-R1 from the cell surface by histamine treatment, to enforce the replenishment of TNF-R1 from the Golgi pool and to optimize the timeframe for metabolic labeling which increased the signal of metabolically labeled TNF-R1 in WB [Wang et al., 2003].

In other receptor systems such as in CD95, TRAILR1, DR6 and CD71, receptor palmitoylation occurs at cysteines which are juxta membranous or even within the TMD [Charollais and van der Goot, 2009; Blaskovic et al., 2013; Rossin et al., 2009; Klíma et al., 2009]. The comparison of the cytoplasmic amino acid sequence of TNF-R1 in different mammalian species revealed four conserved (C223, C248, C395, and C433) and two less conserved (C304 and C442) cysteine residues (Figure 39).

## 5. Discussion

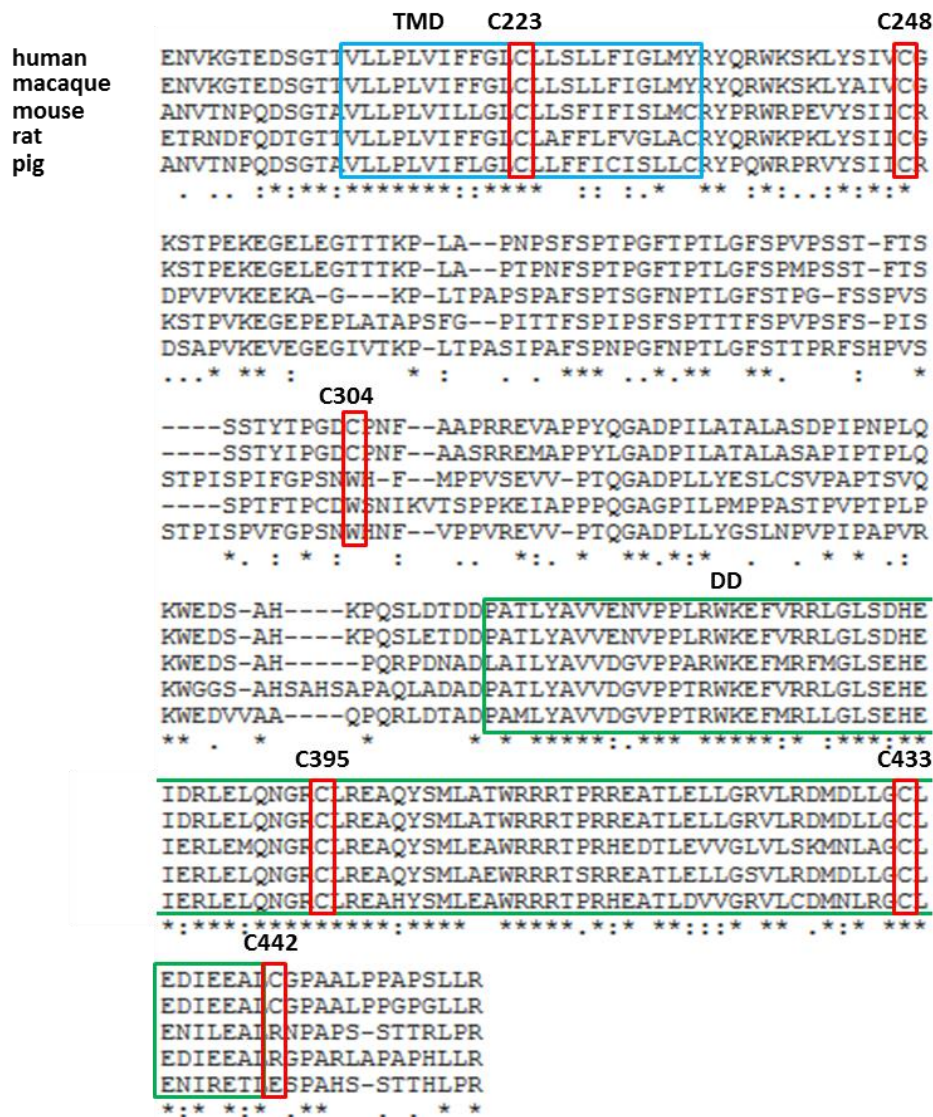


**Figure 39: Alignment of TNF-R1 amino acid sequence from different mammals.** Comparison of the cytoplasmic amino acid sequence of TNF-R1 within different mammal species such as human, macaques, mice, rat and pig (part of the N-terminus is not shown). Conserved (C223, C248, C395, and C433) and less conserved (C304 and C442) cysteine residues represent the putative palmitoylation sites of TNF-R1 and are shown in red boxes. Amino acids belonging to the transmembrane domain (TMD) are shown in the blue box. Amino acids belonging to the death domain (DD) are shown in the green box. The asterisk (\*) indicates conserved residues. The colon (:) indicates conservation in groups of strongly similar properties. The period (.) indicates conservation in groups of weakly similar properties.

Based on data from other receptor systems and palmitoylation site prediction using the CSS-palm algorithm, cysteines C223, C248 and C304 were chosen for mutagenesis experiments in TNF-R1 [Ren et al., 2008]. The hypothesis that cysteines close to or within the TMD are putative receptor palmitoylation sites could be also confirmed for TNF-R1, expressing the mutant receptors in TNF-R1 knockout HeLa80 cells. Under high protein loading on the gel (140 µg/lane), TNF-R1 knockout HeLa80 cells still showed signals for TNF-R1. Therefore, full and short length receptors of the triple mutant were recognized by a FLAG antibody detecting no signal for mutant receptor in the WB. Based on this

observation, cysteines C223, C248 and C304 appear to be the palmitoylation sites of TNF-R1. Thus, it can be concluded that cysteines in the DD (C395, C433) or downstream of the DD (C442) are not palmitoylated.

In U937 cells, full length transduced triple, double and single mutant receptors unfortunately could not be reproducibly detected, although cells were cultured in the selection medium, indicating a successful transduction. The possible reason for the failure to detect these full length TNF-R mutants can have several explanations: The lack or change in the correct palmitoylation status of TNF-R1 could possibly be caused by the proteasomal degradation of misfolded, retained and accumulated mutant TNF-R1 in the Endoplasmic Reticulum (ER) [Rao et al., 2004; Lam et al., 2006; Abrami et al., 2008; Turner et al., 2012]. Alternatively, receptors missing the quality control in the ER can be checked again in the Golgi where they can also receive further palmitoylation. Due to improper conformation or to unfitting hydrophobic mismatches caused by the lack of palmitoylation, receptors in the Golgi compartment can also undergo lysosomal degradation [Schulze et al., 2009; Charollais and van der Goot, 2009; Foot et al., 2017]. Such degenerated (post-) translational products may be responsible for the multiple bands in the WB of overexpressed mutant TNF-R1 observed in this project which appear only after re-transduction of the signal-less TNF-R1 deficient clone. Furthermore, those products may form protein aggregates in their respective compartment resulting in signal bands migrating at higher MW than the predicted protein [Lam et al., 2006; Banfield, 2011]. Another possibility could be different isoforms of TNF-R1 derived from alternative splicing of the pre-mRNA e.g. by exon skipping [Cáceres et al., 1994; López-Urrutia et al., 2017]. Otherwise, other posttranslational modifications such as glycosylation, phosphorylation, sumoylation, myristylation, methylation or acetylation can change the molecular weight or the migration behavior in SDS-PAGEs [Shirai et al., 2008]. Besides that, also the detection of unspecific signals by the antibodies as well as the occasionally huge amounts of total protein in the lysates up to 140 µg per lane could account for additional bands. In addition, transduction of WT TNF-R1 is known also to be lethal in U937 cells which has been shown in earlier experiments of the Schütze group. This is presumably due to a bias of U937 cells to respond to pro-apoptotic stimuli. This is most likely caused by the increased expression of TNF-R1 above the endogenous level, resulting in the killing by endogenously released TNF from the cells after several days of transduction even without selection [Pfizenmaier et al., 1987].



Also, qPCR analysis of the mRNA levels in U937 cells of mutant and WT TNF-R1 was not successful presumably due to the low expression of WT TNF-R1 mRNA in U937 cells which may be only initiated when the Golgi pool of WT TNF-R1 is exhausted [Pfizenmaier et al., 1987; Higuchi and Aggarwal, 1994; Wang et al., 2003; Turner et al., 2012]. In sum, overexpression of mutant TNF-R1 seems highly cell line dependent since detection of all receptor mutants in HeLa80 cells was successful within two experimental series whereas, for most mutant receptors in U937 cells all twelve attempts failed.

The mutagenesis of one putative palmitoylation site C248 in U937 cells resulted in multiple changes in the biological outcome of the active full length mutant receptor C248S. Although protein synthesis of C248S was highly increased compared to WT receptor, the surface expression was reduced while internalization was not affected. Furthermore, the signaling via the NF- $\kappa$ B pathway was blocked whereas apoptosis induction was restored but on a lower level than the WT receptor. It can therefore be assumed that the change of the palmitoylation status of TNF-R1 at cysteine 248 alters the receptor transport from the Golgi to the PM, suggesting the necessity of palmitoylation in this process. In this context, Wang and colleagues could show that membrane resident TNF-R1 is shed from the cell surface upon histamine treatment and that the receptor is replenished from an intracellular Golgi pool [Wang et al., 2003]. This was verified in the Schütze group by imaging flow cytometry. Additionally, subsequent to cell surface depletion of TNF-R1 by histamine stimulation, TNF-R1 delivered from the Golgi pool to the PM could be labeled with the palmitate analog 17-ODYA. This was futile without prior histamine treatment. This indicates that due to the changed palmitoylation of mutant receptor C248S, the receptor is retained either in the ER or the Golgi where further transport to the PM is terminated e.g. due to the hydrophobic mismatch of the receptors TMD in the respective membrane by improper tilting. To prove this hypothesis, 17-ODYA labeling could be performed using C248S cells where the signal of the metabolic labeled mutant receptor should be decreased compared to the WT TNF-R1 due to its retention in the ER or Golgi [Tanimura et al., 2006; Lam et al., 2006; Joseph and Nagaraj 1995; Mitra et al., 2004; Charollais and van der Goot, 2009]. Moreover, besides impaired PM transport, lipid raft localization of TNF-R1 also appears to be altered by the C248S mutagenesis. We could confirm the report of Legler and colleagues having shown the TNF-R1 localization into lipid raft by sucrose density gradient ultracentrifugation in U937 cells [Legler et al., 2003]. As shown in this work, upon TNF stimulation the receptor shifted into the lipid raft fractions, determined by flotillin-2 colocalization in the sucrose fractions. Interestingly, analysis of the mutant receptor C248S distribution revealed a more pronounced

localization of the receptor in lipid raft fractions as well as in fractions with higher buoyancy even without TNF stimulation. Together, this suggests that palmitoylation also affects the distribution and order within the fluid plasma membrane, shuttling the receptor between different membrane microdomains from non-raft, raft and caveolae-like structures, finally determining the biological outcome [Lillemeier et al., 2006; Schneider-Brachert et al., 2004; Ko et al., 1999; Helms and Zurzolo, 2004].

Translocation of TNF-R1 into lipid rafts has been described to be crucial for NF- $\kappa$ B activation [Legler et al., 2003]. In my experiments, after transduction in HeLa80 cells, only WT TNF-R1 showed a slight degradation of I $\kappa$ B, indicating a modest rescue of WT TNF-R1 mediated activation of NF- $\kappa$ B upon TNF stimulation due to the assembly of complex I. All other full length receptor mutants were unchanged, implying that either mutant receptors are transported to the cell surface with too low frequency for proper NF- $\kappa$ B activation or receptors were excluded from the correct lipid rafts or miss located into other subdomains or protein microdomains due to their altered palmitoylation [Charollais and van der Goot, 2009; Blaskovic et al., 2013].

In earlier reports of the Schütze group, clathrin-mediated receptor internalization has been reported to be required for the execution of apoptosis. According to the literature, this is presumably initiated from non-raft subdomains of the PM [Schneider-Brachert et al., 2004; Kaksonen and Roux, 2018]. Internalization analysis of the mutant receptors compared to WT TNF-R1 showed no significant alteration in their ability to internalize after TNF stimulation, despite mutant receptors were less prominent expressed at the cells surface. However, only mutant receptor C248S restored apoptosis induction, albeit at a lower level than WT TNF-R1. Other full length receptor mutants such as C223S/C248S and C248S/C304S which were expected to potentially induce apoptosis, showed no increase in cell death induction after TNF stimulation. This supports observations that apoptosis is not solely dependent on internalization of the receptor itself but also on the amount of internalized receptors triggering downstream signal cascades [Pfizenmaier et al., 1987; Higuchi and Aggarwal, 1994; Schneider-Brachert et al., 2004]. Moreover, the localization of TNF-R1 within different protein or lipid microdomains of the PM seems to further differentiate TNF-R1 signaling. Besides the clathrin-coated pit mediated internalization of TNF-R1 from non-rafts region, resulting in apoptosis, clathrin-independent internalization from lipid rafts, caveolae or caveolae-like structures has been described causing either cell death or inflammation [Schneider-Brachert et al., 2004; Kaksonen and Roux, 2018; D'Alessio et al., 2005; Pelkmans and Helenius, 2002; Di

Guglielmo et al., 2003; Ko et al., 1999; Lillemeier et al., 2006]. Additionally, disruption of caveolae by methyl- $\beta$ -cyclodextrin (MCD) -mediated cholesterol depletion resulted in the redistribution of TNF-R1 into other subdomains of the PM. In parallel, NF- $\kappa$ B activation was abrogated and cells sensitized for apoptosis [D'Alessio et al., 2005; Legler et al., 2003]. Hence, the diversity of the biological outcomes of TNF seems to be balanced by the relocation of TNF-R1 into different protein clusters or subdomains of the biological membranes. Apparently, the aforementioned diversity of the partly contradictory results in the literature seems to be related to cell-type specificity. In some cell lines, the ability to form caveolae disappears during prolonged cultivation of the cells which results in the relocation of the membrane proteins into lipid rafts [D'Alessio et al., 2005]. In contrast to HT1080 cells where NF- $\kappa$ B is activated from lipid raft regions, lipid rafts and caveolae rather signal for the MAPK/ERK pathway but not for NF- $\kappa$ B in primary mouse macrophages [Ko et al., 1999]. However, also lipid raft independent pathways have been reported in human airway smooth muscle cells, triggering NF- $\kappa$ B and MAPK from non-raft subdomains [Hunter and Nixon, 2006]. This demonstrates that the quality of the lipid raft mediated signal varies greatly between the cell lines used.

### **5.2 APT2 alters TNF-R1 distribution in the plasma membrane by receptor depalmitoylation**

During the long-term treatment of U937 cells with TNF, I could show that the amount of palmitoylated TNF-R1 decreased within one hour, suggesting a receptor depalmitoylation upon TNF stimulation. The initial increase observed after 5 min may be explained by replenishment of TNF-R1 from either the ER or the Golgi pool to the PM after TNF binding, which probably depends on receptor palmitoylation [Wang et al., 2003]. For CD95 this has also been described where the initial ligand binding resulted in an increased fusion of CD95 containing vesicles with the PM, enhancing the amount of CD95 at the cell surface [Stephan et al., 2017].

Interestingly, in HeLa80 cells a decrease in TNF-R1 palmitoylation could not be detected in both, cells treated only with TNF as well as CHX (cycloheximide) pre-incubated HeLa80 cells. Normally, HeLa80 cells as most cell lines mainly trigger the activation of NF- $\kappa$ B upon TNF stimulation and less cell death induction by receptor internalization [Muppidi et al., 2004]. The inhibition of the protein biosynthesis in cells by CHX treatment shifts the pro-survival NF- $\kappa$ B signaling towards cell death induction.

Thus, under CHX treatment, the anti-apoptotic signaling mediated by NF- $\kappa$ B activation is terminated. This enables internalized TNF-R1 to establish the proteolytic caspase cascade, resulting in cell death. However, since in HeLa80 cells less TNF-R1s are internalized than in U937 cells, less receptors need to be depalmitoylated [Pfizenmaier et al., 1987]. This may explain why (de)-palmitoylation of TNF-R1 in HeLa80 cells was not significantly affected upon TNF stimulation at the 90 min time point.

Only a few members of the family of protein thioesterases (PTE) are known so far. However, since APT1 and PPT1 were found in receptosome proteome dataset, immunoprecipitation was used to examine the possible interaction of PTEs with the TNF-R1. Due to the predominant lysosomal localization of PPT1 and its constant interaction with TNF-R1 upon TNF stimulation, we assumed that PPT1 is not involved in receptor depalmitoylation [Verkruyse and Hofmann, 1996]. However, PPT1 appears to be linked to the TNF-R1 signaling independent of its direct interaction with the TNF-R1, since knockout experiment showed a resistance to TNF induced apoptosis induction, correlating with our observations of full cell death induction mediated by the fusion of receptosomes with lysosomes [Tardy et al., 2009; Schneider-Brachert et al., 2004; Edelmann et al., 2011; Fritsch et al., 2014]. On the contrary, APT1 and APT2 revealed a dynamic interaction with TNF-R1 after TNF binding. Both proteins have been reported as cytoplasmic PTEs which are also palmitoylated themselves by yet unknown PATs. This palmitoylation facilitates the localization of APTs from the cytoplasm to specific membranes where they catalyze the depalmitoylation of specific target proteins [Tomatis et al., 2010; Kong et al., 2013].

Upon the discovery that APT2 is activated after TNF stimulation in U937 cells and that TNF-R1 palmitoylation increased in the WB of acylRAC after APT2 specific inhibition, I pre-incubated recombinant APT2 with the membrane fraction used for the acylRAC. This resulted in a decrease of palmitoylated TNF-R1 in the WB, indicating that APT2 depalmitoylates TNF-R1 *in vitro*. Legler and colleagues earlier reported that upon TNF stimulation, TNF-R1 translocates into lipid rafts where it triggers for NF- $\kappa$ B activation [Legler et al., 2003]. In this work it could be shown that TNF-R1 needs to be depalmitoylated by APT2 for efficient translocation into lipid rafts and thus also for NF- $\kappa$ B activation. Investigating the I $\kappa$ B degradation in APT2 inhibited U937 as well as in APT2 down modulated U937 cells, we revealed that in both cases the degradation of I $\kappa$ B was impaired. Hence, the NF- $\kappa$ B pathway in TNF-R1 signaling appears to be blocked by the prevented depalmitoylation and thus also translocation of TNF-R1, suppressed by APT2 inhibition and down modulation.

Interestingly, other known palmitoylated proteins such as CD71, Integrin $\alpha$ 6, PPT1 and Rab5 were not affected by APT2 treatment. Substrate specificity in PTEs and especially in APTs has been described before e.g. growth-associated protein-43 (GAP-43) is to be depalmitoylated by APT2 but not by APT1 [Tomatis et al., 2010]. On the other side, big potassium (BK) channels or H-Ras are only depalmitoylated by APT1 but not by APT2 [Tian et al., 2012; Dekker et al., 2010]. Furthermore, APT1 was found to depalmitoylate APT2 and also itself, ensuring the dynamic re-localization of APTs from the cytoplasm to the PM and Golgi membrane [Kong et al., 2013; Tabaczar et al., 2017].

As shown here, the pharmacological inhibition of APT2 resulted in a dose-dependent reduction of TNF-R1 internalization which was partly reversed by lowering the inhibitors concentrations. This might be caused by compensation by other activated but unknown PTEs which are not affected by the APTs, the applied inhibitors, by depalmitoylation, or the lack of depalmitoylation of other proteins involved in this process [Tabaczar et al., 2017]. Surprisingly, upon APT2 inhibition and down modulation in U937 cells, TNF induced apoptosis was significantly increased. Moreover, this effect was also detectable on the protein level where apoptosis markers such as PARP1 or cleaved caspase-3 increased in signal intensity whereas the involvement of necroptosis in this process could be excluded.

Earlier reports of the Schütze group and others showed that upon TNF-R1 activation the production of the strong pro-apoptotic mediator ceramide is initiated by plasma membrane bound neutral sphingomyelinase (nSMase) [Krut et al., 2006; Neumeyer et al., 2006; Philipp et al., 2010]. We propose that due to APT2 inhibition, TNF-R1 internalization is decreased which enables the PM resident receptor to assemble the nSMase activating protein complex. Therefore, the adaptor protein FAN (factor associated with nSMase) is recruited to TNF-R1 via its NSD (neutral sphingomyelinase activating domain) motif [Adam-Klages et al., 1996]. This further engages RACK1 (receptor for activated C-kinase) and EED (embryonic ectodermal development) to the complex involving integrins [Tcherkasowa et al., 2002; Philipp et al., 2010]. EED serves as a scaffold protein, promoting the recruitment and activation of nSMases-2. Active nSMases-2 hydrolyzes sphingomyelin in the PM, producing ceramide which results in increased cell death [Morales et al., 2007]. This pathway could be also completely blocked by a nSMase inhibitor. nSMase-2 and Integrin $\alpha$ 6 have been reported as being palmitoylated whereas nSMases-3 is known to be localized to lipid rafts where it is activated by TNF [Tani and Hannun, 2007; Sharma et al., 2012; Moylan et al., 2014]. Therefore, it can be assumed

that due to palmitoylation and hence localization to lipid raft, the assembly of this signaling complex is facilitated through accumulation of the proteins in the specific protein microdomains of the PM.

### **5.3 zDHH5 promotes TNF-receptosome maturation in TNF-R1 signaling**

zDHH5 is one of three mainly plasma membrane resident acyltransferases which is, depending on its subcellular localization, also palmitoylated [Ohno et al., 2006; Brigidi et al., 2015]. The dynamic interaction of zDHH5 with the TNF-R1 signaling complex after TNF stimulation could be shown here by several approaches such as the palmitoyl-proteome studies, the TNF-receptosome studies and immunoprecipitation. After TNF stimulation, zDHH5 is palmitoylated, probably for recruiting the PAT to early TNF-receptosomes. In consequence an involvement of zDHH5 within the endocytic maturation of TNF-receptosomes is likely. Indeed, the knockout of zDHH5 in U937 cells showed a decreased apoptosis rate, suggesting a pro-apoptotic function of zDHH5 in TNF-R1 signaling. However, internalization as well as TNF-R1 palmitoylation was not affected by the zDHH5 knockout, indicating that zDHH5 is recruited to TNF receptosomes after membrane fission from the PM but does not directly interfere with the TNF-R1. Substrates of zDHH5 affecting the trafficking and maturation of TNF-receptosomes and apoptosis downstream signaling need to be elucidated in future experiments.

### **5.4 TNF-R2 palmitoylation may contribute to TNF-receptor crosstalk**

TNF-R2 is the closest relative of TNF-R1 and shares an overall amino acid sequence identity with TNF-R1 of 25 % in the extracellular domain [Dembic et al., 1990]. The expression of TNF-R2 is highly regulated in cells of the immune system, endothelial cells, prostate cells and cardiac myocytes. The expression of TNF-R2 varies upon certain stimuli such as LPS, IL-2 and TNF whereas the amount of TNF-R1 is nearly unchanged. Therefore, the ratio between TNF-R1 and TNF-R2 can fluctuate substantially, affecting the biological outcome of TNF signaling [Carpentier et al., 2004]. In U937 cells, the total amount of TNF-R2 is two to three times higher than that of TNF-R1 [Higuchi and Aggarwal, 1994]. TNF-R2 is only fully activated by membrane resident TNF (mTNF) and only slightly by soluble TNF (sTNF) [Grell et al., 1995; Grell et al., 1998]. Intensive crosstalk between TNF-R1 and TNF-R2 but also with other death receptors such as CD95 has been described before [Tartaglia et al., 1993; Varfolomeev et al., 1996; Wajant, 2017]. Due to the lack of a DD, TNF-R2 is

not able to induce apoptosis directly by DISC formation. Nevertheless, in some cell lines, a TNF-R2 mediated apoptosis induction has been described, caused by the increased production of endogenous mTNF, triggering TNF-R1 mediated apoptosis. Furthermore, an “intracellular cooperation model” has been proposed where TNF-R2 enhances TNF-R1 induced caspase-8 activation by the sequestration of cytosolic TRAF2 to the TNF-R2 complex. This leads to the capturing of the anti-apoptotic cIAP proteins which then bind less to the TNF-R1 signaling complex, reducing its anti-apoptotic outcome [Carpentier et al., 2004; Grell et al., 1998; Vercammen et al., 1995; Faustman and Davis, 2010; Chan and Lenardo, 2000; Fotin-Mleczek et al., 2002]. Moreover, the NF- $\kappa$ B regulated expression of other anti-apoptotic proteins can be also prevented by the TNF-R2 mediated TRAF2 depletion, enhancing TNF-R1 induced apoptosis. On the other side, TNF-R2 may also be involved in the upregulation of pro-apoptotic proteins such as Bax and Bak, triggering the MOMP, and thus, promoting apoptosis [Alexander-Miller et al., 1998; Karin and Lin, 2002; Carpentier et al., 2004]. Under normal conditions, TNF-R2 directly recruits TRAF2 via its TRAF domain which in turn engages TRAF1 to the complex leading to the activation of non-apoptotic signaling pathways such as NF- $\kappa$ B, JNK, p38 and ERK [Baud and Karin, 2001; Hehlhans and Pfeffer, 2005]. It has been reported that TRAF2 localization into lipid rafts via its RING finger domain is crucial for the activation of some non-apoptotic signal pathways such as JNK [Arron et al., 2002; Ceccarelli et al., 2017]. In the palmitoyl-proteome studies of the Schütze group TRAF2 was also found to be palmitoylated, which may further direct and stabilize TRAF2 into lipid rafts.

TNF-R2 is also palmitoylated which initially increased after TNF stimulation with sTNF. This is presumably either caused by an increased cell surface transport from the cell interior, by a TNF-R1 induced palmitoylation or by a low affinity binding induced palmitoylation of sTNF to TNF-R2. Both processes may enable the TNF-R2 mediated signaling of JNK by bringing TNF-R2 and TRAF2 into the same lipid raft or protein microdomain and thus, in close proximity for their interaction. Other pathways such as NF- $\kappa$ B or p38 have been reported not to be activated from those rafts, suggesting a further segmentation and distribution of signal pathways in the protein microdomains of the PM [Arron et al., 2002; Carpentier et al., 2004; Lillemeier et al., 2006].

### 5.5 Model of TNF-R1 palmitoylation

Based on the current results generated during this dissertation and on the additional findings in the Schütze group, the following model of de-palmitoylation mediated regulation of TNF-R1 signaling is hypothesized (Figure 40): After the translation of TNF-R1 in the ER, the receptor is presumably palmitoylated in the Golgi which allows the transport to definite membrane compartments of the PM such as caveolae, caveolae-like structures or distinct lipid rafts. Upon ligand binding, TNF-R1 is primed for cell survival by the APT2 mediated depalmitoylation, resulting in the translocation of TNF-R1 in another membrane location like lipid rafts which allows the recruitment of the “complex I” proteins TRADD, RIP1 and TRAF2. During this activation also TRAF2 is palmitoylated, stabilizing its raft residence. Complex I then induces the activation of NF- $\kappa$ B, leading to survival of the cells. Lack of depalmitoylation mediated by APT2 inhibition leads to trapping of activated TNF-R1 in its steady state compartment in the PM. This results in the enhanced activation of nSMase which catalyzes the production of ceramide, shifting the TNF-R1 signaling towards cell death. Apoptosis mediated by internalization, forming TNF-receptosomes, may occur from both subdomains of the PM, the lipid disordered and caveolae compartment where the DISC formation also results in cell death.

Internalization, however, is neither affected by the mutagenesis of Cys 248 in the TNF-R1 nor APT2 down modulation but partially by pharmacological APT2 inhibition. TNF-R2 is also palmitoylated which dynamically changes upon ligand binding, presumably localizing the receptor into lipid rafts which facilitates the recruitment of its signaling complexes, additionally affecting the TNF-R1 signaling by crosstalk. Upon TNF stimulation, zDHHC5 is palmitoylated, resulting in its recruitment to early TNF-receptosomes. Although the knockout of zDHHC5 resulted in the reduction of apoptosis, confirming the involvement of zDHHC5 in receptosome maturation, the substrates inducing this change are still unknown and need to be elucidated.

In sum, in this dissertation it could be shown that the pleiotropic signaling of TNF-R1 is also regulated by the posttranslational modification of palmitoylation, altering the distribution of TNF-R1 in the PM and thus determining the biological outcome in TNF-R1 signaling. However, many questions are still unanswered and need to be clarified in future: What is the purpose and biological consequence of the triple palmitoylation of TNF-R1? Which PATs are involved in TNF-R1 palmitoylation and in which compartment does the multiple palmitoylation occur? Are there cell line or tissue dependent differences due to their lipid composition and PAT/PTE expression? How does the



cross-talk between the TNF-Rs but also between other death receptors such as CD95 and TRAIL-Rs influence their respective signaling? Might this understanding provide access for pharmaceutical intervention in future disease treatment such as for cancer or chronic inflammatory diseases?

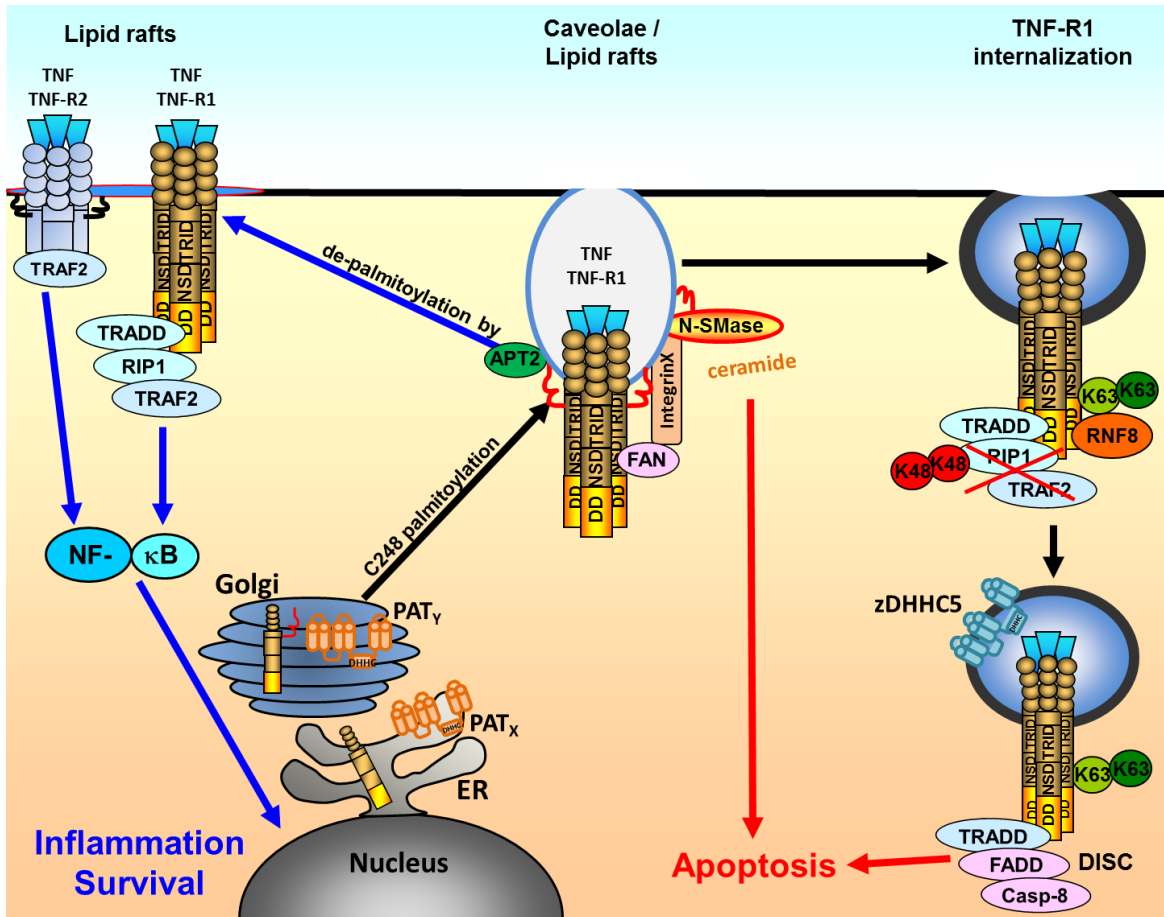


**Figure 40: Model of TNF-R1 palmitoylation,** TNF-R1 is palmitoylated in the Golgi and its C248 palmitoylation enables the transport to caveolae in the PM [D'Alessio et al., 2005]. Upon TNF binding, TNF-R1 is either depalmitoylated by APT2, leading to the translocation into another raft compartment of the PM, triggering NF-κB activation. Alternatively, TNF-R1 activation triggers the translocation out of caveolae into non-raft subdomains where TNF-receptosomes are formed by clathrin-dependent endocytosis, resulting in apoptosis mediated by DISC formation. Under APT2 inhibition or down modulation, active TNF-R1 in caveolae triggers nSMase dependent ceramide production, resulting in apoptosis. The PAT zDHH5 is involved in TNF-receptosome maturation and cell death induction.

## 6. References

- Abrami, L.; Kunz, B.; Iacovache, I.; van der Goot, F. G.** (2008): Palmitoylation and ubiquitination regulate exit of the Wnt signaling protein LRP6 from the endoplasmic reticulum. In: *Proceedings of the National Academy of Sciences of the United States of America* 105 (14), S. 5384–5389. DOI: 10.1073/pnas.0710389105.
- Adam-Klages, S.; Adam, D.; Wiegmann, K.; Struve, S.; Kolanus, W.; Schneider-Mergener, J.; Krönke, M.** (1996): FAN, a novel WD-repeat protein, couples the p55 TNF-receptor to neutral sphingomyelinase. In: *Cell* 86 (6), S. 937–947.
- Aggarwal, B. B.** (2003): Signalling pathways of the TNF superfamily: a double-edged sword. In: *Nature reviews. Immunology* 3 (9), S. 745–756. DOI: 10.1038/nri1184.
- Aggarwal, B. B.; Gupta, S. C.; Kim, J. H.** (2012): Historical perspectives on tumor necrosis factor and its superfamily: 25 years later, a golden journey. In: *Blood* 119 (3), S. 651–665. DOI: 10.1182/blood-2011-04-325225.
- Alexander-Miller, M. A.; Derby, M.A.; Sarin, A.; Henkart, P. A.; Berzofsky, J. A.** (1998): Supraoptimal Peptide–Major Histocompatibility Complex Causes a Decrease in Bcl-2 Levels and Allows Tumor Necrosis Factor  $\alpha$  Receptor II–mediated Apoptosis of Cytotoxic T Lymphocytes. In: *J Exp Med* 188 (8), S. 1391–1399. DOI: 10.1084/jem.188.8.1391.
- Arron, J. R.; Pewzner-Jung, Y.; Walsh, M. C.; Kobayashi, T.; Choi, Y.** (2002): Regulation of the Subcellular Localization of Tumor Necrosis Factor Receptor–associated Factor (TRAF)2 by TRAF1 Reveals Mechanisms of TRAF2 Signaling. In: *J Exp Med* 196 (7), S. 923–934. DOI: 10.1084/jem.20020774.
- Ashkenazi, A.; Dixit, V. M.** (1998): Death receptors: signaling and modulation. In: *Science (New York, N.Y.)* 281 (5381), S. 1305–1308.
- Banfield, D. K.** (2011): Mechanisms of protein retention in the Golgi. In: *Cold Spring Harbor Perspectives in Biology* 3 (8), S. a005264. DOI: 10.1101/cshperspect.a005264.
- Baud, V.; Karin, M.** (2001): Signal transduction by tumor necrosis factor and its relatives. In: *Trends in Cell Biology* 11 (9), S. 372–377.
- Birnboim, H. C.; Doly, J.** (1979): A rapid alkaline extraction procedure for screening recombinant plasmid DNA. In: *Nucleic Acids Research* 7 (6), S. 1513–1523.
- Blanc, M.; David, F.; Abrami, L.; Migliozi, D.; Armand, F.; Bürgi, J.; van der Goot, F. G.** (2015): SwissPalm: Protein Palmitoylation database. In: *F1000Research* 4, S. 261. DOI: 10.12688/f1000research.6464.1.
- Blaskovic, S.; Blanc, M.; van der Goot, F. G.** (2013): What does S-palmitoylation do to membrane proteins? In: *The FEBS Journal* 280 (12), S. 2766–2774. DOI: 10.1111/febs.12263.

- Brigidi, G. S.; Santyr, B.; Shimell, J.; Jovellar, B.; Bamji, S. X.** (2015): Activity-regulated trafficking of the palmitoyl-acyl transferase zDHHC5. In: *Nature Communications* 6, S. 8200. DOI:10.1038/ncomms9200.
- Brown, D. A.; London, E.** (1998): Structure and origin of ordered lipid domains in biological membranes. In: *The Journal of Membrane Biology* 164 (2), S. 103–114.
- Cáceres, J. F.; Stamm, S.; Helfman, D. M.; Krainer, A. R.** (1994): Regulation of alternative splicing in vivo by overexpression of antagonistic splicing factors. In: *Science (New York, N.Y.)* 265 (5179), S. 1706–1709.
- Carpentier, I.; Coornaert, B.; Beyaert, R.** (2004): Function and Regulation of Tumor Necrosis Factor Receptor Type 2. In: *CMC* 11 (16), S. 2205–2212. DOI: 10.2174/0929867043364694.
- Carswell, E. A.; Old, L. J.; Kassel, R. L.; Green, S.; Fiore, N.; Williamson, B.** (1975): An endotoxin-induced serum factor that causes necrosis of tumors. In: *Proceedings of the National Academy of Sciences of the United States of America* 72 (9), S. 3666–3670.
- Ceccarelli, A.; Di Venere, A.; Nicolai, E.; Luca, A.; Rosato, N.; Gratton, E.; Mei, G; Caccuri A. M.** (2017): New insight into the interaction of TRAF2 C-terminal domain with lipid raft microdomains. In: *Biochimica et Biophysica Acta. Molecular and Cell Biology of Lipids* 1862 (9), S. 813–822. DOI: 10.1016/j.bbalip.2017.05.003.
- Cendrowski, J.; Mamińska, A.; Miaczynska, M.** (2016): Endocytic regulation of cytokine receptor signaling. In: *Cytokine & Growth Factor Reviews* 32, S. 63–73. DOI: 10.1016/j.cytogfr.2016.07.002.
- Chakrabandhu, K.; Hérincs, Z.; Huault, S.; Dost, B.; Peng, L.; Conchonaud, F.; Marguet, D; He, H.; Hueber A.** (2007): Palmitoylation is required for efficient Fas cell death signaling. In: *The EMBO Journal* 26 (1), S. 209–220. DOI: 10.1038/sj.emboj.7601456.
- Chamberlain, L. H.; Shipston, M. J.** (2015): The physiology of protein S-acylation. In: *Physiological Reviews* 95 (2), S. 341–376. DOI: 10.1152/physrev.00032.2014.
- Chan, F. K.; Lenardo, M. J.** (2000): A crucial role for p80 TNF-R2 in amplifying p60 TNF-R1 apoptosis signals in T lymphocytes. In: *European Journal of Immunology* 30 (2), S. 652–660. DOI: 10.1002/1521-4141(200002)30:2
- Charollais, J.; van der Goot, F. G.** (2009): Palmitoylation of membrane proteins (Review). In: *Molecular Membrane Biology* 26 (1), S. 55–66. DOI: 10.1080/09687680802620369.
- Cohen, G. M.** (1997): Caspases: the executioners of apoptosis. In: *The Biochemical Journal* 326 (Pt 1), S. 1–16.
- Coleman, M. L.; Sahai, E. A.; Yeo, M.; Bosch, M.; Dewar, A.; Olson, M. F.** (2001): Membrane blebbing during apoptosis results from caspase-mediated activation of ROCK I. In: *Nature Cell Biology* 3 (4), S. 339–345. DOI: 10.1038/35070009.
- Corti, A.; Merli, S.; Bagnasco, L.; D'Ambrosio, F.; Marino, M.; Cassani, G.** (1995): Identification of two forms (31-33 and 48 kD) of the urinary soluble p55 tumor necrosis

- factor receptor that are differentially N- and O-glycosylated. In: *Journal of Interferon & Cytokine Research : the Official Journal of the International Society for Interferon and Cytokine Research* 15 (2), S. 143–152. DOI: 10.1089/jir.1995.15.143.
- Cottin, V.; van Linden, A.; Riches, D. W.** (1999): Phosphorylation of tumor necrosis factor receptor CD120a (p55) by p42 (mapk/erk2) induces changes in its subcellular localization. In: *The Journal of Biological Chemistry* 274 (46), S. 32975–32987.
- Cottin, V.; Doan, J. E. S.; Riches, D. W. H.** (2002): Restricted localization of the TNF receptor CD120a to lipid rafts: a novel role for the death domain. In: *Journal of Immunology (Baltimore, Md. : 1950)* 168 (8), S. 4095–4102.
- Crawford, E. D.; Wells, J. A.** (2011): Caspase substrates and cellular remodeling. In: *Annual Review of Biochemistry* 80, S. 1055–1087. DOI: 10.1146/annurev-biochem-061809-121639.
- D'Alessio, A.; Al-Lamki, R. S.; Bradley, J. R.; Pober, J. S.** (2005): Caveolae participate in tumor necrosis factor receptor 1 signaling and internalization in a human endothelial cell line. In: *The American Journal of Pathology* 166 (4), S. 1273–1282. DOI: 10.1016/S0002-9440(10)62346-2.
- D'Alessio, A.; Kluger, M. S.; Li, J. H.; Al-Lamki, R.; Bradley, J. R.; Pober, J. S.** (2010): Targeting of tumor necrosis factor receptor 1 to low density plasma membrane domains in human endothelial cells. In: *The Journal of Biological Chemistry* 285 (31), S. 23868–23879. DOI: 10.1074/jbc.M110.122853.
- Dargelos, E.; Renaud, V.; Decossas, M.; Bure, C.; Lambert, O.; Poussard, S.** (2018): Caveolae-mediated effects of TNF- $\alpha$  on human skeletal muscle cells. In: *Experimental Cell Research* 370 (2), S. 623–631. DOI: 10.1016/j.yexcr.2018.07.027.
- Degterev, A.; Huang, Z.; Boyce, M.; Li, Y.; Jagtap, P.; Mizushima, N.; Cuny, G. D.; Mitchison, T. J.; Moskowitz, M. A.; Yuan, J.** (2005): Chemical inhibitor of nonapoptotic cell death with therapeutic potential for ischemic brain injury. In: *Nature Chemical Biology* 1 (2), S. 112–119. DOI: 10.1038/nchembio711.
- Dekker, F. J.; Rocks, O.; Vartak, N.; Menninger, S.; Hedberg, C.; Balamurugan, R.; Wetzel, S.; Renner, S.; Gerauer, M.; Schölermann, B.; Rusch, M.; Kramer, J. W.; Rauh, D.; Coates, G. W.; Brunsveld, L.; Bastiaens, P. I. H.; Waldmann, H.** (2010): Small-molecule inhibition of APT1 affects Ras localization and signaling. In: *Nature Chemical Biology* 6 (6), S. 449–456. DOI: 10.1038/nchembio.362.
- Dembic, Z.; Loetscher, H.; Gubler, U.; Pan, Y. C.; Lahm, H. W.; Gentz, R.; Brockhaus, M.; Lesslauer, W.** (1990): Two human TNF receptors have similar extracellular, but distinct intracellular, domain sequences. In: *Cytokine* 2 (4), S. 231–237.
- Derfuss, T.; Fickenscher, H.; Kraft, M. S.; Henning, G.; Lengenfelder, D.; Fleckenstein, B.; Meini, E.** (1998): Antiapoptotic activity of the herpesvirus saimiri-encoded Bcl-2 homolog: stabilization of mitochondria and inhibition of caspase-3-like activity. In: *Journal of Virology* 72 (7), S. 5897–5904.

- Di Guglielmo, G. M.; Le Roy, C.; Goodfellow, A. F.; Wrana, J. L.** (2003): Distinct endocytic pathways regulate TGF-beta receptor signalling and turnover. In: *Nature Cell Biology* 5 (5), S. 410–421. DOI: 10.1038/ncb975.
- Doan, J. E. S.; Windmiller, D. A.; Riches, D. W. H.** (2004): Differential regulation of TNF-R1 signaling: lipid raft dependency of p42mapk/erk2 activation, but not NF-kappaB activation. In: *Journal of Immunology (Baltimore, Md. : 1950)* 172 (12), S. 7654–7660.
- Doherty, J.; Baehrecke, E. H.** (2018): Life, death and autophagy. In: *Nature Cell Biology* 20 (10), S. 1110–1117. DOI: 10.1038/s41556-018-0201-5.
- Draber, P.; Kupka, S.; Reichert, M.; Draberova, H.; Lafont, E.; Miguel de, D.; Spilgies, L.; Surinova, S.; Taraborelli, L.; Hartwig, T.; Rieser, E.; Martino, L.; Rittinger, K; Walczak, H.** (2015): LUBAC-Recruited CYLD and A20 Regulate Gene Activation and Cell Death by Exerting Opposing Effects on Linear Ubiquitin in Signaling Complexes. In: *Cell Reports* 13 (10), S. 2258–2272. DOI: 10.1016/j.celrep.2015.11.009.
- Dumitru, C. A.; Gulbins, E.** (2006): TRAIL activates acid sphingomyelinase via a redox mechanism and releases ceramide to trigger apoptosis. In: *Oncogene* 25 (41), S. 5612–5625. DOI: 10.1038/sj.onc.1209568.
- Eckelman, B. P.; Salvesen, G. S.; Scott, F. L.** (2006): Human inhibitor of apoptosis proteins: why XIAP is the black sheep of the family. In: *EMBO Reports* 7 (10), S. 988–994. DOI: 10.1038/sj.embor.7400795.
- Edelmann, B.; Bertsch, U.; Tchikov, V.; Winoto-Morbach, S.; Perrotta, C.; Jakob, M.; Adam-Klages, S.; Kabelitz, D.; Schütze, S.** (2011): Caspase-8 and caspase-7 sequentially mediate proteolytic activation of acid sphingomyelinase in TNF-R1 receptosomes. In: *The EMBO Journal* 30 (2), S. 379–394. DOI: 10.1038/emboj.2010.326.
- Elmore, S.** (2007): Apoptosis: a review of programmed cell death. In: *Toxicologic Pathology* 35 (4), S. 495–516. DOI: 10.1080/01926230701320337.
- Enari, M.; Sakahira, H.; Yokoyama, H.; Okawa, K.; Iwamatsu, A.; Nagata, S.** (1998): A caspase-activated DNase that degrades DNA during apoptosis, and its inhibitor ICAD. In: *Nature* 391 (6662), S. 43–50. DOI: 10.1038/34112.
- Falschlehner, C.; Emmerich, C. H.; Gerlach, B.; Walczak, H.** (2007): TRAIL signalling: decisions between life and death. In: *The International Journal of Biochemistry & Cell Biology* 39 (7-8), S. 1462–1475. DOI: 10.1016/j.biocel.2007.02.007.
- Faustman, D.; Davis, M.** (2010): TNF receptor 2 pathway: drug target for autoimmune diseases. In: *Nature Reviews. Drug Discovery* 9 (6), S. 482–493. DOI: 10.1038/nrd3030.
- Feig, C.; Tchikov, V.; Schütze, S.; Peter, M. E.** (2007): Palmitoylation of CD95 facilitates formation of SDS-stable receptor aggregates that initiate apoptosis signaling. In: *The EMBO Journal* 26 (1), S. 221–231. DOI: 10.1038/sj.emboj.7601460.
- Foot, N.; Henshall, T.; Kumar, S.** (2017): Ubiquitination and the Regulation of Membrane Proteins. In: *Physiological Reviews* 97 (1), S. 253–281. DOI: 10.1152/physrev.00012.2016.

- Forrester, M. T.; Hess, D. T.; Thompson, J. W.; Hultman, R.; Moseley, M. A.; Stamler, J. S.; Casey, P. J.** (2011): Site-specific analysis of protein S-acylation by resin-assisted capture. In: *Journal of Lipid Research* 52 (2), S. 393–398. DOI: 10.1194/jlr.D011106.
- Fotin-Mleczek, M.; Henkler, F.; Samel, D.; Reichwein, M.; Hausser, A.; Parmryd, I.; Scheurich, P.; Schmid, J. A.; Wajant, H.** (2002): Apoptotic crosstalk of TNF receptors: TNF-R2-induces depletion of TRAF2 and IAP proteins and accelerates TNF-R1-dependent activation of caspase-8. In: *Journal of Cell Science* 115 (Pt 13), S. 2757–2770.
- Fritsch, J.; Stephan, M.; Tchikov, V.; Winoto-Morbach, S.; Gubkina, S.; Kabelitz, D.; Schütze, S.** (2014): Cell fate decisions regulated by K63 ubiquitination of tumor necrosis factor receptor 1. In: *Molecular and Cellular Biology* 34 (17), S. 3214–3228. DOI: 10.1128/MCB.00048-14.
- Fritsch, J.; Zingler, P.; Särchen, V.; Heck, A. L.; Schütze, S.** (2017): Role of ubiquitination and proteolysis in the regulation of pro- and anti-apoptotic TNF-R1 signaling. In: *Biochimica et Biophysica Acta. Molecular Cell Research* 1864 (11 Pt B), S. 2138–2146. DOI: 10.1016/j.bbamcr.2017.07.017.
- Garrido, C.; Galluzzi, L.; Brunet, M.; Puig, P. E.; Didelot, C.; Kroemer, G.** (2006): Mechanisms of cytochrome c release from mitochondria. In: *Cell Death and Differentiation* 13 (9), S. 1423–1433. DOI: 10.1038/sj.cdd.4401950.
- Gille, J. J.; Joenje, H.** (1989): Chromosomal instability and progressive loss of chromosomes in HeLa cells during adaptation to hyperoxic growth conditions. In: *Mutation Research* 219 (4), S. 225–230.
- Gonzalvez, F.; Ashkenazi, A.** (2010): New insights into apoptosis signaling by Apo2L/TRAIL. In: *Oncogene* 29 (34), S. 4752–4765. DOI: 10.1038/onc.2010.221.
- Graham, F. L.; Smiley, J.; Russell, W. C.; Nairn, R.** (1977): Characteristics of a human cell line transformed by DNA from human adenovirus type 5. In: *The Journal of General Virology* 36 (1), S. 59–74. DOI: 10.1099/0022-1317-36-1-59.
- Greaves, J.; Chamberlain, L. H.** (2007): Palmitoylation-dependent protein sorting. In: *The Journal of Cell Biology* 176 (3), S. 249–254. DOI: 10.1083/jcb.200610151.
- Greaves J.; Chamberlain L. H.** (2011): DHHC palmitoyl transferases: substrate interactions and (patho)physiology. In: *Trends in Biochemical Sciences* 36 (5), S. 245-253. DOI: 10.1016/j.tibs.2011.01.033.
- Greaves, J.; Chamberlain, L. H.** (2014): New links between S-acylation and cancer. In: *The Journal of Pathology* 233 (1), S. 4–6. DOI: 10.1002/path.4339.
- Green, D. R.; Llambi, F.** (2015): Cell Death Signaling. In: *Cold Spring Harbor Perspectives in Biology* 7 (12). DOI: 10.1101/cshperspect.a006080.
- Grell, M.; Douni, E.; Wajant, H.; Löhden, M.; Clauss, M.; Maxeiner, B.; Georgopoulos, S.; Lesslauer, W.; Kollias, G.; Pfizenmaier, K.; Scheurich, P.** (1995): The transmembrane form

of tumor necrosis factor is the prime activating ligand of the 80 kDa tumor necrosis factor receptor. In: *Cell* 83 (5), S. 793–802.

**Grell, M.; Wajant, H.; Zimmermann, G.; Scheurich, P.** (1998): The type 1 receptor (CD120a) is the high-affinity receptor for soluble tumor necrosis factor. In: *Proceedings of the National Academy of Sciences of the United States of America* 95 (2), S. 570–575.

**Gump, J. M.; Thorburn, A.** (2011): Autophagy and apoptosis: what is the connection? In: *Trends in Cell Biology* 21 (7), S. 387–392. DOI: 10.1016/j.tcb.2011.03.007.

**Han, L.; Zhang, D.; Tao, T.; Sun, X.; Liu, X.; Zhu, G.; Xu, Z.; Zhu, L.; Zhang, Y.; Liu, W.; Ke, K.; Shen, A.** (2015): The role of N-glycan modification of TNFR1 in inflammatory microglia activation. In: *Glycoconjugate Journal* 32 (9), S. 685–693. DOI: 10.1007/s10719-015-9619-1.

**Hehlgans, T.; Pfeffer, K.** (2005): The intriguing biology of the tumour necrosis factor/tumour necrosis factor receptor superfamily: players, rules and the games. In: *Immunology* 115 (1), S. 1–20. DOI: 10.1111/j.1365-2567.2005.02143.x.

**Heinrich, M.; Neumeyer, J.; Jakob, M.; Hallas, C.; Tchikov, V.; Winoto-Morbach, S.; Wickel, M.; Schneider-Brachert W.; Trauzold, A.; Hethke, A.; Schütze, S.** (2004): Cathepsin D links TNF-induced acid sphingomyelinase to Bid-mediated caspase-9 and -3 activation. In: *Cell Death and Differentiation* 11 (5), S. 550–563. DOI: 10.1038/sj.cdd.4401382.

**Helms, J. B.; Zurzolo, C.** (2004): Lipids as targeting signals: lipid rafts and intracellular trafficking. In: *Traffic (Copenhagen, Denmark)* 5 (4), S. 247–254. DOI: 10.1111/j.1600-0854.2004.0181.x.

**Higuchi, M.; Aggarwal, B. B.** (1994): TNF induces internalization of the p60 receptor and shedding of the p80 receptor. In: *Journal of Immunology (Baltimore, Md. : 1950)* 152 (7), S. 3550–3558.

**Hill, M. M.; Adrain, C.; Duriez, P. J.; Creagh, E. M.; Martin, S. J.** (2004): Analysis of the composition, assembly kinetics and activity of native Apaf-1 apoptosomes. In: *The EMBO Journal* 23 (10), S. 2134–2145. DOI: 10.1038/sj.emboj.7600210.

**Holdbrooks, A. T.; Britain, C. M.; Bellis, S. L.** (2018): ST6Gal-I sialyltransferase promotes tumor necrosis factor (TNF)-mediated cancer cell survival via sialylation of the TNF receptor 1 (TNFR1) death receptor. In: *The Journal of Biological Chemistry* 293 (5), S. 1610–1622. DOI: 10.1074/jbc.M117.801480.

**Hunter, I.; Nixon, G. F.** (2006): Spatial compartmentalization of tumor necrosis factor (TNF) receptor 1-dependent signaling pathways in human airway smooth muscle cells. Lipid rafts are essential for TNF-alpha-mediated activation of RhoA but dispensable for the activation of the NF-kappaB and MAPK pathways. In: *The Journal of Biological Chemistry* 281 (45), S. 34705–34715. DOI: 10.1074/jbc.M605738200.

**Igney, F. H.; Krammer, P. H.** (2002): Death and anti-death: tumour resistance to apoptosis. In: *Nature Reviews. Cancer* 2 (4), S. 277–288. DOI: 10.1038/nrc776.

- Jennings, B. C.; Linder, M. E.** (2012): DHHC protein S-acyltransferases use similar ping-pong kinetic mechanisms but display different acyl-CoA specificities. In: *The Journal of Biological Chemistry* 287 (10), S. 7236–7245. DOI: 10.1074/jbc.M111.337246.
- Joseph, M.; Nagaraj, R.** (1995): Interaction of peptides corresponding to fatty acylation sites in proteins with model membranes. In: *The Journal of Biological Chemistry* 270 (28), S. 16749–16755.
- Kaksonen, M.; Roux, A.** (2018): Mechanisms of clathrin-mediated endocytosis. In: *Nature Reviews. Molecular Cell Biology* 19 (5), S. 313–326. DOI: 10.1038/nrm.2017.132.
- Kang, J. U.; Koo, S. H.; Kwon, K. C.; Park, J. W.; Kim, J. M.** (2008): Gain at chromosomal region 5p15.33, containing TERT, is the most frequent genetic event in early stages of non-small cell lung cancer. In: *Cancer Genetics and Cytogenetics* 182 (1), S. 1–11. DOI: 10.1016/j.cancergencyto.2007.12.004.
- Karin, M.; Lin, A.** (2002): NF-kappaB at the crossroads of life and death. In: *Nature Immunology* 3 (3), S. 221–227. DOI: 10.1038/ni0302-221.
- Kathayat, R. S.; Elvira, P. D.; Dickinson, B. C.** (2017): A fluorescent probe for cysteine depalmitoylation reveals dynamic APT signaling. In: *Nature Chemical Biology* 13 (2), S. 150–152. DOI: 10.1038/nchembio.2262.
- Kerr, J. F.; Wyllie, A. H.; Currie, A. R.** (1972): Apoptosis: a basic biological phenomenon with wide-ranging implications in tissue kinetics. In: *British Journal of Cancer* 26 (4), S. 239–257.
- Ketteler, R.; Glaser, S.; Sandra, O.; Martens, U. M.; Klingmüller, U.** (2002): Enhanced transgene expression in primitive hematopoietic progenitor cells and embryonic stem cells efficiently transduced by optimized retroviral hybrid vectors. In: *Gene Therapy* 9 (8), S. 477–487. DOI: 10.1038/sj.gt.3301653.
- Klíma, M.; Zájedová, J.; Doubravská, L.; Andera, L.** (2009): Functional analysis of the posttranslational modifications of the death receptor 6. In: *Biochimica et Biophysica Acta* 1793 (10), S. 1579–1587. DOI: 10.1016/j.bbamcr.2009.07.008.
- Klotzsch, E.; Schütz, G. J.** (2013): A critical survey of methods to detect plasma membrane rafts. In: *Philosophical transactions of the Royal Society of London. Series B, Biological Sciences* 368 (1611), S. 20120033. DOI: 10.1098/rstb.2012.0033.
- Ko, P.; Dixon, S. J.** (2018): Protein palmitoylation and cancer. In: *EMBO Reports* 19 (10). DOI: 10.15252/embr.201846666.
- Ko, Y. G.; Lee, J. S.; Kang, Y. S.; Ahn, J. H.; Seo, J. S.** (1999): TNF-alpha-mediated apoptosis is initiated in caveolae-like domains. In: *Journal of immunology (Baltimore, Md. : 1950)* 162 (12), S. 7217–7223.
- Kong, E.; Peng, S.; Chandra, G.; Sarkar, C.; Zhang, Z.; Bagh, M. B.; Mukherjee, A. B.** (2013): Dynamic palmitoylation links cytosol-membrane shuttling of acyl-protein thioesterase-1 and acyl-protein thioesterase-2 with that of proto-oncogene H-ras product



and growth-associated protein-43. In: *The Journal of Biological Chemistry* 288 (13), S. 9112–9125. DOI: 10.1074/jbc.M112.421073.

**Kothakota, S.; Azuma, T.; Reinhard, C.; Klippel, A.; Tang, J.; Chu, K.; McGarry, T. J.; Kirschner, M. W.; Koths, K.; Kwiatkowski, D. J.; Williams L. T.** (1997): Caspase-3-generated fragment of gelsolin: effector of morphological change in apoptosis. In: *Science (New York, N.Y.)* 278 (5336), S. 294–298.

**Krut, O.; Wiegmann, K.; Kashkar, H.; Yazdanpanah, B.; Krönke, M.** (2006): Novel tumor necrosis factor-responsive mammalian neutral sphingomyelinase-3 is a C-tail-anchored protein. In: *The Journal of Biological Chemistry* 281 (19), S. 13784–13793. DOI: 10.1074/jbc.M511306200.

**Kvansakul, M.; Hinds, M. G.** (2013): Structural biology of the Bcl-2 family and its mimicry by viral proteins. In: *Cell Death & Disease* 4, S. e909. DOI: 10.1038/cddis.2013.436.

**Laemmli, U. K.** (1970): Cleavage of structural proteins during the assembly of the head of bacteriophage T4. In: *Nature* 227 (5259), S. 680–685.

**Lam, K. K. Y.; Davey, M.; Sun, B.; Roth, A. F.; Davis, N. G.; Conibear, E.** (2006): Palmitoylation by the DHHC protein Pfa4 regulates the ER exit of Chs3. In: *The Journal of Cell Biology* 174 (1), S. 19–25. DOI: 10.1083/jcb.200602049.

**Legler, D. F.; Micheau, O.; Doucey, M.; Tschopp, J.; Bron, C.** (2003): Recruitment of TNF receptor 1 to lipid rafts is essential for TNF $\alpha$ -mediated NF- $\kappa$ B activation. In: *Immunity* 18 (5), S. 655–664.

**Levental, I.; Grzybek, M.; Simons, K.** (2010): Greasing their way: lipid modifications determine protein association with membrane rafts. In: *Biochemistry* 49 (30), S. 6305–6316. DOI: 10.1021/bi100882y.

**Liao, W.; Fujita, K.; Xiao, Q.; Tchikov, V.; Yang, W.; Gunsor, M.; Garfield, S.; Goldsmith, P.; El-Deiry, W. S.; Schütze, S.; Srinivasula, S. M.** (2009): Response. CARP1 regulates induction of NF- $\kappa$ B by TNF $\alpha$ . In: *Current Biology* 19 (1), S. R17-R19. DOI: 10.1016/j.cub.2008.11.041.

**Liao, W.; Xiao, Q.; Tchikov, V.; Fujita, K.; Yang, W.; Wincovitch, S.; Garfield, S.; Conze, D.; Goldsmith, P.; El-Deiry, W. S.; Schütze, S.; Srinivasula, S. M.** (2008): CARP-2 is an endosome-associated ubiquitin ligase for RIP and regulates TNF-induced NF- $\kappa$ B activation. In: *Current Biology: CB* 18 (9), S. 641–649. DOI: 10.1016/j.cub.2008.04.017.

**Lillemeier, B. F.; Pfeiffer, J. R.; Surviladze, Z.; Wilson, B. S.; Davis, M. M.** (2006): Plasma membrane-associated proteins are clustered into islands attached to the cytoskeleton. In: *Proceedings of the National Academy of Sciences of the United States of America* 103 (50), S. 18992–18997. DOI: 10.1073/pnas.0609009103.

**Linder, M. E.; Deschenes, R. J.** (2007): Palmitoylation: policing protein stability and traffic. In: *Nature reviews. Molecular Cell Biology* 8 (1), S. 74–84. DOI: 10.1038/nrm2084.

## 6. References

---

- Lingwood, D.; Simons, K.** (2010): Lipid rafts as a membrane-organizing principle. In: *Science (New York, N.Y.)* 327 (5961), S. 46–50. DOI: 10.1126/science.1174621.
- Lockshin, R. A.; Zakeri, Z.** (2001): Programmed cell death and apoptosis: origins of the theory. In: *Nature Reviews. Molecular Cell Biology* 2 (7), S. 545–550. DOI: 10.1038/35080097.
- Lockshin, R. A.; Williams, C.M.** (1964): Programmed cell death—II. Endocrine potentiation of the breakdown of the intersegmental muscles of silkmoths. In: *Journal of Insect Physiology* 10 (4), S. 643–649. DOI: 10.1016/0022-1910(64)90034-4.
- Locksley, R. M.; Killeen, N.; Lenardo, M. J.** (2001): The TNF and TNF receptor superfamilies: integrating mammalian biology. In: *Cell* 104 (4), S. 487–501.
- López-Urrutia, E.; Campos-Parra, A.; Herrera, L. A.; Pérez-Plasencia, C.** (2017): Alternative splicing regulation in tumor necrosis factor-mediated inflammation. In: *Oncology Letters* 14 (5), S. 5114–5120. DOI: 10.3892/ol.2017.6905.
- Maguy, A.; Hebert, T. E.; Nattel, S.** (2006): Involvement of lipid rafts and caveolae in cardiac ion channel function. In: *Cardiovascular Research* 69 (4), S. 798–807. DOI: 10.1016/j.cardiores.2005.11.013.
- Martin, B. R.** (2013): Nonradioactive analysis of dynamic protein palmitoylation. In: *Current Protocols in Protein Science* 73, S. Unit 14.15. DOI: 10.1002/0471140864.ps1415s73.
- Meng, X. W.; Peterson, K. L.; Dai, H.; Schneider, P.; Lee, S.; Zhang, J.; Koenig, A.; Bronk, S.; Billadeau, D. D.; Gores, G. J.; Kaufmann, S. H.** (2011): High cell surface death receptor expression determines type I versus type II signaling. In: *The Journal of Biological Chemistry* 286 (41), S. 35823–35833. DOI: 10.1074/jbc.M111.240432.
- Micheau, O.; Tschoop, J.** (2003): Induction of TNF receptor I-mediated apoptosis via two sequential signaling complexes. In: *Cell* 114 (2), S. 181–190.
- Mitchell, D. A.; Mitchell, G.; Ling, Y.; Budde, C.; Deschenes, R. J.** (2010): Mutational analysis of *Saccharomyces cerevisiae* Erf2 reveals a two-step reaction mechanism for protein palmitoylation by DHHC enzymes. In: *The Journal of Biological Chemistry* 285 (49), S. 38104–38114. DOI: 10.1074/jbc.M110.169102.
- Mitchell, D. A.; Vasudevan, A.; Linder, M. E.; Deschenes, R. J.** (2006): Protein palmitoylation by a family of DHHC protein S-acyltransferases. In: *Journal of Lipid Research* 47 (6), S. 1118–1127. DOI: 10.1194/jlr.R600007-JLR200.
- Mitra, K.; Ubarretxena-Belandia, I.; Taguchi, T.; Warren, G.; Engelman, D. M.** (2004): Modulation of the bilayer thickness of exocytic pathway membranes by membrane proteins rather than cholesterol. In: *Proceedings of the National Academy of Sciences of the United States of America* 101 (12), S. 4083–4088. DOI: 10.1073/pnas.0307332101.

- Morales, A.; Lee, H.; Goñi, F. M.; Kolesnick, R.; Fernandez-Checa, J. C.** (2007): Sphingolipids and cell death. In: *Apoptosis: an International Journal on Programmed Cell Death* 12 (5), S. 923–939. DOI: 10.1007/s10495-007-0721-0.
- Moylan, J. S.; Smith, J. D.; Wolf Horrell, E. M.; McLean, J. B.; Deevska, G. M.; Bonnell, M. R.; Nikolova-Karakashian, M. N.; Reid, M. B.** (2014): Neutral sphingomyelinase-3 mediates TNF-stimulated oxidant activity in skeletal muscle. In: *Redox Biology* 2, S. 910–920. DOI: 10.1016/j.redox.2014.07.006.
- Muppidi, J. R.; Tschopp, J.; Siegel, R. M.** (2004): Life and death decisions: secondary complexes and lipid rafts in TNF receptor family signal transduction. In: *Immunity* 21 (4), S. 461–465. DOI: 10.1016/j.immuni.2004.10.001.
- Muszbek, L.; Haramura, G.; Cluette-Brown, J. E.; van Cott, E. M.; Laposata, M.** (1999): The pool of fatty acids covalently bound to platelet proteins by thioester linkages can be altered by exogenously supplied fatty acids. In: *Lipids* 34 Suppl, S. S331-7.
- Napetschnig, J.; Wu, H.** (2013): Molecular basis of NF- $\kappa$ B signaling. In: *Annual Review of Biophysics* 42, S. 443–468. DOI: 10.1146/annurev-biophys-083012-130338.
- Neumeyer, J.; Hallas, C.; Merkel, O.; Winoto-Morbach, S.; Jakob, M.; Thon, L.; Adam, D.; Schneider-Brachert, W.; Schütze, S.** (2006): TNF-receptor I defective in internalization allows for cell death through activation of neutral sphingomyelinase. In: *Experimental Cell Research* 312 (11), S. 2142–2153. DOI: 10.1016/j.yexcr.2006.03.014.
- Ohno, Y.; Kihara, A.; Sano, T.; Igarashi, Y.** (2006): Intracellular localization and tissue-specific distribution of human and yeast DHHC cysteine-rich domain-containing proteins. In: *Biochimica et Biophysica Acta* 1761 (4), S. 474–483. DOI: 10.1016/j.bbaliip.2006.03.010.
- Orzechowska, S.; Pajak, B.; Gajkowska, B.; Orzechowski, A.** (2011): Cholesterol level determines viability and mitogenicity, but it does not affect sodium butyrate-dependent sensitization of Colo 205 cells to TNF- $\alpha$ -induced apoptosis. In: *Oncology Reports* 25 (2), S. 573–582. DOI: 10.3892/or.2010.1081.
- Oyama, T.; Miyoshi, Y.; Koyama, K.; Nakagawa, H.; Yamori, T.; Ito, T.; Matsuda, H.; Arakawa, H.; Nakamura, Y.** (2000): Isolation of a novel gene on 8p21.3-22 whose expression is reduced significantly in human colorectal cancers with liver metastasis. In: *Genes, Chromosomes & Cancer* 29 (1), S. 9–15.
- Pelkmans, L.; Helenius, A.** (2002): Endocytosis via caveolae. In: *Traffic (Copenhagen, Denmark)* 3 (5), S. 311–320.
- Peter, M. E.; Budd, R. C.; Desbarats, J.; Hedrick, S. M.; Hueber, A.; Newell, M. K.; Owen, L. B.; Pope, R. M.; Tschopp, J.; Wajant, H.; Wallach, D.; Wilttrout, R. H.; Zörnig, M.; Lynch, D. H.** (2007): The CD95 receptor: apoptosis revisited. In: *Cell* 129 (3), S. 447–450. DOI: 10.1016/j.cell.2007.04.031.

- Pfizenmaier, K.; Krönke, M.; Scheurich, P.; Nagel, G. A.** (1987): Tumor necrosis factor (TNF) alpha: control of TNF-sensitivity and molecular mechanisms of TNF-mediated growth inhibition. In: *Blut* 55 (1), S. 1–10.
- Philipp, S.; Puchert, M.; Adam-Klages, S.; Tchikov, V.; Winoto-Morbach, S.; Mathieu, S.; Deerberg, A.; Kolker, L.; Marchesini, N.; Kabelitz, D.; Hannun, Y. A.; Schütze, S.; Adam, D.** (2010): The Polycomb group protein EED couples TNF receptor 1 to neutral sphingomyelinase. In: *Proceedings of the National Academy of Sciences of the United States of America* 107 (3), S. 1112–1117. DOI: 10.1073/pnas.0908486107.
- Pike, L. J.** (2006): Rafts defined: a report on the Keystone Symposium on Lipid Rafts and Cell Function. In: *Journal of Lipid Research* 47 (7), S. 1597–1598. DOI: 10.1194/jlr.E600002-JLR200.
- Rai, N. K.; Tripathi, K.; Sharma, D.; Shukla, V. K.** (2005): Apoptosis: a basic physiologic process in wound healing. In: *The International Journal of Lower Extremity Wounds* 4 (3), S. 138–144. DOI: 10.1177/1534734605280018.
- Ran, F. A.; Hsu, P. D.; Wright, J.; Agarwala, V.; Scott, D. A.; Zhang, F.** (2013): Genome engineering using the CRISPR-Cas9 system. In: *Nature Protocols* 8 (11), S. 2281–2308. DOI: 10.1038/nprot.2013.143.
- Rao, R. V.; Ellerby, H. M.; Bredesen, D. E.** (2004): Coupling endoplasmic reticulum stress to the cell death program. In: *Cell Death and Differentiation* 11 (4), S. 372–380. DOI: 10.1038/sj.cdd.4401378.
- Ren, J.; Wen, L.; Gao, X.; Jin, C.; Xue, Y.; Yao, X.** (2008): CSS-Palm 2.0: an updated software for palmitoylation sites prediction. In: *Protein Engineering, Design & Selection: PEDS* 21 (11), S. 639–644. DOI: 10.1093/protein/gzn039.
- Resh, M. D.** (2016): Fatty acylation of proteins: The long and the short of it. In: *Progress in Lipid Research* 63, S. 120–131. DOI: 10.1016/j.plipres.2016.05.002.
- Ricci, J.; Muñoz-Pinedo, C.; Fitzgerald, P.; Bailly-Maitre, B.; Perkins, G. A.; Yadava, N.; Scheffler, I. E.; Ellisman, M. H.; Green, D. R.** (2004): Disruption of mitochondrial function during apoptosis is mediated by caspase cleavage of the p75 subunit of complex I of the electron transport chain. In: *Cell* 117 (6), S. 773–786. DOI: 10.1016/j.cell.2004.05.008.
- Richter, C.; Messerschmidt, S.; Holeiter, G.; Tepperink, J.; Osswald, S.; Zappe, A.; Branschädel, M.; Boschert, V.; Mann, D. A.; Scheurich, P.; Krippner-Heidenreich, A.** (2012): The tumor necrosis factor receptor stalk regions define responsiveness to soluble versus membrane-bound ligand. In: *Molecular and Cellular Biology* 32 (13), S. 2515–2529. DOI: 10.1128/MCB.06458-11.
- Rossin, A.; Durivault, J.; Chakhtoura-Feghali, T.; Lounnas, N.; Gagnoux-Palacios, L.; Hueber, A-O** (2015): Fas palmitoylation by the palmitoyl acyltransferase DHHC7 regulates Fas stability. In: *Cell Death and Differentiation* 22 (4), S. 643–653. DOI: 10.1038/cdd.2014.153.

- Rossin, A.; Derouet, M.; Abdel-Sater, F.; Hueber, A-O** (2009): Palmitoylation of the TRAIL receptor DR4 confers an efficient TRAIL-induced cell death signalling. In: *The Biochemical Journal* 419 (1), S. 185-92, 2 p following 192. DOI: 10.1042/BJ20081212.
- Roth, A. F.; Wan, J.; Bailey, A. O.; Sun, B.; Kuchar, J. A.; Green, W. N.; Phinney, B. S.; Yates III, J. R.; Davis, N. G.** (2006): Global analysis of protein palmitoylation in yeast. In: *Cell* 125 (5), S. 1003–1013. DOI: 10.1016/j.cell.2006.03.042.
- Rubio-Moscardo, F.; Blesa, D.; Mestre, C.; Siebert, R.; Balasas, T.; Benito, A.; Rosenwald A.; Climent J.; Martinez J. I.; Schilhabel M.; Karran E. L.; Gesk S.; Esteller M.; deLeeuw R.; Staudt L. M.; Fernandez-Luna J. L.; Pinkel D.; Dyer M. J. S.; Martinez-Climent J. A.** (2005): Characterization of 8p21.3 chromosomal deletions in B-cell lymphoma: TRAIL-R1 and TRAIL-R2 as candidate dosage-dependent tumor suppressor genes. In: *Blood* 106 (9), S. 3214–3222. DOI: 10.1182/blood-2005-05-2013.
- Saelens, X.; Festjens, N.; Vande Walle, L.; van Gurp, M.; van Loo, G.; Vandenabeele, P.** (2004): Toxic proteins released from mitochondria in cell death. In: *Oncogene* 23 (16), S. 2861–2874. DOI: 10.1038/sj.onc.1207523.
- Salaun, C.; Greaves, J.; Chamberlain, L. H.** (2010): The intracellular dynamic of protein palmitoylation. In: *The Journal of Cell Biology* 191 (7), S. 1229–1238. DOI: 10.1083/jcb.201008160.
- Scaffidi, C.; Schmitz, I.; Krammer, P. H.; Peter, M. E.** (1999): The role of c-FLIP in modulation of CD95-induced apoptosis. In: *The Journal of Biological Chemistry* 274 (3), S. 1541–1548.
- Schlesinger, M. J.; Magee, A. I.; Schmidt, M. F.** (1980): Fatty acid acylation of proteins in cultured cells. In: *The Journal of Biological Chemistry* 255 (21), S. 10021–10024.
- Schneider-Brachert, W.; Tchikov, V.; Neumeyer, J.; Jakob, M.; Winoto-Morbach, S.; Held-Feindt, J.; Heinrich, M.; Merkel, O.; Ehrenschwender, M.; Adam, D.; Mentlein, R.; Kabelitz, D.; Schütze, S.** (2004): Compartmentalization of TNF receptor 1 signaling: internalized TNF receptors as death signaling vesicles. In: *Immunity* 21 (3), S. 415–428. DOI: 10.1016/j.immuni.2004.08.017.
- Schulze, H.; Kolter, T.; Sandhoff, K.** (2009): Principles of lysosomal membrane degradation: Cellular topology and biochemistry of lysosomal lipid degradation. In: *Biochimica et Biophysica Acta* 1793 (4), S. 674–683. DOI: 10.1016/j.bbamcr.2008.09.020.
- Schütze, S.; Tchikov, V.; Schneider-Brachert, W.** (2008): Regulation of TNFR1 and CD95 signalling by receptor compartmentalization. In: *Nature Reviews. Molecular Cell Biology* 9 (8), S. 655–662. DOI: 10.1038/nrm2430.
- Sezgin, E.; Levental, I.; Mayor, S.; Eggeling, C.** (2017): The mystery of membrane organization: composition, regulation and roles of lipid rafts. In: *Nature Reviews. Molecular Cell Biology* 18 (6), S. 361–374. DOI: 10.1038/nrm.2017.16.

- Sharma, C.; Rabinovitz, I.; Hemler, M. E.** (2012): Palmitoylation by DHHC3 is critical for the function, expression, and stability of integrin  $\alpha 6\beta 4$ . In: *Cellular and Molecular Life Sciences : CMLS* 69 (13), S. 2233–2244. DOI: 10.1007/s00018-012-0924-6.
- Shirai, A.; Matsuyama, A.; Yashiroda, Y.; Hashimoto, A.; Kawamura, Y.; Arai, R.; Komatsu, Y.; Horinouchi, S.; Yoshida, M.** (2008): Global analysis of gel mobility of proteins and its use in target identification. In: *The Journal of Biological Chemistry* 283 (16), S. 10745–10752. DOI: 10.1074/jbc.M709211200.
- Stephan, M.; Edelmann, B.; Winoto-Morbach, S.; Janssen, O.; Bertsch, U.; Perrotta, C.; Schütze, S.; Fritsch, J.** (2017): Role of caspases in CD95-induced biphasic activation of acid sphingomyelinase. In: *Oncotarget* 8 (12), S. 20067–20085. DOI: 10.18632/oncotarget.15379.
- Sundström, C.; Nilsson, K.** (1976): Establishment and characterization of a human histiocytic lymphoma cell line (U-937). In: *International Journal of Cancer* 17 (5), S. 565–577.
- Tabaczar, S.; Czogalla, A.; Podkalicka, J.; Biernatowska, A.; Sikorski, A. F.** (2017): Protein palmitoylation: Palmitoyltransferases and their specificity. In: *Experimental Biology and Medicine (Maywood, N.J.)* 242 (11), S. 1150–1157. DOI: 10.1177/1535370217707732.
- Tani, M.; Hannun, Y. A.** (2007): Analysis of membrane topology of neutral sphingomyelinase 2. In: *FEBS Letters* 581 (7), S. 1323–1328. DOI: 10.1016/j.febslet.2007.02.046.
- Tanimura, N.; Saitoh, S.; Kawano, S.; Kosugi, A.; Miyake, K.** (2006): Palmitoylation of LAT contributes to its subcellular localization and stability. In: *Biochemical and Biophysical Research Communications* 341 (4), S. 1177–1183. DOI: 10.1016/j.bbrc.2006.01.076.
- Tardy, C.; Sabourdy, F.; Garcia, V.; Jalanko, A.; Therville, N.; Levade, T.; Andrieu-Abadie, N.** (2009): Palmitoyl protein thioesterase 1 modulates tumor necrosis factor alpha-induced apoptosis. In: *Biochimica et Biophysica Acta* 1793 (7), S. 1250–1258. DOI: 10.1016/j.bbamcr.2009.03.007.
- Tartaglia, L. A.; Pennica, D.; Goeddel, D. V.** (1993): Ligand passing: the 75-kDa tumor necrosis factor (TNF) receptor recruits TNF for signaling by the 55-kDa TNF receptor. In: *The Journal of Biological Chemistry* 268 (25), S. 18542–18548.
- Tcherkasowa, A. E.; Adam-Klages, S.; Kruse, M.-L.; Wiegmann, K.; Mathieu, S.; Kolanus, W.; Krönke, M.; Adam, D.** (2002): Interaction with Factor Associated with Neutral Sphingomyelinase Activation, a WD Motif-Containing Protein, Identifies Receptor for Activated C-Kinase 1 as a Novel Component of the Signaling Pathways of the p55 TNF Receptor. In: *The Journal of Immunology* 169 (9), S. 5161–5170. DOI: 10.4049/jimmunol.169.9.5161.
- Thon, L.; Mathieu, S.; Kabelitz, D.; Adam, D.** (2006): The murine TRAIL receptor signals caspase-independent cell death through ceramide. In: *Experimental Cell Research* 312 (19), S. 3808–3821. DOI: 10.1016/j.yexcr.2006.08.017.

- Tian, L.; McClafferty, H.; Knaus, H.; Ruth, P.; Shipston, M. J.** (2012): Distinct acyl protein transferases and thioesterases control surface expression of calcium-activated potassium channels. In: *The Journal of Biological Chemistry* 287 (18), S. 14718–14725. DOI: 10.1074/jbc.M111.335547.
- Ting, A. T.; Bertrand, M. J. M.** (2016): More to Life than NF- $\kappa$ B in TNFR1 Signaling. In: *Trends in Immunology* 37 (8), S. 535–545. DOI: 10.1016/j.it.2016.06.002.
- Tomatis, V. M.; Trenchi, A.; Gomez, G. A.; Daniotti, J. L.** (2010): Acyl-protein thioesterase 2 catalyzes the deacylation of peripheral membrane-associated GAP-43. In: *PloS One* 5 (11), S. e15045. DOI: 10.1371/journal.pone.0015045.
- Turner, M. D.; Chaudhry, A.; Nedjai, B.** (2012): Tumour necrosis factor receptor trafficking dysfunction opens the TRAPS door to pro-inflammatory cytokine secretion. In: *Bioscience Reports* 32 (2), S. 105–112. DOI: 10.1042/BSR20110089.
- Van Linden, A. A.; Cottin, V.; Frankel, S. K.; Riches, D. W. H.** (2005): Hierarchical phosphorylation of the TNF-alpha receptor, TNF-R1, by p42Mapk/Erk at basic Pro-directed kinase sites. In: *Biochemistry* 44 (18), S. 6980–6989. DOI: 10.1021/bi050058w.
- Varfolomeev, E. E.; Boldin, M. P.; Goncharov, T. M.; Wallach, D.** (1996): A potential mechanism of "cross-talk" between the p55 tumor necrosis factor receptor and Fas/APO1: proteins binding to the death domains of the two receptors also bind to each other. In: *The Journal of Experimental Medicine* 183 (3), S. 1271–1275.
- Vartak, N.; Papke, B.; Grecco, H. E.; Rossmannek, L.; Waldmann, H.; Hedberg, C.; Bastiaens, P. I. H.** (2014): The autodepalmitoylating activity of APT maintains the spatial organization of palmitoylated membrane proteins. In: *Biophysical Journal* 106 (1), S. 93–105. DOI: 10.1016/j.bpj.2013.11.024.
- Veldman, R. J.; Maestre, N.; Aduib, O. M.; Medin, J. A.; Salvayre, R.; Levade, T.** (2001): A neutral sphingomyelinase resides in sphingolipid-enriched microdomains and is inhibited by the caveolin-scaffolding domain: potential implications in tumour necrosis factor signalling. In: *The Biochemical Journal* 355 (Pt 3), S. 859–868.
- Vercammen, D.; Vandenabeele, P.; Declercq, W.; van de Craen, M.; Grooten, J.; Fiers, W.** (1995): Cytotoxicity in L929 murine fibrosarcoma cells after triggering of transfected human p75 tumour necrosis factor (TNF) receptor is mediated by endogenous murine TNF. In: *Cytokine* 7 (5), S. 463–470. DOI: 10.1006/cyto.1995.0063.
- Verkruyse, L. A.; Hofmann, S. L.** (1996): Lysosomal targeting of palmitoyl-protein thioesterase. In: *The Journal of Biological Chemistry* 271 (26), S. 15831–15836.
- Wagner, S. A.; Satpathy, S.; Beli, P.; Choudhary, C.** (2016): SPATA2 links CYLD to the TNF- $\alpha$  receptor signaling complex and modulates the receptor signaling outcomes. In: *The EMBO Journal* 35 (17), S. 1868–1884. DOI: 10.15252/embj.201694300.
- Wajant, H.; Pfizenmaier, K.; Scheurich, P.** (2003): Tumor necrosis factor signaling. In: *Cell Death and Differentiation* 10 (1), S. 45–65. DOI: 10.1038/sj.cdd.4401189.

- Wajant, H.** (2002): The Fas signaling pathway: more than a paradigm. In: *Science (New York, N.Y.)* 296 (5573), S. 1635–1636. DOI: 10.1126/science.1071553.
- Wajant, H.** (2017): TRAIL- and TNF-induced signaling complexes-so similar yet so different. In: *The EMBO Journal* 36 (9), S. 1117–1119. DOI: 10.15252/embj.201796997.
- Wajant, H.; Scheurich, P.** (2011): TNFR1-induced activation of the classical NF- $\kappa$ B pathway. In: *The FEBS Journal* 278 (6), S. 862–876. DOI: 10.1111/j.1742-4658.2011.08015.x.
- Wang, J.; Al-Lamki, R. S.; Zhang, H.; Kirkiles-Smith, N.; Gaeta, M. L.; Thiru, S.; Pobers, J. S.; Bradley, J. R.** (2003): Histamine Antagonizes Tumor Necrosis Factor (TNF) Signaling by Stimulating TNF Receptor Shedding from the Cell Surface and Golgi Storage Pool. In: *Journal of Biological Chemistry* 278 (24), S. 21751–21760. DOI: 10.1074/jbc.M212662200.
- Yamamoto, Y.; Chochi, Y.; Matsuyama, H.; Eguchi, S.; Kawauchi, S.; Furuya, T.; Oga, A.; Kang, J. J.; Naito, K.; Sasaki, K.** (2007): Gain of 5p15.33 is associated with progression of bladder cancer. In: *Oncology* 72 (1-2), S. 132–138. DOI: 10.1159/000111132.
- Yan, S.; Tang, J.; Huang, C.; Xi, S.; Huang, M.; Liang, J.; Jiang, Y.; Li, Y.; Zhou, Z.; Ernberg, I.; Wu, Q.; Du, Z.** (2013): Reduced expression of ZDHHC2 is associated with lymph node metastasis and poor prognosis in gastric adenocarcinoma. In: *PloS One* 8 (2), S. e56366. DOI: 10.1371/journal.pone.0056366.
- Yang, E.; Zha, J.; Jockel, J.; Boise, L. H.; Thompson, C. B.; Korsmeyer, S. J.** (1995): Bad, a heterodimeric partner for Bcl-XL and Bcl-2, displaces Bax and promotes cell death. In: *Cell* 80 (2), S. 285–291.
- Young, F. B.; Butland, S. L.; Sanders, S. S.; Sutton, L. M.; Hayden, M. R.** (2012): Putting proteins in their place: palmitoylation in Huntington disease and other neuropsychiatric diseases. In: *Progress in Neurobiology* 97 (2), S. 220–238. DOI: 10.1016/j.pneurobio.2011.11.002.
- Yu, J.; Fischman, D. A.; Steck, T. L.** (1973): Selective solubilization of proteins and phospholipids from red blood cell membranes by nonionic detergents. In: *Journal of Supramolecular Structure* 1 (3), S. 233–248. DOI: 10.1002/jss.400010308.
- Yuan, J.; Kroemer, G.** (2010): Alternative cell death mechanisms in development and beyond. In: *Genes & Development* 24 (23), S. 2592–2602. DOI: 10.1101/gad.1984410.
- Zhang, Q.; Lenardo, M. J.; Baltimore, D.** (2017): 30 Years of NF- $\kappa$ B: A Blossoming of Relevance to Human Pathobiology. In: *Cell* 168 (1-2), S. 37-57. DOI: 10.1016/j.cell.2016.12.012.



## 7. List of publication

**Fritsch J, Zingler P, Särchen V, Heck AL, Schütze S** (2017) Role of ubiquitination and proteolysis in the regulation of pro- and anti-apoptotic TNF-R1 signaling. *Biochim. Biophys. Acta*, 1864, 2138-2146.

**Fritsch J, Fickers R, Klawitter J, Särchen V, Zingler P, Adam D, Janssen O, Krause E, Schütze S** (2016) TNF induced cleavage of HSP90 by cathepsin D potentiates apoptotic cell death. *Oncotarget*, 15; 7(46), 75774-75789.

Submitted for publication

**Zingler P, Särchen V, Glatter T, Canning L, Saggau C, Kathayat RS, Pagel O, Tenev T, Dickinson BC, Zahedi RP, Lucius R, Meier P, Adam D, Schneider-Brachert W, Schütze S, Fritsch J** (2018) Dynamic protein palmitoylation regulates TNF-R1 signaling.

## 8. Eidesstattliche Erklärung

Hiermit versichere ich, Philipp Zingler (Geb.: 06.10.1990, Weimar), an Eides statt, dass ich die vorliegende wissenschaftliche Abhandlung mit dem Titel:

**„Regulation of the Tumor Necrosis Factor Receptor-1 signaling by palmitoylation“**

nach den Regeln guter wissenschaftlicher Praxis eigenständig verfasst und keine anderen als die angegebenen Hilfsmittel und Quellen benutzt habe. Dabei habe ich keine Hilfe, außer der wissenschaftlichen Beratung durch meinen Doktorvater Prof. Dr. rer. nat. Axel Scheidig und durch die namentlich erwähnten Kooperationspartner in Anspruch genommen.

Weder wurde diese Arbeit bisher im Rahmen eines Prüfungsverfahrens vorgelegt, noch wurde ein akademischer Grad entzogen. Teile dieser Arbeit sind zur Veröffentlichung eingereicht worden.

Kiel, März 2019

---

Philipp Zingler

## 9. Danksagung

Meinen ersten besonderen und ausdrücklichen Dank richte ich an meinen Betreuer Prof. Dr. rer. nat. Stefan Schütze, denn er eröffnete mir mit der Bereitstellung dieses überaus spannenden Themas die Möglichkeit, mich mit diesem zu beschäftigen und es bearbeiten zu dürfen. Weiterhin danke ich ihm für das stete Vertrauen und die Wertschätzung, die er mir in den letzten drei Jahren entgegen brachte sowie für die motivierenden und kritischen wissenschaftlichen Diskussionen, die maßgeblich zum Gelingen dieser Arbeit beitrugen, aber auch mich persönlich in meiner wissenschaftlichen Wissensaneignung intensiv prägten und entwickelten.

Des Weiteren gilt mein ausdrücklicher Dank Prof. Dr. rer. nat. Axel Scheidig, welcher mich seit meiner wissenschaftlichen Ausbildungszeit in Kiel stets zuverlässig betreute und der sich auch für die Begutachtung dieser Arbeit bereit erklärte.

Ebenfalls danke ich den Direktoren des Instituts für Immunologie, Prof. Dr. med. Dietrich Kabelitz und Prof. Dr. rer. nat. Alexander Scheffold, für die Möglichkeit meine Dissertation an ihrem Institut anfertigen zu dürfen.

Ich danke allen Mitarbeitern des Institutes für Immunologie für die freundschaftliche und optimistische Arbeitsatmosphäre, ihre Hilfe und ihren Beistand, auch wenn nicht alles immer zeit- und planmäßig reibungslos verlief.

Weiterhin widme ich einen besonderen Dank an Dr. Jürgen Fritsch für die unablässige Betreuung und die vielseitigen wissenschaftlichen Diskussionen während der drei Jahre, die ebenfalls zu meiner wissenschaftlichen Reifung beigetragen haben. Ich bedanke mich herzlich bei den folgenden temporären Mitarbeitern der AG Schütze: Vinzenz Särchen, Lotta Caning, Matthias von Garrel, Lena Hennig und Anna Laura Heck, ohne die der Laboralltag wesentlich trostloser gewesen wäre. Überdies gilt mein Dank Parvin Davarnia für ihre Unterstützung in der Molekularbiologie, Carina Saggau für die Zusammenarbeit bezüglich der Institutsaufgaben sowie Doreen Gänslar für die Hilfestellungen während aller bürokratischen Hürden.

Außerdem danke ich Sascha Rahn, Florian Peters, Fred Armbrust, Johanna Ehlers und Vivian Adamski für ihre Freundschaft und die Unterstützung während unserer gemeinsamen Studien- und PhD-Zeit in Kiel, in der wir uns gegenseitig Mut zugesprochen und auch Frust von der Seele geredet haben. Darüber hinaus danke ich Todi, Domi, Made, Brille, Kevin, Dicker und Mary für die entschleunigenden und erdenden Momente.

Zuletzt gilt mein tiefer Dank meiner gesamten Familie, besonders jedoch meinen Eltern Sibylle und Thomas, ohne deren unermüdliche Unterstützung in all den Jahren dieser Lebensabschnitt nicht hätte vollendet werden können.

## 10. Wissenschaftlicher Werdegang

### Persönliche Daten

Name: Philipp Zingler  
Geburtsdatum und –ort: 06.10.1990 in Weimar  
Adresse: Brunswiker Str. 41 in 24103 Kiel  
Staatsangehörigkeit: deutsch

### Akademische Ausbildung

seit 11/2015 Promotionsarbeit im Rahmen des Sonderforschungsbereichs SFB877 „*Proteolysis as a Regulatory Event in Pathophysiology*“ in der Arbeitsgruppe von Prof. Dr. Stefan Schütze, Christian-Albrechts-Universität zu Kiel

10/2013 – 11/2015 Masterstudium der Biochemie und Molekularbiologie an der Christian-Albrechts-Universität zu Kiel

11/2015 Abschluss: *Master of Science*  
  
Thema der Masterarbeit: „*Deletion of antiapoptotic genes by multi-step homologous recombination and its effects on the replication of self-repairing rhadinovirus vectors*“

10/2010 – 09/2013 Bachelorstudium der Biochemie und Molekularbiologie an der Martin-Luther-Universität, Halle-Wittenberg

09/2013 Abschluss: *Bachelor of Science*  
  
Thema der Bachelorarbeit: „Charakterisierung der putativen [Ni-Fe] Hydrogenase Vhu in *Dehalococcoides mccartyi* CBDB1“

07/2001 - 07/2009 Gymnasium „Prof. Fritz Hofmann“, Kölleda  
Abschluss: Abitur